EFFECTS OF Ag-NANOPARTICLES DISPERSED GLYCERYL LACTATE MATRIX ON THE CRYSTALLIZATION, THERMAL AND ELECTRICAL PROPERTIES OF POLY (LACTIC ACID)

GETACHEW TADESSE GURMU

A Thesis Submitted to

The department of Chemical Engineering

School of Mechanical, Chemical and Materials Engineering

Presented in Partial Fulfilment of the Requirement for the Degree of Master of Science in Chemical Engineering (Specialization in Process engineering)

Office of Graduate Studies

Adama Science and Technology University

June, 2022 G.C

Adama, Ethiopia

EFFECTS OF Ag-NANOPARTICLE DISPERSED GLYCERYL LACTATE MATRIX ON THE CRYSTALLIZATION, THERMAL AND ELECTRICAL PROPERTIES OF POLY (LACTIC ACID)

GETACHEW TADESSE GURMU

Advisor

Dr. Melaku Tesfaye

Co-Advisor

Dr. Tatek Temesgen

A Thesis Submitted to

The department of Chemical Engineering

School of Mechanical, Chemical and Materials Engineering

Presented in Partial Fulfilment of the Requirement for the Degree of Master of Science in Chemical Engineering (Specialization in Process engineering)

Office of Graduate Studies

Adama Science and Technology University

June, 2022 G.C

Adama, Ethiopia

DECLARATION

I hereby declare that this Master Thesis entitled “Effects of Ag-nanoparticles Dispersed Glyceryl lactate Matrix on the Crystallization, Thermal and Electrical Properties of Poly (lactic acid)” is my original work, it has not been submitted for the award of any academic degree, diploma or certificate in any other university. All sources of materials that are used for this thesis have been duly acknowledged through citation. It is being submitted for the award of the degree of Master of Science in Chemical Engineering (Specialization in Process engineering) at Adama Science and Technology University, School of Mechanical, Chemical and Materials Engineering.

Getachew Tadesse Gurmu	_____	_____
Name of the Student	Signature	Date

RECOMMENDATION

We, the advisors of this thesis, hereby certify that we have read the revised version of the thesis entitled “Effects of Ag-nanoparticles Dispersed Glyceryl lactate Matrix on the Crystallization, Thermal and Electrical Properties of Poly (lactic acid)” prepared under our guidance by Getachew Tadesse Gurmu submitted in partial fulfilment of the requirements for the degree of Master of Science in Chemical Engineering. Therefore, we recommend the submission of the revised version of the thesis to the department following the applicable procedures.

Melaku Tesfaye (PhD)	_____	_____
Major Advisor	Signature	Date
Tatek Temesgen (PhD)	_____	_____
Co-Advisor	Signature	Date

APPROVAL

We, the advisors of the thesis entitled “Effects of Ag-nanoparticles Dispersed Glyceryl lactate Matrix on the Crystallization, Thermal and Electrical Properties of Poly (lactic acid)” and developed by Getachew Tadesse Gurmu, hereby certify that the recommendation and suggestions made by the board of examiners are appropriately incorporated into the final version of the thesis.

Melaku Tesfaye (PhD)	_____	_____
Major Advisor	Signature	Date
Tatek Temesgen (PhD)	_____	_____
Co-Advisor	Signature	Date

We, the undersigned, members of the Board of Examiners of the thesis by Getachew Tadesse Gurmu have read and evaluated the thesis entitled “Effects of Ag-nanoparticles Dispersed Glyceryl lactate Matrix on the Crystallization, Thermal and Electrical Properties of Poly (lactic acid)” and examined the candidate during the open defence. This is, therefore, to certify that the thesis is accepted for partial fulfilment of the requirement of the degree of Master of Science in Chemical Engineering.

_____	_____	_____
Chairperson	Signature	Date
_____	_____	_____
Internal Examiner	Signature	Date
_____	_____	_____
Eternal Examiner	Signature	Date
_____	_____	_____
Department Head	Signature	Date
_____	_____	_____
School Dean	Signature	Date
_____	_____	_____
Office of Postgraduate Studies, Dean	Signature	Date

ACKNOWLEDGMENTS

First of all, I would like to thank GOD Almighty, for the protection and ability to do work that has granted me countless blessings, wisdom, and peace of mind. This thesis becomes a reality with the kind support and assistance of many people. I would like to express my heartfelt gratitude to every one of them. I would like to express my deepest appreciation to my major advisor Dr. Melaku Tesfaye for his intellectual guidance, and valuable advice on doing the experiments, giving me intellectual freedom in my work and preparing my thesis. I would also like to extend my deepest gratitude to Dr. Tatek Temsegen for taking the time to advise and assist me through every stage of this study, especially in searching for characterization equipment. It was a pleasure working with both of them.

Thanks to my family, for the numerous times they have helped and prayed for me. This thesis is heartily dedicated to my mother (Yeshi Shiferaw) who took the lead to heaven. I believe that all of my family's efforts will gain something great shortly. When times were tough, their encouragement, financial assistance, and constant prayer were much welcomed and acknowledged.

I would like to thank my best friends and ASTU classmates for always being there for me when I needed them; without them, I would never have enjoyed so many opportunities.

I'm also grateful to my friends and my co-workers at Adama Science and Technology University (ASTU) for helping me through this master's thesis. Finally, I would like to thank all the people who contributed in one way or another to the work described in this thesis.

TABLE OF CONTENTS

LIST OF TABLES

LIST OF FIGURES

LIST OF EQUATIONS

LIST OF ABBREVIATIONS AND ACRONYMS

^{13}C-NMR	^{13}C-NMR Carbon Nuclear Magnetic resonance
1HNMR	^{1}HNMR Hydrogen Nuclear Magnetic resonance
3D	Three Dimensional
Ag	Silver
AgNPs	Silver Nanoparticles
ASTM	American Society for Testing and Materials
Au	Gold
AV	Acid value
CB	Carbon Black
CNTs	Carbon Nanotubes
CPCs	Conductive Polymer Composites
CPs	Conductive Polymers
CS	Chitosan
DSC	Differential scanning calorimeter
DW	Distilled water
E/DW	Ethanol with distilled water
EA	Ethyl acetate
EC	Electrical Conductivity
EDC	Ethyl carbodiimide hydrochloride
FGO	Amide-functionalized Graphene oxide
FTIR	Fourier-transform infrared spectroscopy
GLY	Glycerol
LAC	Lactic acid
LAOLG	L-lactic acid Oligomer
M/DW	Methanol with distilled water

NAs	Nucleating agents
NB	Nitrobenzene
NMR	Nuclear magnetic resonance
ODCB	O-dichlorobenzene
OMBH	Octamethylenedicarboxylic di(2-hydroxybenzohydrazide)
PBAT	Poly(butylene adipate-co-terephthalate)
PDLA	Poly D-lactic Acid
PEG	Poly ethylene glycol
PLA	Poly lactic Acid
PLA-g-GMA	Polylactide-graft-glycidyl methacrylate
PLA-g-PEGMA	Polylactide-graft-poly (ethylene glycol) methyl ether methacrylate
PLLA/Zn (D-Ala)2	Poly L-lactic Acid zinc L -alanine
PLLA/Zn (DL-Ala)2	Poly L-lactic Acid zinc DL -alanine
PLLA/Zn (DL-Phe)2	Poly L-lactic Acid zinc DL-phenylalaninate
PLLA/Zn (DL-Pro)2	Poly L-lactic Acid zinc DL-proline
PLLA/Zn (D-Phe)2	Poly L-lactic Acid zinc D-phenylalaninate
PLLA/Zn (D-Pro)2	Poly L-lactic Acid zinc D-proline
PLLA/Zn (L-Ala)2	Poly L-lactic Acid zinc L -alanine
PLLA/Zn (L-Phe)2	Poly L-lactic Acid zinc L-phenylalaninate
PLLA/Zn (L-Pro)2	Poly L-lactic Acid zinc L-proline
POCFA	Phosphorus oxychloride furfurylamine
PSA	Particle size analyser
SEM	Scanning electron microscope
$t_{1/2}$	Half-life
TMC	Tetramethylene-dicarboxylic dibenzoyl-hydrazide,

UV-Vis	Ultra violet -visible spectroscopy
V. amygdalina	Vernonia amygdalina
X_c	Degree of crystallinity
XRD	X-ray diffraction spectroscopy
T_g	Glass transition temperature
T_m	Melting temperature
TC	Thermal conductivity
EC	Electrical conductivity

LIST OF NOTATIONS

%	Percentage
µg	Microgram
Cm	Centimetre
cP	Centipoise
GLY-LAC 1:12	1 to 12 Glycerol to lactic acid ratio
GLY-LAC 1:3	1 to 3 Glycerol to lactic acid ratio
GLY-LAC 1:6	1 to 6 Glycerol to lactic acid ratio
GLY-LAC 1:9	1 to 9 Glycerol to lactic acid ratio
hr	hour
kV	Kilovolt
mM	Millimolar
mW	Milliwatt
Nm	Nano meter
^{o}C	Degree Celsius
Sec	Second
w/v	Weight per volume

ABSTRACT

Polymers were utilized in different areas for longer periods of time. Nowadays, biodegradable polymers such as poly (lactic acid) (PLA) are highly applicable. To increase the application of PLA for diversified purposes, its poor crystallinity and insulating property needs to be improved, using green synthesis approaches. Glyceryl lactate (GLY-LAC) with different chain lengths (1:3, 1:6, 1:9 and 1:12) was derived from glycerol and lactic acid through a condensation reaction, then purified through solubility in two different miscible liquid methods and used as a nucleating agent (NAs) to increase PLA crystallinity. Silver nanoparticles (AgNPs) which was synthesised from silver nitrate ($AgNO_3$) through a biological method using Vernonia amygdalina (V. amygdalina) leaf extract as reducing, stabilizing and capping agents was used for improvement.

The formation and synthesis of GLY-LAC was confirmed through acid value calculation and 75.73%, 137.44%, 148.66%, 157.08% and 33.023%, 89%, 92.54%, 112.86% was calculated for before and after purification. NMR and FTIR analysis also confirmed the formation and synthesis of GLY-LAC. Dispersions of AgNPs within the GLY-LAC matrix were done using ultra sonication. The impacts of nucleating agent (GLY-LAC) and AgNPs were examined through the preparation of biopolymer films, using the solution casting method. The effects of annealing time (30, 90 and 150 minutes), annealing temperature (90 ℃, 100 ℃, 110 ℃ and 120 ℃) and loading rate of GLY-LAC (1wt%, 3wt%, 5wt%, and 10wt%,) on the degree of crystallinity were examined. The conformity of green synthesised AgNPs was done with UV-Vis, XRD, FTIR and PSA. UV-Vis spectra showed absorption peaks at 415, 418 and 423 nm after synthesis of 6 hr, 24 hr and after 5 months.

Formations of four major peaks on XRD attributed to the formation of AgNPs and also FTIR spectrum at 625 and 454 attributed to Ag-OH and Ag^o formation. Particle size for the AgNPs was also found to be 3.05 and 56.45 nm. The higher degree of crystallinity achieved was 85.2% with 10wt% GLY-LAC loading at 110 ℃ and for 150 minutes annealing time with using differential scanning calorimeter (DSC). The thermal conductivity enhanced from 0.2 to 0.7 W m^{-1} k^{-1} with 5wt% AgNPs loading, however, the electrical conductivity was not changed, this was due to the encapsulation and shielding effects of plant extract. Therefore, it was possible to conclude that GLY-LAC and AgNPs were good fillers and that AgNPs dispersed GLY-LAC/PLA matrix could be used in biomedical, packing and 3D printing areas.

***Keywords**: AgNPs, Bio-film, GLY-LAC, PLA, Vernonia amygdalina.*

CHAPTER ONE

1. INTRODUCTION

1.1 Background of the study

Conductive, flexible and tough polymers are nowadays very important for biomedical and 3D printing filaments as well as electrical and electronics parts. These materials are required to fulfil the property of biocompatibility and biodegradability. The need for replacing conventionally existing polymers (petroleum-based materials) by using degradable, recyclable and biocompatible polymers such as poly (lactic acid) (PLA) gets high attention from many scholars, because of the growing need of reducing the non-degradable nature and waste generations of petroleum-based materials.

PLA is a thermoplastic polymer that possesses the ability to substitute existing petroleum-based commercially available polymers, to overcome the accumulation of plastic waste in landfills. PLA is produced from the monomers of lactic acid, which are obtained from sugar-based compounds through direct poly-condensation and ring-opening polymerization (Sin, 2012; Tarani et al., 2021; N. Wang et al., 2021; Xiaoyu Wang et al., 2020).

Due to its production from vegetable sources, PLA has a lot of advantages such as biodegradability, recyclability, biocompatibility, eco-friendly, and energy-saving properties. Other properties make this polymer to be used for the application of biomedical (compatibility in the human body), packaging materials, fibre/textile and others. Besides those advantages and applications, PLA has some limitations that lower its further applications such as; poor crystallinity (resulting in a long processing cycle), hydrophobicity, poor toughness, slow degradation rate, thermal instability and insulators for thermal and electrical conductivity. Enhancing those limitations will make PLA applicable in different areas such as bio-3D printing materials, fashion products, ECG applications, electrodes, pipes, apparel, home textiles and other applications (Tarani et al., 2021; Xiaoyu Wang et al., 2020).

There are different mechanisms for improving the limited properties of PLA such as using blending, plasticization, composition, NAs addition, cross-linking, copolymerization and others (Rasal et al., 2010). From those techniques addition of a NAs is the new focus of the vast majority of scientists due to its less input requirement and huge impact to speed up the

crystallization of PLA by giving low energy of obstruction to nucleation and allowing crystallization at higher crystallization temperatures (J. Wu et al., 2020; L. Yang et al., 2019). Some of the nucleating agents are not compatible with the PLA matrix and are less effective on X_C, as well as, migrate into PLA matrix.

Therefore, it is necessary to use NAs that are compatible and do not migrate. To use PLA in packing industries, especially in the food packing industry, its antiviral, antibacterial, antifungal and ant parasitic effects must be improved, for this purpose using nanoparticles will have the greatest impact. For synergistic impacts, using AgNPs with several of their unique features will offer the potential for the combined improvement of PLA properties, (AgNPs) has a property to improve the antiviral, antibacterial, antifungal as well as thermal and electrical conductivity (Ding et al., 2021; Sheikh et al., 2021; Yuan et al., 2016).

In this research, the main goal was to synthesise and purify glyceryl lactate (GLY-LAC) NAs for the application of improving the crystallization, thermal and electrical properties of PLA through the incorporation of AgNPs using green synthesis approaches to apply the high compatibility, green and degradability nature of GLY-LAC and PLA matrix. GLY-LAC has an amazing structure, with a 3-armed OH functional group which gives it the ability to hold other additional elements or compounds that minimize the migration rate of compounds. In these case for the study of the effects of the filler on PLA's insulating property (thermal and electrical), AgNPs were dispersed into the GLY-LAC matrix and then into PLA. Here the research was conducted trying to improve the engineering properties of PLA (crystallization, conductivity) without compromising its biodegradability.

1.2 Statements of problem

In addition to vast applications of PLA, due to some limiting properties its application window is limited. From those limiting properties below some of them are listed:

- ✓ Poor crystallization rates
- ✓ Slow degradation rates
- ✓ Poor toughness
- ✓ Low thermal stability
- ✓ Poor thermal and electrically conductivity
- ✓ Poor heat resistance
- ✓ High brittleness

With those and other limiting properties PLA exhibits rapid loss of molecular weight, can't recycle PLA easily an and also incredibly low crystallization rates, lower PLA handling prospects application window, bringing about a long processing time and low toughness, t are restricting its broad applications, such as with its poor crystalllinity PLA cannot applied in 3D printing areas, in agricultural films, as pipes and its low thermal stability makes PLA to restrict to low service temperatures equipment. Due to its insulating properties using PLA in electronics as well as in communication also limited. Most of those limiting properties are directly related with crystallinity and crystallization ability, therefore, improving the crystallinity of PLA the other performance of PLA improved. To overcome those limitations and apply them for wide applications using different nucleating agents is a current and very effective method to control the crystallization process and crystallinity.

The other problems related with the nucleating agents, most of the existing nucleating agents were non-degradable, require high cost of synthesis because during their synthesis they need catalyst and surfactants, and also they became toxic because they leached out from the polymer due to lack of host matrix, therefore degradable, biocompatible and environmental friendly nucleating agent are required.

1.3 Research question, hypothesis and choice of systems

Research questions: this research work aims to answer the following major research questions

- Can it possible to synthesise and purify biodegradable 3-armed macromolecules from lactic acid and glycerol which can be applied as polymer additive?
- Is it possible to form a stable dispersion of AgNPs in synthesized 3-armed biodegradable macromolecules and disperse it into a PLA matrix?
- Is it possible to enhance the slow crystallization of PLA using 3-armed GLY-LAC?
- Is it possible to improve the thermal and electrical conductivity of PLA using nanomaterial dispersed 3-armed biodegradable macromolecules?

From the above research questions the choice of the systems, methodology and characterization techniques are framed as follows:

- PLA, GLY-LAC and AgNPs are selected based on: -
    - PLA is a biodegradable and biocompatibility polymer synthesized from renewable resources such as corn. PLA is now produced on a large scale and can be used for various applications in different fields: electrical and thermal conductive instruments (biosensors, electronics, energy, biomedicine, chemical industries, and aerospace) packaging, pharmaceutical, agriculture, 3D printing, different films (in mulch film and in medical films).
    - GLY-LAC is selected due to its production from renewable resources, which is obtained from the esterification reaction between lactic acid and glycerol. GLY-LAC is biodegradable, non-toxic, and biocompatible with PLA and other natural products.
    - AgNPs are selected due to their highest thermal and electrical conductance among all metals (420 W m^{-1} k^{-1} and 62.1 S/m respectively).

Hypothesis: if the stable dispersion of AgNPs in the GLY-LAC is successfully incorporated into the PLA matrix, the crystallization, thermal and electrical conductivity and other properties of PLA can be enhanced.

1.4 Objectives

1.4.1 General objective

The general objective of this research work is to synthesise, purify and characterize AgNPs dispersed glyceryl lactate based nucleating agents and study their effects on crystallization, thermal and electrical conductivities of PLA.

1.4.2 Specific objectives

The specific objectives of the research work were

- Synthesis, purification and characterization of glyceryl lactate (GLY-LAC).
- Synthesis and characterization of AgNPs.
- Study the stability of AgNPs within purified glyceryl lactate (GLY-LAC).
- Study the nucleating effect of GLY-LAC on crystallization properties of PLA
- Investigate the effects of AgNPs dispersed GLY-LAC on the thermal and electrical conductivity of PLA.

1.5 Significance of the study

Due to low crystallinity, low toughness, thermal instability and thermally and electrically insulator properties of PLA, the application areas are limited, therefore, if improvements will take place on those properties PLA applications become expanded for further use. Greenly synthesized AgNPs using *V.amygdalina* plant leaf extract which contains different phytochemicals as reducing agents and a stabilizing agent, used as conductive fillers to improve PLA's insulating properties, due to its multifunctional properties such as antimicrobial, excellent thermal and electrical conductivity and also its higher surface area to volume ratio their impacts as conductive filler will be great.

If GLY-LAC will be successfully incorporated into the polymer backbone it allows PLA to be modified for specific applications. GLY-LAC which is made from the combination of glycerol stereoisomers and lactic acid, make it biocompatible with PLA. The ease of incorporation of various nucleating agents into PLA allows for the control of the crystallization rate. GLY-LAC acts as a crystallizer, plasticizer and also carrier matrix for the AgNPs dispersion. Due to its end chain of GLY-LAC (OH), it could be easily compatible with AgNPs for uniform and stable dispersion. Its impact on the improvements of poor properties of PLA will be interesting.

Therefore, incorporating those two multifunctional fillers into PLA to improve its limiting properties through ultra-sonication and solution casting method will be effective after AgNPs dispersed uniformly within GLY-LAC. The application areas of the PLA become increased if those poor property improved and it could be applied in different applications, such as packing, 3D printing, the medical industry, tea bags, different films (in mulch film, medical films), biodegradable cups and others.

1.6 Scope of the study

The study covers analysing effects of NAs starting from its synthesis from glycerol and lactic acid through poly-condensation reaction and purification using solubility in two different miscible liquid methods and also characterizes the final product GLY-LAC, which is within different mixing ratios. The other focusing areas are:

- ✓ These researches also focus on the preparation of AgNPs through a biological method, with the consideration of the impacts of the plant extract.
- ✓ Study the physical (Viscosity and AV) and chemical (functional group) properties of prepared NAs through different characterizing instruments.
- ✓ The researchers also focus on the study of the effects of NAs on PLA properties with each parameter on the degree of crystallinity of PLA.
- ✓ Study the effects of biologically synthesized AgNPs on PLA properties, such as thermal conductivity, and electrical conductivity through dispersing AgNPs with different ratios.

During the research work, there were some limiting properties which limit the study to go further beyond all of the above areas. These limitations include a lack of characterizing instruments such as TEM, SEM (nano scale), stability characterizing instruments and others.

CHAPTER TWO

2. LITERATURE REVIEW

2.1 Overview of PLA

Generally, there are two major categories of polymers; natural and synthetic polymers which are also categorized as; non-degradable and biodegradable. Those polymers are made of different raw materials. Biodegradable polymers can be partitioned into two classifications petrol determined and microorganism-inferred biodegradable polymers (Sin, 2012; Trifol et al., 2019). People have been utilizing polymers for millennia. In old occasions, normal plant gum was utilized to follow bits of wood in house building. Around then individuals didn't have the foggiest idea about the degree to which polymers could be put to utilize, so their utilization was restricted to quite certain applications (Sin, 2012). The first synthetic polymer was invented by Leo Hendrik Baekeland in 1907. In past years, the quick improvement of polymers has made a huge commitment to innovation with the development of a profoundly viable polymerization measure (Sin, 2012; Trifol et al., 2019).

Nowadays, degradable polymers are getting high intention from many scholars due to their environmentally friendly; one of them is PLA. Because of its, slow crystallization behaviour, high brittleness, poor barrier properties, low heat distortion temperature and longer crystallization time, PLA is not highly commercialized. The other important properties required from PLA are its thermal and electrical conductivity. By its nature, PLA is an insulating polymer, but by incorporating conductive fillers it became conductive. From many properties crystallization and conductivity properties of PLA are highly related, when PLA become highly crystallized it becomes a good conductor, due to the orderly arrangement of the PLA matrix. Its biodegradability, flexibility, ease to process and stretch ability using PLA in electronic, communication as well as the medical application as a conductive polymer make it a very interesting polymer (Xiaoxue Wang et al., 2018).

PLA is completely bio-based, biodegradable and harmless to the ecosystem because it is made from sustainable resources and can be produced through ring-opening polymerization and condensation polymerization. PLA can't be considered a new polymer. As ahead of schedule as 1845, PLA was integrated by Theophile - Jules Pelouze by the build-up of lactic acid The base material of PLA is a lactic acid monomer, which is

obtained from normal assets like corn, wheat, rice and so on, and is acquiring the common consideration (Sin, 2012; Zhao et al., 2017).

Biopolymer films are polymer-based thin films for different applications, especially in medical applications; they are produced from different biodegradable as well as petroleum-based materials such as living organisms, and microbial systems, from plants and also can be synthesized chemically from biological systems. Polymer-based films are one part of the polymer's form of application as PLA-based films can be manufactured for packaging, especially for edible food packaging. The PLA-based thin film could be used for different PLA properties (Rebelo et al., 2017).

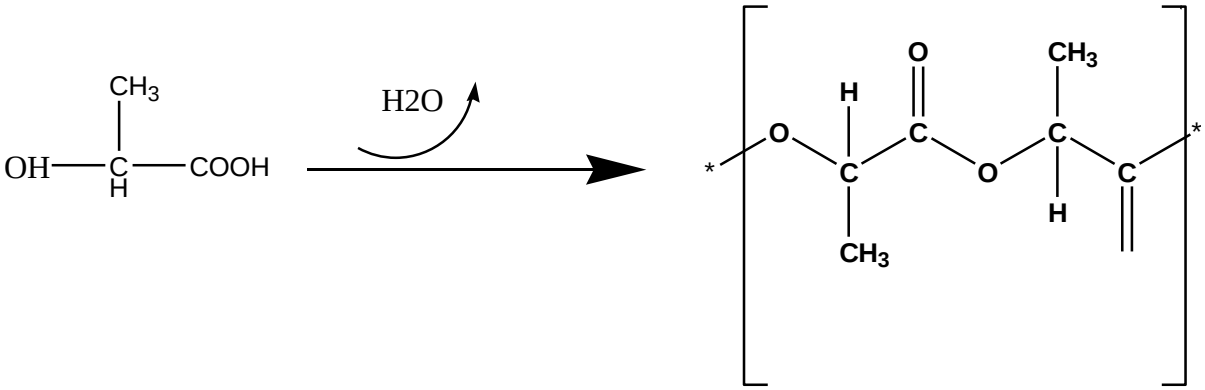

Figure 2-1: Polylactic acid (PLA) production process

2.2 Crystallization property of PLA

PLA is utilized in the worldwide market because of its mix of awesome properties and minimal cost. PLA is a semi-crystalline polymer, a large number of its properties rely upon its glasslike attributes, which can be altered through various mechanisms and procedures. The addition of nucleating agents will prompt a more uniform precious ordered size and gem structure. This will initiate a higher crystallization temperature, which ultimately will bring about a more limited crystallization time. Upgrades in the mechanical and thermal properties incorporate expanded modulus without forfeiting way strength, expanded thermal solidness and expanded clearness for extraordinarily enhanced visualizations while concerning the optical properties (Botkin et al., 2002).

In industry, quick crystallization is regularly required. At present, the crystallization rate of PLA is excessively low contrasted with modern requirements (Carbone et al., 2015). To be appropriate for specific biomedical applications, the PLA has been modified mainly concerning two aspects: bulk properties and surface chemistry (Jinhao Sun et al., 2019;

Xiao et al., 2012). PLA ordinarily has low crystallinity, which restricts the scope of utilization in different areas. Therefore, a great deal of exertion in scientific research was taken to upgrade the cores thickness or nuclei density and the general crystallization. PLA with a specific measure of crystallinity is needed for commercial application. Then again, the mechanical properties and biodegradability of PLA are perfectly subject to the crystal morphology and structure, while, it is trying to foster high crystallinity. Along these lines, enhancing PLA crystallinity is required (Jing et al., 2016).

Various techniques help to enhance the crystallization properties of PLA as shown in figure 2-2, methods of crystallization enhancement can be broadly classified as surface chemistry modification and bulk properties modification. Surface chemistry modification is a process of modifying the surface of a material instead of using it as it is; such modification includes topography, surface chemical functionalities, hydrophilicity, roughness and smoothness, and surface energy. Bulk properties methods focus in detail on the modification of biodegradability, thermal stability, crystallinity and others properties of polymers, through the changing polymers tacticity and also structures. There are two ways of bulk modification system, physical and chemical method, under physical there are different nucleating agents, which are highly applicable in many research areas as well as industrial scales due to their fast response and little amount requirement. Chemical methods include copolymerization and cross linking, which focus mainly on structural modification of PLA (Jin et al., 2019; Saeidlou et al., 2012; Xiao et al., 2012).

2.2.1 Nucleation mechanisms

From the above mentioned methods, NA is the new and the vast majority of the scientists centre on this strategy. Adding NAs is one of the simplest, recent and most proficient approaches. NAs are used to speed up the crystallization of PLA by giving a low energy obstruction to nucleation and allowing crystallization at higher crystallization temperatures (H. Bai et al., 2014; Jin et al., 2019; Wei et al., 2019). NAs would reduce the nucleation induction period and increase the number of primary nucleation sites. In a general classification, nucleation can be either physical/epitaxial nucleation or chemical nucleation (Saeidlou et al., 2012). Considering the chemical nucleation, the NAs typically disintegrate in the polymer solution and respond with the polymer chains, bringing about another nucleation substance on which other polymer chains could nucleate.

The scission of polymer chains is going with the result, bringing about the decrease of atomic weight. In terms of the epitaxial nucleation mechanism, polymer crystals grow on NA substance by physical interaction. Currently, the epitaxial nucleation mechanism based on lattice matching was widely used to explain the enhanced crystallization of polymers with NAs (Wei et al., 2019). Specifically, there are three methods of incorporating NAs with PLA as shown in figure 2-3.

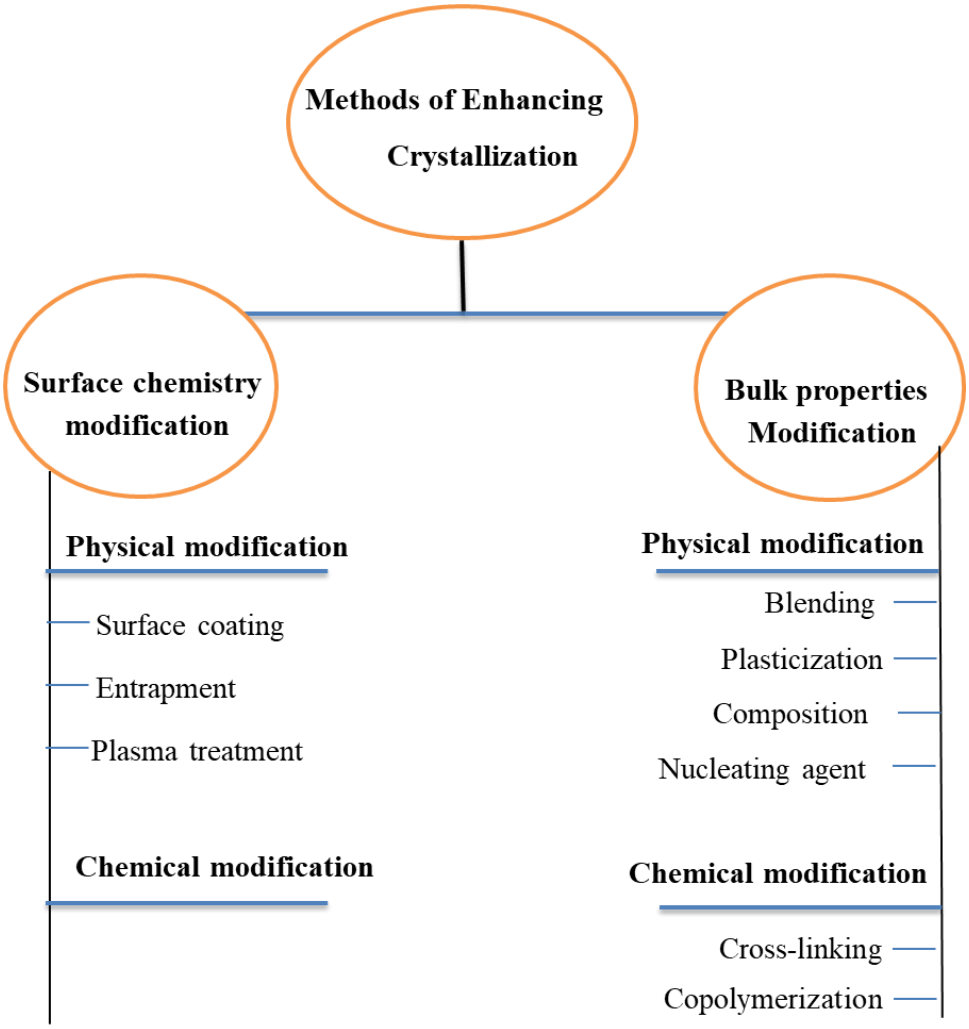

Figure 2-2: Methods of enhancing crystallization

1) Melting mixing**:** PLA beads are first melted at high temperatures then the NAs are incorporated within it during melting. Melt blending is performed at different temperatures based on the materials' properties. During melt blending the higher molecular NAs are became flexible at high temperatures within the PLA matrix.

2) Solution mixing: it is a very simple method in which the biocompatibility of the solvent and the polymer give homogenous dispersion of fillers through agitation, after the NAs

and polymer are mixed, they are cast or processed with different mouldings. Then solvent will be evaporated slowly or at high temperatures (Jingru Sun et al., 2011).

3) In-situ polymerization: is also used for the dispersion of NAs within the PLA matrix, this process works through side by side formation of polymer from the monomers, at the instantaneous formation of polymers through the polymerization process, the NAs are dispersed then the composite is formed, on this method heat used as an initiator.

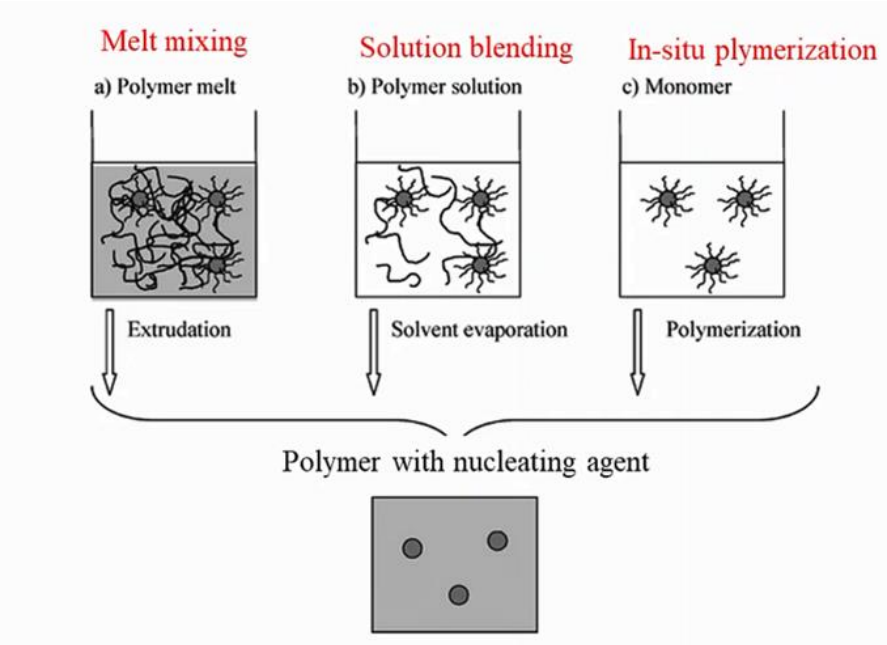

Figure 2-3: Nucleation mechanisms (Source:(Althues et al., 2007))

Based on the above studies on the nucleation mechanisms as well as crystallinity improvement by NAs, different nucleating agents have been used to enhance the slow crystallization behaviour of PLA as well as to improve its crystallization time.

2.2.2 Nucleating agents and crystallization enhancement of PLA

Among the previously mentioned improving strategies for crystallization of PLA, the expansion of NAs modification has the attributes of less expansion, huge impact and usefulness, later and at present viable (K. Li et al., 2021). The NAs have a beneficial outcome on crystallinity and mechanical properties, which increase with the nucleant concentration (Aliotta et al., 2017; L. Yang et al., 2019). Indeed, even in industrial production, the crystallinity control of infusion-shaped PLA can be accomplished by adding NAs during expulsion which is biocompatible NAs (Lim et al., 2008).

Different NAs have been reported to be effective in increasing crystallinity content in PLA such as talc, calcium carbonate, and boron nitrate (Jin et al., 2019; L. Yang et al., 2019) (Aliotta et al., 2017). The addition of a NAs is an effective means to control the crystallization process which enables improvements in PLA by providing a low energy barrier for nucleation and permitting crystallization at higher crystallization temperatures (T_C) (H. Bai et al., 2014; L. Yang et al., 2019). The NAs could push down the nucleation energy boundary and initiate crystallization at higher temperatures after cooling (Urayama et al., 2003). There are different NAs based on different criteria. Based on their properties they are classified as degradable and non-degradable NAs, as well as based on methods of production they are classified as, bio-based and synthetic NAs. Based on their origin they are classified as inorganic NAs and organic NAs.

Of synthetic NAs, GLY-LAC is one of them, which is an organic and biodegradable NAs and also it is prepared through green method.

2.2.3 Comparison of different nucleating agents

Based on the improvement on crystallization time and crystallization performance of PLA different NAs are compared. Below some are listed.

(Jinhao Sun et al., 2019) studied the effects of POCFA derivative on flame retardancy and crystallization behaviours of PLA. POCFA was synthesized using furfuryl amine (FA) and phosphorus oxychloride (POC). The $t_{1/2}$ of PLA is 6.41 minutes and with crystallinity (X_C) of 38.9%, which means PLA needs a relatively long time to complete this much crystallization. When POCFA is added to PLA, the half-life ($t_{1/2}$) decreases rapidly with its content increasing. The $t_{1/2}$ of PLA5 (95% PLA with 5% POCFA) is decreased to 1.27 min while the X_C is increased to 50.0%, suggesting the crystallization rate and crystallinity are both improved (Jinhao Sun et al., 2019). In table 2-1, there are different NAs with their impacts on the degree of crystallinity.

Table 2.1: Comparison of different nucleating agents

Nucleating agent	T_m(℃)	**Crystallinity (%)**	**Half-life (min)**	**Reference**
Neat PLA/PB	169	9		(Ding et al., 2021)
5% diatomite	105.47	5		(Ding et al., 2021)
5% talc	105	60.8		(Ding et al., 2021)
Neat /PLA0	105	38.9	6.41	(Jinhao Sun et al., 2019)
5% POCFA	105	50.0	1.27	(Jinhao Sun et al., 2019)
Neat PLA	103	broad crystallization peak	146.9 min	(H. Bai et al., 2014)
0.2% TMC-306	132	much sharper	0.5 wt% TMC-306- 8.8 min	(H. Bai et al., 2014)
Neat PLLA	110		35.2	(Wei et al., 2019)
PLLA/Zn(L-Ala)$_2$	108	51		(Wei et al., 2019)
PLLA/Zn(D-Ala)$_2$	109	49		(Wei et al., 2019)
PLLA/Zn(DL- Ala)2	107	50		(Wei et al., 2019)
PLLA/Zn(L-Pro)$_2$	108	50		(Wei et al., 2019)
PLLA/Zn(D-Pro)$_2$	105	51		(Wei et al., 2019)

PLLA/Zn(DL-Pro)$_2$	98	45		(Wei et al., 2019)
PLLA/Zn(L-Phe)$_2$	100	48	22.2	(Wei et al., 2019)
PLLA/Zn(D-Phe)$_2$	94.5	56	1.8	(Wei et al., 2019)
PLLA/Zn(DL-Phe)$_2$	102	51	15.8	(Wei et al., 2019)
Neat PLA	113	10.5%		(Sheikh et al., 2021)
Ag nanoparticles	104	7.9%		(Sheikh et al., 2021)
PCNAg5 Ag (wt %) =5, 94 (wt%) PLA, CNF (wt.%) =1				

Recently, synthesizes of glycerol-based macromolecules are extensively studied targeting different applications to expand the application areas of waste glycerol. Nowadays one of the targets is the development of degradable nucleating agents for polymers, such as GLY-LAC, which is produced from waste glycerol, GLY-LAC is an organic and bio-degradable nucleating agent.

2.2.4 GLY-LAC bio-conjugate as a nucleating agent

Different NAs have been reported to be effective in increasing crystallinity content in PLA such as talc, calcium carbonate, and boron nitrate. The addition of a NAs is an effective means to control the crystallization process which enables improvements in PLA by providing a low energy barrier for nucleation and permitting crystallization at higher crystallization temperatures (T_C) (H. Bai et al., 2014; L. Yang et al., 2019). Three-armed GLY-LAC is a type of evolved branching polymer with a hyperbranched core and liner arms. Here focus would give to using of glycerol and lactic acid-based NAs. Conversion of glycerol to other products is used widely; however green way of synthesizing glycerol-based macromolecules with branched structure can have the possibility to be used as a bio-based macromolecule targeting different engineering and medical applications.

Additionally, it can also be applied as a plasticizer to enhance the flexibility of different polymer matrices. In recent years, the development of fully bio-based materials has been the core research direction. Among these materials, the development of fully biodegradable and compatible structurally controlled viscoelastic materials is a need in the development of base matrix for skincare products as well as for polymer additives. We focus on using three armed GLY-LAC as a NAs for PLA crystallizer through the development of glycerol as a base matrix using lactic acid as a growing chain.

The reaction between glycerol and lactic acid is between the three OH groups of glycerol to react with 3-molecules of Lactic acid via a condensation reaction. In this case, there is the possibility of ester bond formation. This bond is formed by either the reaction between the hydroxyl group of glycerol and a carboxyl group of lactic acid or by the reaction between the hydroxyl groups of one lactic acid monomer. The other properties of PLA which rely on the degree of crystallinity will be discussed in detail below. The more the crystallized polymer matrix is the more the chance of improvement in the conductive network formation between the polymer matrixes due to order arrangement.

2.3 Conductivity Properties of Poly Lactic Acid (PLA)

In the early stages polymers are considered insulators (Akande et al., 2021; A. K. Mishra, 2018; Park et al., 2010; Sury et al., 2021), but because of their advanced properties inclusive of a wide range of controllable conductivity, low price relative to metals, smooth synthesizing techniques, huge industrial viability and optical properties transforming those polymers into thermally and electrically conductive polymers can open up opportunities for advanced thermal and current managements (Inzelt, 2012; Taghizadeh et al., 2020), (Anis et al., 2020; Mekonnen et al., 2016).

The era of CPs started in 1962 by John Pople and S.H. Walmsley (Grancarić et al., 2018; Rasmussen, 2018), and Shirakawa prepared the first polymer capable of conducting electricity which is polyacetylene (Akande et al., 2021; A. K. Mishra, 2018). Conductivity is a measure of thermal and electric conduction within the materials, which indicates the capacity to pass heat and current (Diantoro et al., 2016; Lakatos, 2018; Qu et al., 2019). When metal conductors (He et al., 2020; Ye et al., 2020) and conductive polymers are compared, CPs composites have the advantages of low density, ease of shaping, and an enormous range of thermal and electrical conductivities with corrosion resistance (Anis et al., 2020; J. Chen et al., 2019; Yaqun Wang et al., 2019). CPs are expected to control the

generation of heat in electronic devices as heat dissipating material which prevents devices from failure or used to increase the lifetime of the materials (Fallahi et al., 2017; Lule et al., 2019; Shen, Wu, Liu, Wang, & Zhang, 2020; Shen, Wu, Liu, Wang, & Huang, 2020).

CPs give us the potential of having both metals properties (highest thermal & electrical conductivity) and conventional polymers properties (flexibility, ease of process, stretch ability) (Halvaee et al., 2017; A. Li et al., 2017). Due to the requirement for flexible, stretchable, lightweight, thermally and electrically conductive devices brought about the generation of smart substances referred to as conductive polymers (CPs) (S. Kumar et al., 2021; Lee et al., 2019; Nezakati et al., 2018), Besides to those interesting advantages most of the polymers have drawbacks (Carbone et al., 2015), such as most of the polymers are produced from petroleum-based materials which makes them non-biodegradable (Tarani et al., 2019; Tarani et al., 2021) and environmental problems as consumption rate of synthetic polymers increasing, therefore to solve those problems using biodegradable polymers are used as one alternative way (Demirci et al., 2020; Tarani et al., 2021).

Nowadays electronic wastes are the most abundant wastes in the world (Ambaye et al., 2020; Dev et al., 2020; S. Mishra et al., 2021). There is a need to replace them as much as possible with green, renewable, biocompatible and biodegradable materials (El-Taweel et al., 2020; Y. Li et al., 2018; W. Wu et al., 2017). Electronic wastes are generated due to the usage of petroleum-based products for computers and other electronic parts. Additional costs are also required for the removal of those non-degradable electronic parts (Arroyo et al., 2018; Terzopoulou et al., 2019). PLA can be used as thermally conductive but electrically insulating or electrically conductive but thermally insulating or can be used as both conductive, based on the end application its properties also changed.

2.3.1 Thermal and electrical conductivity of PLA

As shown in figure 2-4, to conduct thermal as well as electrical conductivity within a polymer arranged conductive networks are required, and to create such network conductive fillers are also required. Polymer-based thermally conductive materials are therefore often desired in many applications, to control overheating of electronic materials required to dissipate heat within the materials which was created by temperature difference that comes through movement or vibration of particles.

In order to increase the service life and operating temperature of PLA based electronic and communication products, the removal of heat which was generated during device usage

time is very important (Shen, Wu, Liu, Wang, & Zhang, 2020), (Anis et al., 2020), (A. Li et al., 2017). For this purpose, the improvements of the thermal conductivity of PLA is one of the solutions, due to the quick elimination of heat from the system (Jiang et al., 2020). There are two modes of heat transport within the PLA: 1) by charge carriers (electrons and holes) and 2) by phonons (thermal carriers/vibrations/phonon scattering) they are thermal carriers in polymers (Z. Chen et al., 2018; Y. Huang et al., 2020). Previously polymers are generally taken into consideration as thermal insulators (R. Kumar et al., 2015; A. Li et al., 2017), and their application are confined due to their low thermal conductivity, which is 0.1-0.2 W m^{-1} k^{-1} (H. Chen et al., 2016; Shen, Wu, Liu, Wang, & Zhang, 2020; B. Yang et al., 2019). Some conductive fillers are listed in table 2-2, with their enhancements on thermal conductivity (TC).

An electrically conductive polymer (10^{-8}-10^{3} S/cm) is a mixture of the polymer matrix which is the insulator and conductive fillers, such as graphite, carbon black (CB), metal and carbon nanotube. Polymers are highly required in different areas due to their versatility in applications such as 3D printing, packaging (Namsheer et al., 2021), LED (Evgin et al., 2016), pharmaceuticals, textiles, engineering, chemical industries, automotive composites, and bio medicals (Grancarić et al., 2018; Y. Huang et al., 2020). The formed conduction networks within the polymer matrix shown in figure 2-5, give the polymer to change its properties from insulating to a conductive polymer.

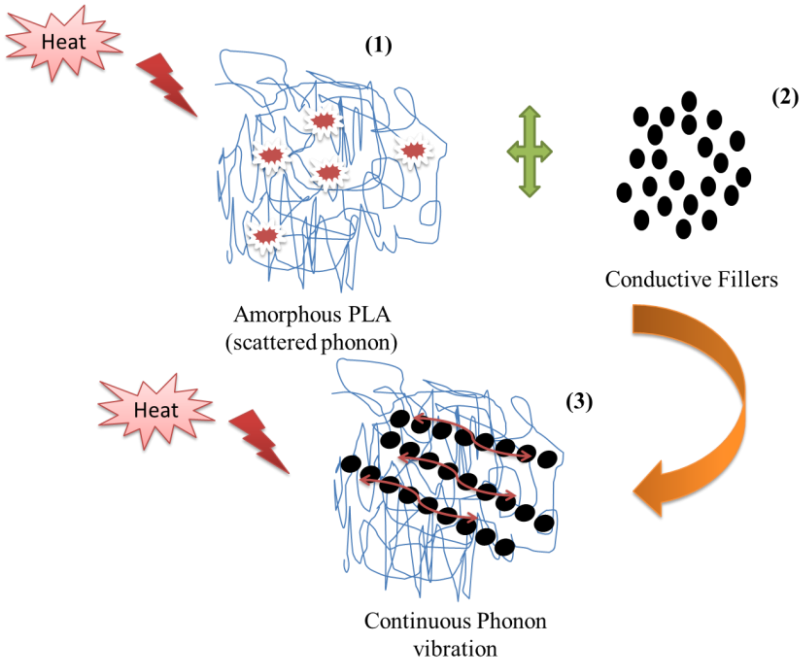

Figure 2-4: Thermal conduction mechanism in semi-crystalline PLA by phonon vibration

Table 2.2: Effects of different fillers on thermal conductivity of PLA

Polymer	Fillers	Loading volume fraction (wt. %)	Thermal conductivity (W/m k)	Reference
PLA	Graphene	1	2.4	(Jiang et al., 2020)
	Alumina	70		
PLA	Boron nitride	25	from 0.71 to 1.09	(Shen, Wu, Liu, Wang, & Huang, 2020)
PLA	Alumina	40	0.715	(Lule et al., 2019)
PLA and poly (butylene adipate-co-butylene terephthalate) (PBAT)	GNPs	40	3.15	(Yichen Guo et al., 2020)
PLA	GNPs	4.5	0.4692	(Ivanov et al., 2019)
	MWCNT	1.5		
PLA	GNPs	6	From 0.205 to 0.577	(Ivanov et al., 2019)
PLA	GNPs	12	0.664	(Spinelli, Lamberti, Tucci, Kotsilkova, et al., 2019)
PLA	MWCNTs	12	0.365	(Spinelli, Lamberti, Tucci,

				Kotsilkova, et al., 2019)
PLA	Combination of both GNPs + MWCNTs (1:1)	12	0.533	(Spinelli, Lamberti, Tucci, Kotsilkova, et al., 2019)
PLA	Tannic acid (TA)-functionalized nano-graphite	12.5	0.47	(R. Guo et al., 2019)
PLA	Graphite	30	0.193 to 2.73	(Lebedev et al., 2017)
PLA	Graphite	40		(Lebedev et al., 2017)
	CNT	1	3.8	
PLA/PA	Boron nitride	50 phr	0.28-0.86	(Pai et al., 2020)

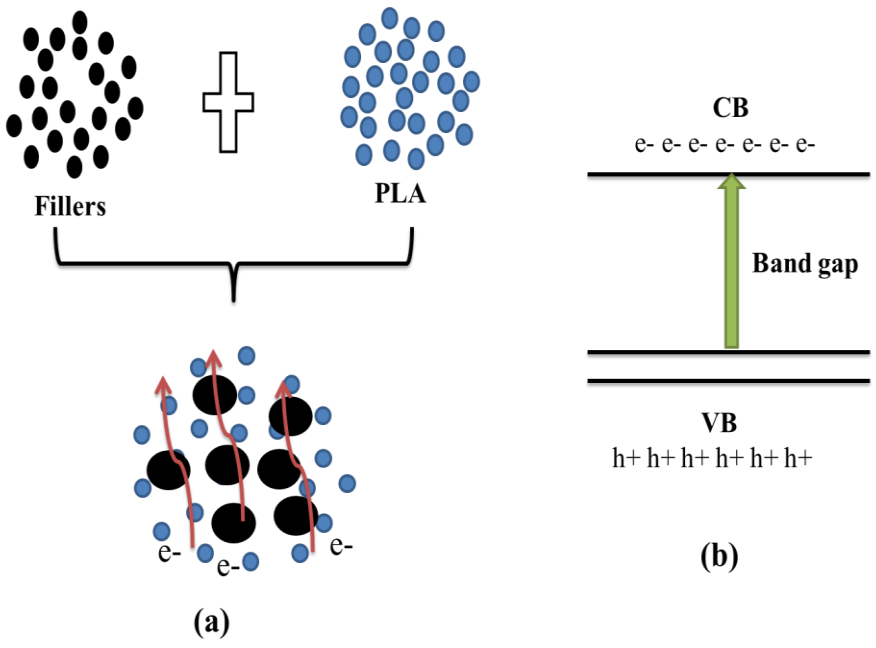

Figure 2-5: Electrical conduction mechanism in semi-crystalline PLA

2.3.2 Conductive fillers

Conductive fillers: are materials which can exist in form of powders, fibres and other forms, materials that are added to polymers for making them easier for electricity/heat, to pass through them or to make them conductive. Based on their composition properties those conductive fillers can be classified: a) Ceramic fillers have the capacity of thermally

Table 2.3: Effects of different fillers on Electrical conductivity of PLA

Polymer	Fillers	Loading volume fraction (Wt. %)	Electrical conductivity (S /m)	Reference
PLA	MWCNTs	12	4.54	(Spinelli, Lamberti, Tucci, Ivanova, et al., 2019)
	GNPs		6.27	
	MWCNT/GNP		0.95	
PLA and (PBAT)	GNPs	40	338	(Yichen Guo et al., 2020)
PLA	GNP	12	0.276	(Kotsilkova et al., 2019)
		20		
PLA	CNT	12	1.973	(Kotsilkova et al., 2019)
PLA	PAni	2.5	0.23	(Bertuoli et al., 2019)
PLA	PAni	10	0.99	(Bertuoli et al., 2019)
PLA	PEG-g-GN and GN	1	$9.69 * 10^{-4}$	(K. Huang et al., 2019)
PLA	Graphene (GR)	15	1.11 S/cm	(Horst et

				al., 2020)
PLA	CB	15	1.42 S/cm	(Horst et al., 2020)
PLA	CNTs	15	0.71 S/cm	(Horst et al., 2020)
PLA/PCL	CB	10	1	(Kim et al., 2020)
PLA	MWCNTs	5	0.4 S/cm	(Luo et al., 2018)
PLA	GNPs	4.5		
	MWCNT	1.5	0.00244	(Ivanov et al., 2019)
PLA	GNPs	6	8.4 × 10−3	(Ivanov et al., 2019)
PLA	MWCNTs	6	2.1 × 10−2	(Ivanov et al., 2019)
PP/PLA blend	MWCNTs	2	From $10^{-}10$ to 10^{-1}	(Azizi et al., 2019)
PLA	CNT	1	44 mS/cm (DC)	(Ceregatti et al., 2017)
PLA	CNT	1	85 mS/cm (AC)	(Ceregatti et al., 2017)
PLA	GNPs	15	5.6	(Mármol et al., 2021)
PLA	GNPs	12	6.27	(Spinelli, Lamberti, Tucci, Kotsilkova, et al., 2019)

as well as electrically conductive properties (Miranzo et al., 2017), and also they can be produced on a large scale, because their impacts on thermal conductivity is great, b) Carbon-based filters, all of the carbon-based fillers increase both thermal and electrical conductivity and mechanical properties of the polymers. They are less expensive regarding other fillers, carbon-based fillers includes carbon nanotube, carbon black and carbon fibre. c) Metallic based fillers, are fillers which based on metals such as aluminium, silver, copper, etc. They have the advantage of increasing both thermal and electrical conductivity of polymers, due to their higher conductivity properties and also they have multi-applications such as antibacterial and others.

There are three methods based on filler type dispersion and are most frequently used to obtain a dispersion of nanofillers into a PLA matrix to produce a filament solution mixing, melt blending and in-situ polymerization. In addition to filler type, other dispersions methods are called intrinsic and extrinsic methods (Yongqiang Guo et al., 2020). In intrinsic method backbone of polymers made up of extensive conjugated system, which is responsible for conductance methods and conductive charged transfer agent are mixed with insulating polymers. In extrinsic methods conventional polymer are mixed with a conducting polymer either physically or chemically and also externally added ingredients makes the polymers conductive. Polymers in which their insulating properties are improved can be used in different areas such as the electronic industry and others areas.

2.3.3 Applications areas of conductive polymers

In most electronic devices very biocompatibility, flexible, small and highly conductive materials are required; polymers are very interesting in such areas due to their flexibility, lightweight, low-cost outstanding corrosion resistance, and smooth processing polymers, which are broadly utilized in all elements of our everyday lifestyles and industry. The details of different application areas of CP are shown in figure 2-6.

2.4 Nanoparticles/Nanotechnology

Nanotechnology refers to technology at the nano-scale level in which materials, devices, or systems are developed via controlling matter at the nano-scale length to stimulate the unique properties of the material at the nano-level. In our daily life, those nano-scale materials become very important as emerging fields due to their great impacts with a small amount of loading.

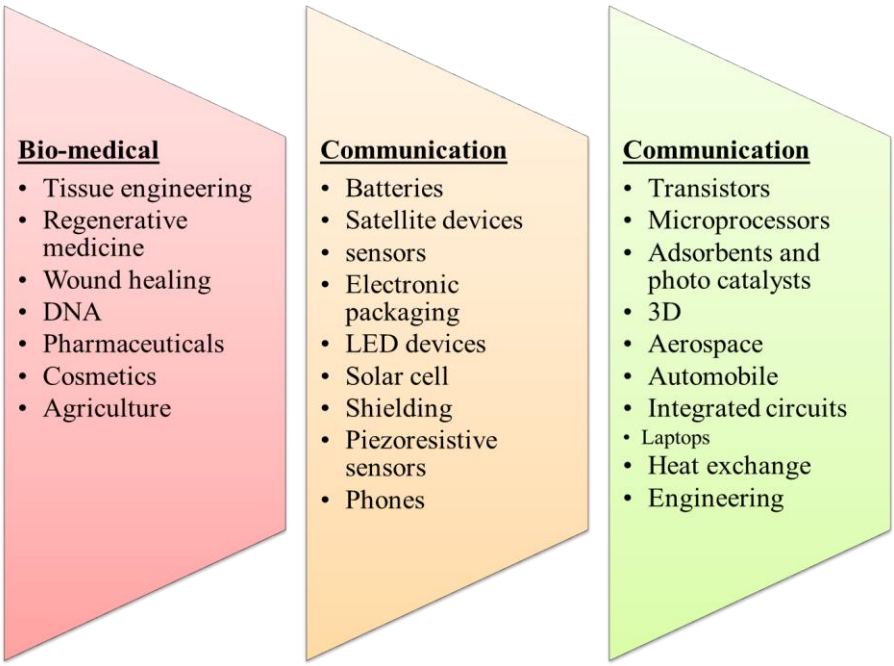

Figure 2-6: Application areas of both thermal and electrical conductive polymers.

To consider any materials like nano, size, morphology and other size-dependent properties are needs to be considered, the one and best properties that need to be fulfilled is their size (<100 nm), because this is why those nanoscale materials have great effects, in nano-scale, they have large surface areas, then high surface-area-to-volume ratio enhances the surface properties (E. Abbasi et al., 2016; Qiao et al., 2021). In 1957 Michael faraday was the first person to describe nanoparticles (Amechi, 2018).

Nano-materials differ in size, shape, and stability which gives them often unique and considerably changed physical, chemical and biological properties compared to their micron scaled particles (Baig et al., 2021). Large amounts of AgNPs can be produced using silver nitrate and different reducing agents. This technology is an emerging field of the present-day and they get great attention from researchers due to its many application, currently used in various areas, such as life sciences, analytical chemistry, genetic engineering, food and environmental industry, medicine, disease diagnosis and clinic treatment (Pan et al., 2021; Speranza, 2021). Nanoparticles can be used in different areas based on their conductivity range and type, whether they are electrically or thermally conductive or both conductors.

2.4.1 Application areas

Based on their large surface area to volume ratios nanoparticles are can be used in different areas such as medical applications**:** in the medicinal application point of view nanoparticle (NPs) interests are increasing among many researchers because of their ability to deliver drugs in the required dosage amount. From many of application areas such as Antimicrobial activity, anticancer activity, Anti-inflammatory activity, Antiviral activity, Antioxidant activity, Anti-diabetic activity, Anti-plasmodial activity, Anti-diabetic activity, are some of them (Aghebati-Maleki et al., 2020; Dulińska-Litewka et al., 2019; Nakamura et al., 2019; Singh et al., 2018). Gold (Au) NPs efficiently convert the strongly absorbed light into localized heat which can be exploited for the selective laser photo thermal therapy of cancer (I. Khan et al., 2019)**.** For applications in manufacturing and materials; nanocrystalline materials provide very interesting substances for material science since their properties deviate from respective bulk materials in a size-dependent manner (Qiu et al., 2020).

Applications in the environment: the contamination of water bodies had a great impact on human as well as aquatic life, therefore treating or removing heavy metals such as mercury, lead, thallium, cadmium and arsenic by using nanoparticles is one solution (J. Yang et al., 2019). One nanoparticle which is highly applicable to super-paramagnetic iron oxide nanoparticles is an effective sorbent material for this toxic soft material (Bhateria et al., 2019). Photo degradation is also another technique to treat those pollutants (I. Khan et al., 2019). Applications in electronics: due to their flexibility, low cost, large area and heat dissipation capability using nanoparticles in electronics for different purposes such as sensors (J. Li et al., 2021) (Anis et al., 2020), is very useful. Applications in mechanical industries: to make the materials strong a coating of nanoparticles will make them mechanically stronger nano devices for various purposes (Brighenti et al., 2020; I. Khan et al., 2019).

2.4.2 Methods of nanoparticles synthesis

Generally, there are two ways of silver nanoparticle synthesis: The bottom-up approach (from the atomic level to nanoparticles) and the Top-down approach (from bulk materials to nanoparticles). Both methods finally give the best nanomaterial and also they are classified as physical, chemical and biological-based on their operation, reaction conditions and adopted protocols. Physical and chemical routes required high energy and

toxic chemicals that are expensive and difficult to scale up in large quantities (Yuliang Wang et al., 2004). As a result of these effects, biosynthesis of nanoparticles circumventing the aforementioned effects has been adopted recently to enhance the properties of the nanoparticles using micro-organisms, animals' chitin, and crude extract from the plant's leaves. This method of synthesis is free of toxicity, biocompatible, cost-effective, and eco-friendly (Arif et al., 2021). Methods of nano particles synthesise are broadly classified into two: bottom-up approach and top-down approach. The methods are summarized in figure 2.7.

2.4.2.1 Bottom-up approach

This approach is employed in reverse as NPs are formed from relatively simpler substances; therefore this approach is also called the building up approach. Examples of this case are sedimentation and reduction techniques. It includes sol-gel, green synthesis, spinning, and biochemical synthesis.

Chemical Methods; it is the most commonly known nanoparticle synthesis method; being a low cost and high yield approach. This method involves chemical reduction by using different reducing agents like Sodium citrate, Ascorbate, Sodium borohydride (NaBH4), tollens reagent elemental hydrogen. Amines, alcohols and acids are used as a surfactant to avoid particle growth and agglomeration. Toxicity, being expensive, poor reducing ability and impurity are some of the limitations of this method (Jamkhande et al., 2019). The sol-gel method is an effective method for the production of high-quality metal and metal oxide nanoparticles. This process involves the conversion of monomers into colloidal solution (sol). The solution acts as a precursor. Highly pure and transparent antimony doped tin oxide (ATO) aerogel nanoparticles were successfully synthesized using the sol-gel method because it has good mechanical hardness and environmental stability (Qiao et al., 2021).

Biological Methods The synthesis of metal nanoparticles may be done in a variety of ways. Physical approaches have several disadvantages, including a greater energy need. Although the chemical technique approach overcomes these disadvantages, it is ecologically dangerous owing to the usage of chemicals (hydrazine). Chemical methods include drawbacks such as toxicity, instability, and low biocompatibility (Gahlawat et al., 2019). For nanomaterial manufacture, green synthesis refers to the use of biogenic materials such as plant extracts, biopolymers, and microbial sources such as bacteria, fungus, algae, and yeast.

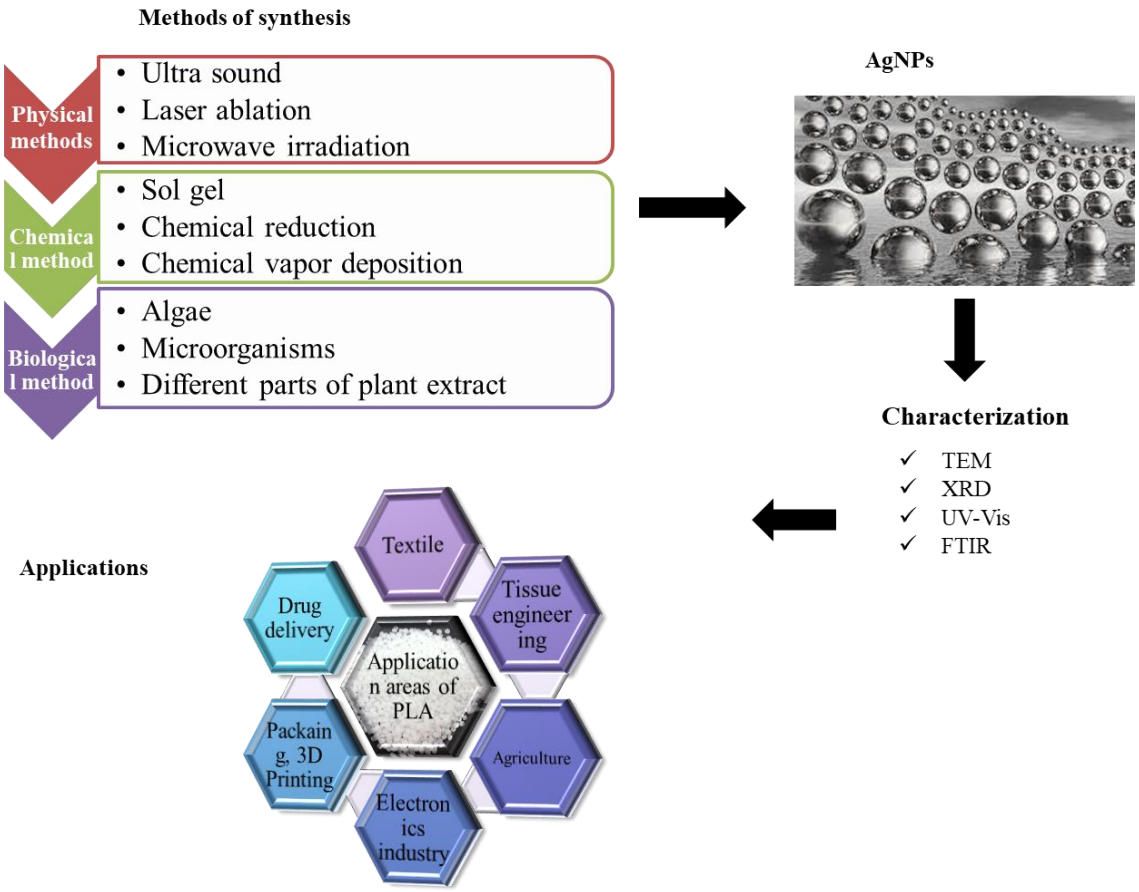

Figure 2-7: Silver nanoparticles from synthesis to end applications

The development of biocompatible, non-toxic and eco-friendly methods for the synthesis of nanoparticles is a topic of concern in biological methods (Salem et al., 2021). Generally, the synthesis of nanoparticles involves three stages, reduction of metal ions, formation of clusters and growth of nanoparticles.

Biosynthesis involves the use of green technology such as crude extracts from leaves of plants that are rich in metabolites such as flavonoid, alkaloid, tannin, saponin and phenolic acid that are responsible mainly for the reduction process of metal ions into bulk metallic nanoparticles formulation in the redox reaction to obtain nano-sized particle that is not toxic by converting Ag^{+} to Ag^{0} (Aisida et al., 2019). The use of different plants as shown in figure 2.8, for synthesising nanoparticles are rapid, low cost, eco-friendly, and a single-step method for the biosynthesis process.

In this method presence of biomolecules which act as capping and reducing agents and are advantageous over other methods by increasing the rate of reduction and stabilization of nanoparticles. Among many metallic nanoparticles used in biomedical applications, AgNPs are one of the most important and intriguing. Physical and chemical properties of

AgNPs which include optical, electrical, and thermal capabilities, as well as strong antimicrobial activities have been utilized for a variety of applications, such as sensory application, cell imaging, textile, cosmetics, dye degradation, food packaging application, antioxidant and antimicrobial agents. AgNPs role as a disinfectant and antimicrobial agent has been given considerable application (Moradi et al., 2021).

Figure 2-8: Different plants used for the synthesis of nanoparticles **(**Source: (Malik et al., 2014)

2.4.2.2 Top-down approach

In this method, a destructive approach is employed. Starting from a larger molecule, which decomposed into smaller units and then these units are converted into suitable nanoparticles.

Physical Methods In physical methods, metal nanoparticles like Gold, platinum, silver, titanium, zinc, cerium, iron, thallium and their compounds are synthesized by evaporation, grinding system, ultra sonication, mechanical milling and laser ablation present as an attractive method for preparing nanoparticles. In the mechanical method ball milling system bulk powder is crushed into particle-sized by using high energy vibrating ball mill. This method does not require several reaction steps and is applicable for the large scale production of nanoparticles but requires high energy for a long period of milling (A. M. R. Abbasi et al., 2013). (Rafique et al., 2019) reported synthesis of nanoparticles using continuous wave (CW) laser has been utilised to AgNPs in the de-ionized water by comparing with a pulsed laser. A pulsed laser and continuous-wave diode-pumped solid-state laser were used for the synthesis of AgNPs in deionized water. Then the colour

change was indicated formation of AgNPs. Microwave assisted organic synthesis employed in the synthesis of nanoparticles due to enhanced reaction rates, higher yields.

2.4.3 Types of nanoparticles

Organic Nanoparticles: Lipid nanoparticles (prepared from warm oil-in-water and triglycerides/fatty acids), Nanometric protein aggregates (prepared from whey protein water-in-limonene) (Margulis-Goshen et al., 2012), and Dendrimers, micelles, liposomes and ferritin, also commonly know the organic nanoparticles or polymers which are biodegradable and non-toxic. Liposomes are spherical vesicles made of one or more phospholipid bilayers. They are used extensively as carriers for numerous molecules in the pharmaceutical and cosmetic industries, and in the encapsulation of insoluble or unstable compounds in pharmaceutical, food, and farming industries (Margulis-Goshen et al., 2012). Polymeric nanoparticles are obtained from synthetic polymers, such as polycaprolactone, polyacrylamide, and polyacrylate, or natural polymers like albumin, which improve the pharmacodynamics and pharmacokinetics properties of different drugs (Herizchi et al., 2016).

Inorganic Nanoparticles: inorganic nanomaterials can be synthesised with those approaches, top-down approaches and bottom-up approaches. In the top-down approach, particles have different size distributions and shapes, for example, etching and lithography. Metal and Metal oxide nanoparticles are well-known types of inorganic nanoparticles and are manufactured from metal salts to nano-metric sizes using destructive or constructive processes. Metal nanoparticles have recently attracted a lot of attention due to their unique properties like a large surface area to volume ratios, high stability, facile chemical modification, enhanced permeability, and easily synthesis (Giner-Casares et al., 2016). Nano-sized inorganic particles of either simple or complex nature, display unique, physical and chemical properties and represent an increasingly important material. They are applicable in several areas such as drag delivery sensor application, energy science, cosmetic products, and cell imaging application (Núñez et al., 2018), catalytic activity (Ko et al., 2016).

Silver nanoparticles: Using metallic nanoparticles for the properties enhancement is very effective due to their higher reactivity. Metallic fillers are prepared through technique biological and physical. From metallic nanoparticles such as silver, gold, zinc, iron, and nickel, platinum has been used for many applications over the years, through various

syntheses. Among these, silver nanoparticles could be synthesised in different ways, the familiar one from the chemical method is a sol-gel method, and from the biological method green synthesis is environmentally friendly and uses different plants as reducing agents of silver nitrate. From many of the synthesis methods, green synthesis is acceptable due to its no-toxic properties. The synthesised silver nanoparticles can be applied in different areas such as food, medical, antibacterial, health care as well as industrial purpose. Silver nanoparticles can be used as conductive filler in the making of conductive polymers (Garibo et al., 2020; Ghosh et al., 2010).

2.4.4 Vernonia amygaldiyan/Bitter leaf extract

The application of various parts of medicinal plants for the treatment of varieties of illnesses of man has been vital and common in many parts of the world for centuries. Ethiopia is one of the six facilities of biodiversity in the world. Traditional medicine performs a tremendous role in Ethiopia, in which the massive majority of Ethiopia's population uses locally grown plant species (Desalegn et al., 2021). After thorough bioassays and analysis, many medicinal plants have been validated in a scientific empirical framework. A large number of medicinal plant species were successfully applied to cure several diseases. *Vernonia amygdalina* Del., is one of the medicinal plants found in Ethiopia with a significant application in traditional medicine. The leaves of *Vernonia amygdalina* plant are served in soups for the people belonging to the diverse cultures of Africa. In the present work, we selected this plant, *Vernonia amygdalina* to investigate the influence of its biomolecules on the green synthesis of AgNPs and also to evaluate the cumulative effect of biomolecules and AgNPs against a few selected bacterial strains (Murthy et al., 2021).

Bitter leaf is a shrub of about 2-5 m high popularly found in the African continent. It has a green leave with a bitter taste. It is often referred to as a medicinal plant because of its therapeutic and prophylactic properties which are widely used for the prevention, treatment of disease, and symptom relief. Dry bitter leaves (DBL) have high turbidity, and low pH compared with the fresh BL. DBL is very rich in phytochemicals such as alkaloid, tannins, saponins, flavonoids, and a steroid which can function as metal-reducing as well as a capping agent on the metal nanoparticles in a single route. The bitter taste of the DBL is a result of anti-nutritional factors, such as alkaloid, saponins, and tannins (Aisida et al., 2019).

CHAPTER THREE

3. MATERIALS AND METHODS

3.1 Materials and Reagents

Reagents: For the preparation of GLY-LAC bio-conjugate, PLA based films, and for the purification of glyceryl lactate as well as the synthesis of silver nanoparticles, different reagents were used. All the chemicals, silver nitrate (99.5%, alpha chemika India), methanol (99.8% Fisher chemicals), ethyl acetate (99.5%, Loba chemie Pvt Ltd chemical manufacturer in Mumbai, India), chloroform (99.99%, Fisher chemicals the scientific UK), L-lactic acid (88% aqueous solution, analytical-reagent grade, Loba Chemie Pvt. Ltd chemical manufacturer in Mumbai, India), glycerol (99% Uttar Pradesh, India Rankem Liquid Laboratory chemicals), sodium hydroxide, distilled water, sodium chloride, potassium hydroxide, phenophtaline, hydrochloric acid, were analytical grade and they were purchased from the local markets except the film grade PLA beads. PLA beads were purchased from Aturker trade Istanbul Turkey and Vernonia amygdalina leaves were collected from Adama Science and Technology University premises, Ethiopia.

Materials: Some of the materials and equipment which was used were: 500-2000 ml RBF, measuring cylinder, horizontal condenser, temperature-controlled reactor/oven, simple distillation apparatus, vacuum pump, chillier, separatory funnel, hot plate with a magnetic stirrer, rod, Petri dishes, measuring balance, centrifuge, Erlenmeyer flask, Pipet, ITO (Indium Tin Oxide) glass, XRD, DSC, TGA, FTIR, NMR, UV-Vis, PSA (particle size analyser), QTM-500 (quick thermal conductivity meter), SP-300 Potentiostat, digital multi-meter (DL-2080) and probe station.

3.2 Methods

3.2.1 Synthesis of glyceryl lactate/ GLY-LAC

Esterification reaction: The esterification of glycerol (99 %) and Lactic acid (88 %) via a condensation reaction was performed in a temperature-controlled heating oven with four different molar contents of glycerol and lactic acid (1:3, 1:6, 1:9, 1:12). The two reactants were added into one neck round bottom flask (RBF), equipped with a horizontal condenser for water segregation. It was then placed in a temperature-controlled oven at a temperature of 190 ℃ and reaction time of 8 hr. The reaction condition was selected based on the preliminary investigation. In the esterification process, three-hydroxyl groups in glycerol

molecule required three moles of lactic acid, as shown below in figure 3.1. For the commercially available 99% pure glycerol, one mole which is equal to 74 ml of liquid glycerol. Whereas for the commercially available 88%, three moles of lactic acid is equal to 255 ml was used. Therefore, in the case of glyceryl lactate (GLY-LAC), 1:3 bio-conjugate syntheses of 74 ml of glycerol were reacted with 255 ml of lactic acid at a temperature of 190 ℃ for an 8 hr. For the rest of the GLY-LAC, the same methods were used, for GLY-LAC 1:6, 1:9 and 1:12, the only difference was a variation of lactic acid 510, 765, and 1020 ml which was used with a constant volume of glycerol. The water was produced as a by-product of the reaction between the hydroxyl group of glycerol and the molecules of lactic acid.

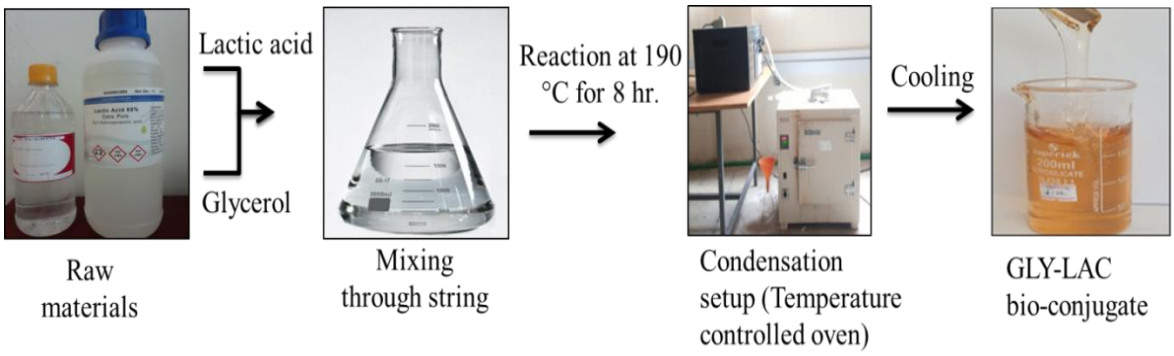

Figure 3-1: Synthesis of nucleating agent (GLY-LAC) bio-conjugate

3.2.2 Purification of synthesised GLY-LAC

The synthesised of GLY-LAC in this research is used as a nucleating agent. It was necessary to purify by-products formed due to side reactions and residual lactic acid as well as glycerol. This was performed using solubility in two different miscible liquid methods. From the purification process, only pure glyceryl lactate bio-conjugate was collected. During the purification, ethyl acetate was used as a solvent with a one to one (1:1) mixing ratio with crude glyceryl lactate within the beaker.

First glyceryl lactate was dissolved with saturated sodium chloride a one to two (1:2) to precipitate unwanted components, then the solution was poured into a separatory funnel and ethyl acetate was added to separate the residual glycerol and lactic acid from the solution. Due to the advantage of the insolubility of glycerol in ethyl acetate and the better solubility of lactic acid in water than in ethyl acetate, removal of residuals took place. After sufficient time (1 hr) was given for the solution, the unreacted lactic acid, glycerol and sodium chloride were precipitated at the bottom of the separatory funnel and it were removed (Yuan et al., 2016).

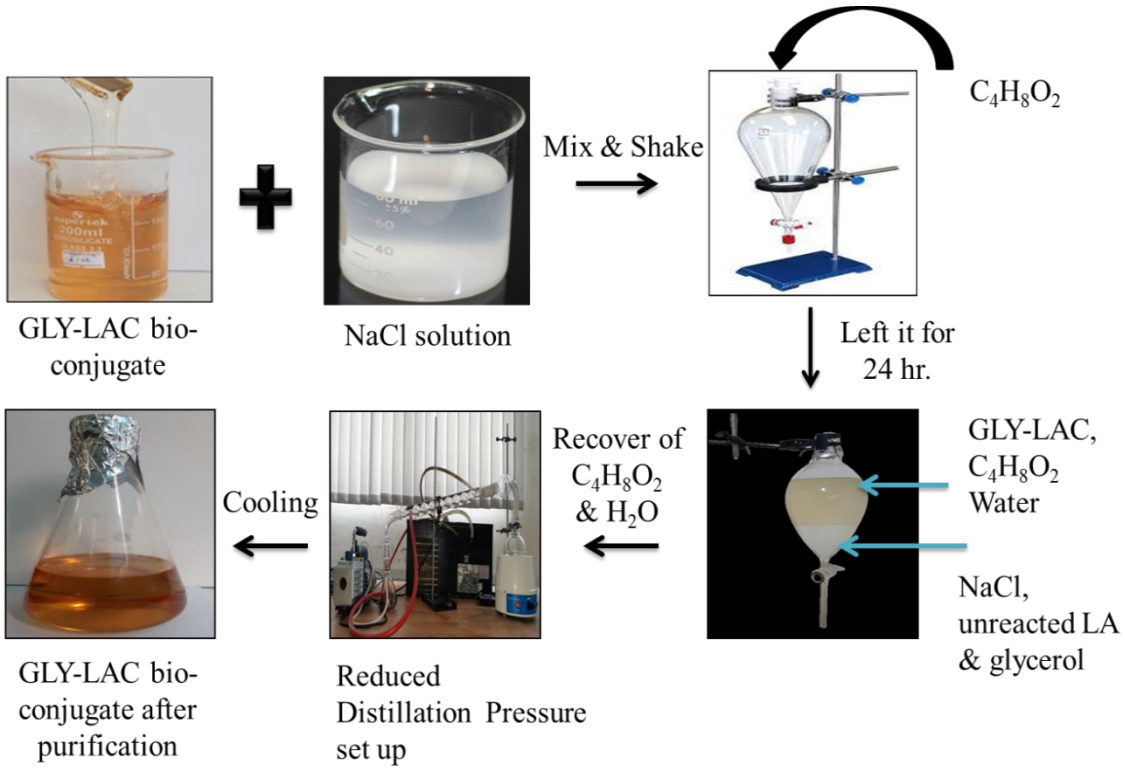

Figure 3-2: Purification of synthesised GLY-LAC bio-conjugate

This procedure was repeated three times to make sure that the removal of residuals is effective. The supernatant liquid of the upper layer, which contains ethyl acetate, water and the GLY-LAC, was collected and then vacuum distillation or reduced-pressure distillation was carried out to remove the ethyl acetate and water. Finally, the pure glyceryl lactate was obtained and the sample was ready for characterization, to check its purity using NMR and FTIR. The above mixing ratio was determined in a preliminary study. The overall procedure of purification of GLY-LAC bio-conjugate was illustrated in figure 3-2 (Yuan et al., 2016).

3.2.3 Extraction of plant Leaf extract

For the green synthesis of silver nanoparticles, plant leaves extract was synthesised as shown in figure 3-3, to use as a reducing agent, stabilizing and capping agent of AgNPs from silver nitrate. *V. amygdalina* or Girawa leaves were collected from Adama Science and Technology University compound, then washed and cleaned with tap water repeatedly to remove dust particles and then rinsed with distilled water. The leaves were dried in shade dry to remove moisture from the leaves for 15 days. The dried leaf samples were grounded by POLYMIX® PX-MFC 90D laboratory miller, which was equipped with a 0.2 mm mesh sieve. Finally, the prepared powder was packed and stored under dry conditions for further applications.

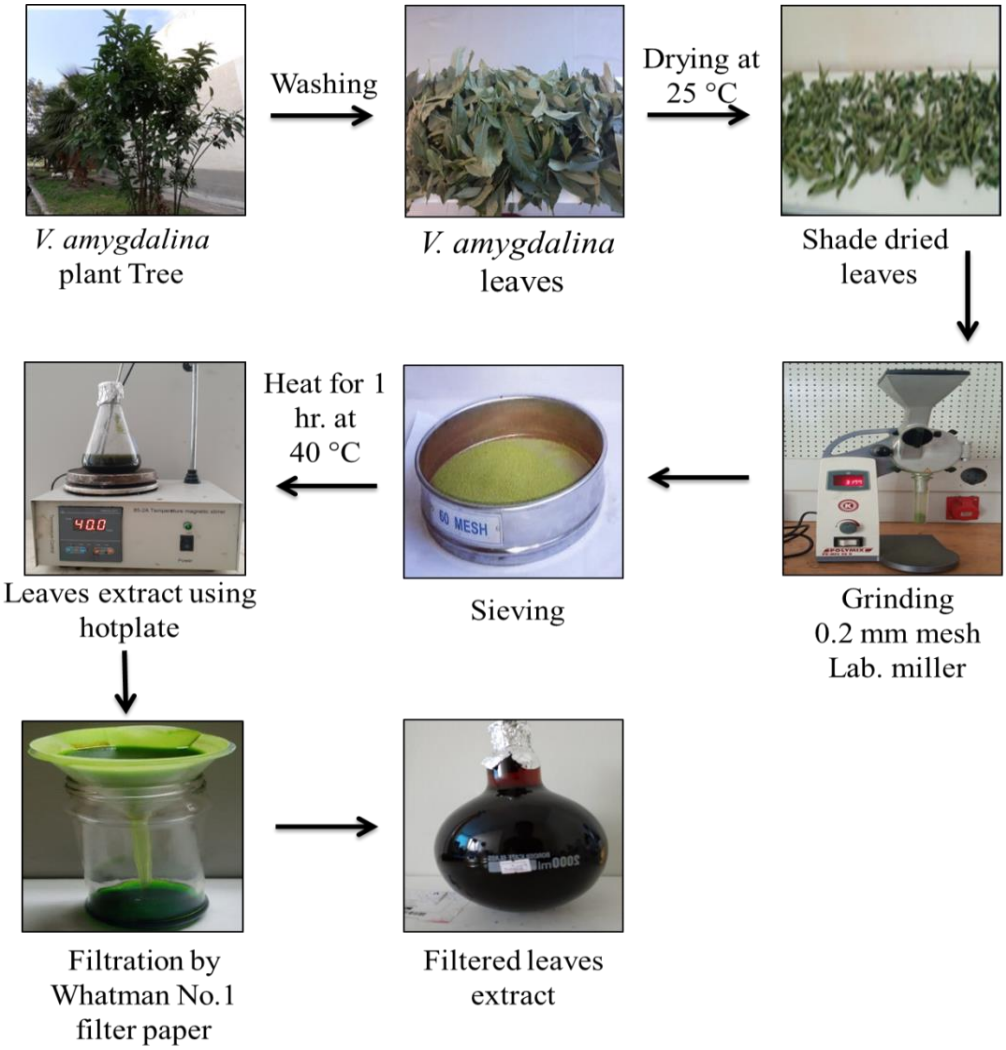

Figure 3-3: Extraction process of *V. amygdalina* plant leaves

Methanol and distilled water were used as a solvent for the extraction process of the crushed plant leaves, with a ratio of 40:60 ml respectively. The extraction was carried out using 2 g of plant leaves powder. The leaves powder was soaked within a conical flask of 100 ml solvent for 1 hr. Extraction time under controlled temperatures of 40 ℃, and then the leaves extract was cooled at room temperature and filtered by using Whatman filter paper. Then by repeating this procedure the plant leaf extract was collected and stored for the next experiment. The overall procedure of powder preparation from *V. amygdalina* leave and the detail of the extraction process are illustrated in figure 3-3. All the parameters were adapted from the previous research, the optimizations were done for all the parameters and solvent selection (Yodahe, 2021).

3.2.4 Green Synthesis of silver nanoparticles (AgNPs)

The reduction of silver nitrate into AgNPs was done using the green or biogenic method (Top-down approach), (L. Xu et al., 2021). For the synthesis of AgNPs, 20 ml of plant leaves extract was added into an Erlenmeyer flask containing 80 ml of 8 mM $AgNO_3$. Then the solution was heated to a temperature of 40 ℃ through continuous stirring with a magnetic stirrer for 30 minutes and the reaction was protected from sunlight to prevent $AgNO_3$ from photoactivation. NaOH was added in drops to the mixture to enhance the precipitation of AgNPs and to maintain the pH at 7.

After the completion of synthesis, the precipitated AgNPs were collected and poured into the petri-dish then put into oven at 40 ℃. When the solvent was evaporated after 12 h, again the other solution was poured into the petri-dish, and this was repeated 5 to 10 times to collect the powder in mass. The solution was purified through centrifugation (NF 200 Bench Top Centrifuge) at 5,000 rpm for 30 min, this process was repeated 2-3 times to ensure the removal of any adsorbed or unreacted substances from the solution through washing with distilled water, as shown in figure 3.4.

The nanoparticles precipitate out of the reaction medium and collected, then the precipitated AgNPs were dried by using an oven (NE9-56S model number) at the temperature of 45-60 ℃ to remove liquid (Jain et al., 2009; S. A. Khan et al., 2018; Oluwaniyi et al., 2016). All the parameters were adapted from the previous research, the optimization was done for all the parameters and solvent selection (Yodahe, 2021).

3.2.5 Dispersions of nanoparticles within purified GLY-LAC

To get uniform and stable dispersion of AgNPs within GLY-LAC for the preparation of biopolymer films (AgNPs/GLY-LAC). The first step was preparing of AgNPs solution, with different ratio (1wt%, 3wt%, 5wt%, 7wt%, and 10wt%). Powder AgNPs were dispersed and mixed with different solvents (10 ml of DW, chloroform, ethanol and methanol), then stirred with magnetic stirrer for 1 hr and then ultra-sonicated by using CASTELNUOVO D.BOSO (AT) ultra-sonicator, for 2 hr. Best-solubilizing solvent was selected through physical detection (which was DW).

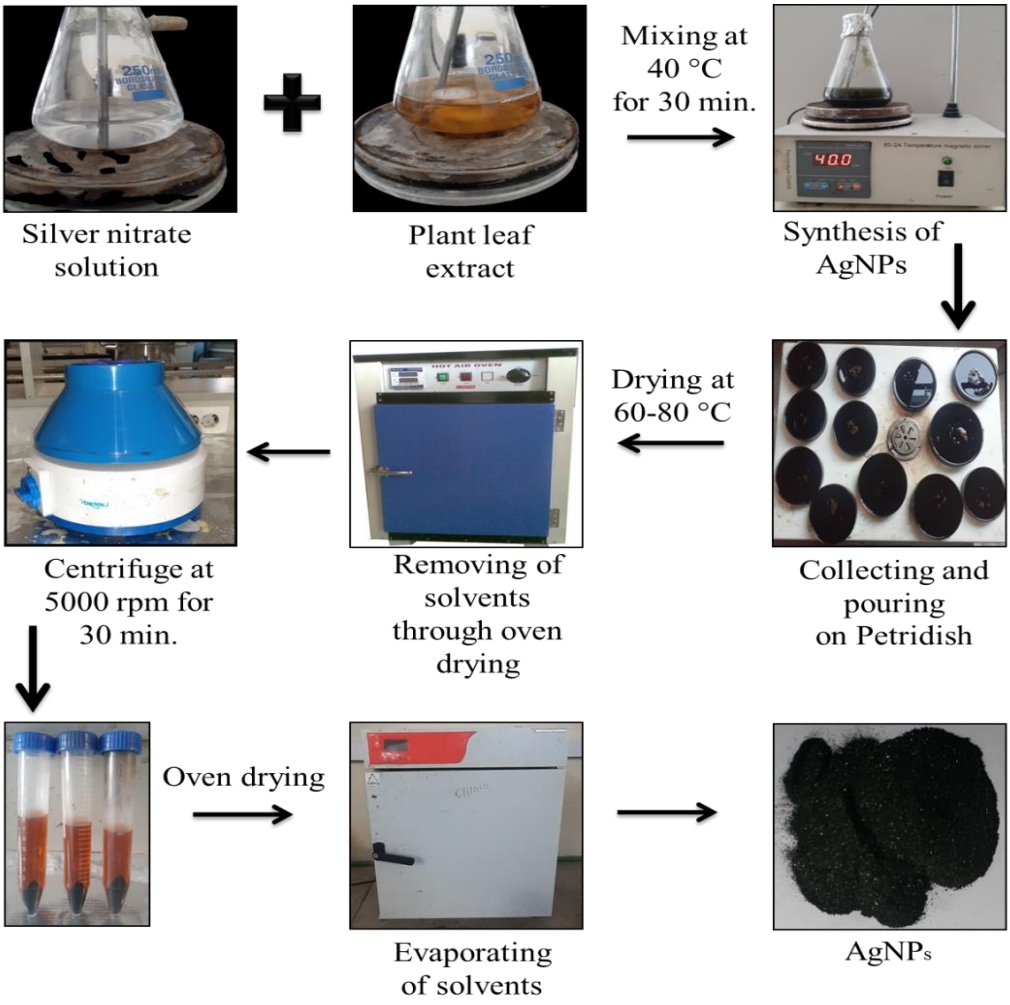

Figure 3-4: Synthesis of AgNPs by using *V. amygdalina* plant extract

Then 10wt% of PLA (base matrix) purified GLY-LAC 1:6 was added into AgNPs solution under the continuous stirring, and the solution was sonicated for 1 hr in 40 ℃. Then stable nanofluid was prepared. Each solution was dried for 36 hr. at 105 ℃ to remove the solvent. The prepared solution was washed with chloroform and dispersed into a PLA matrix to prepare biopolymer films through the solution casting method and stability and uniformity of dispersion were studied. This method of dispersing nanoparticles was based on a preliminary study through different mixing ratios. Effects of drying time on stability were also studied for 12 hr, 24 hr and 36 hr. The detailed process of dispersion of nanoparticles into GLY-LAC macromolecule was illustrated in figure 3-5.

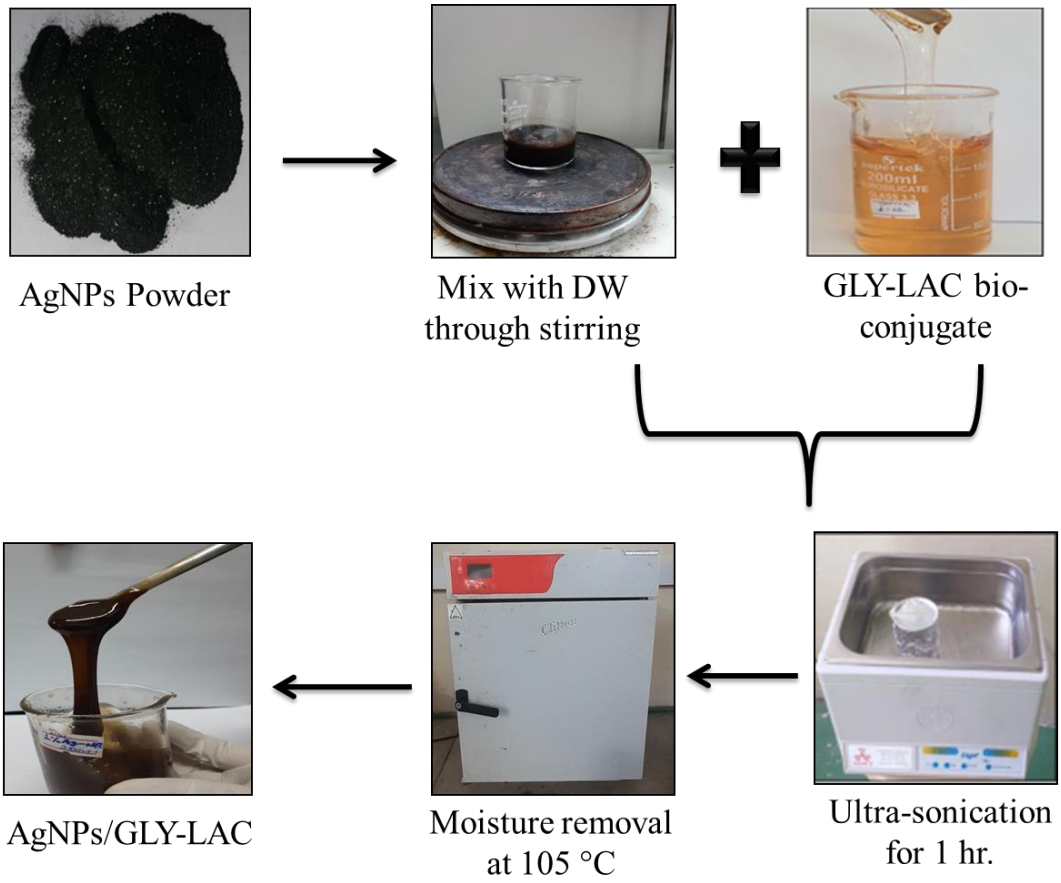

Figure 3-5: Homogenous dispersion of AgNPs within GLY-LAC bio-conjugate

3.2.6 Preparation of PLA based films

3.2.6.1 GLY-LAC/PLA based biopolymer film

Biopolymer films were prepared through the solution casting method, purified GLY-LAC (1:3, 1:6, 1:9 and 1:12) mixed with PLA solution. Based on the PLA mass, 1wt%, 3wt%, 5wt%, and 10wt% based films were prepared for the study of the effects of mixing ratios as well as the effects of GLY-LAC chain length on the degree of crystallinity of the PLA. In the first step, the prepared GLY-LAC was dispersed into the PLA matrix, by preparing PLA solution, PLA beads (3g) were pre-dissolved with chloroform (90ml) for at least 15 minutes using a magnetic stirrer at a rotational speed of 17 rpm.

As shown in figure 3-6, the dispersion of purified nucleating agent into PLA was done with different concentrations; first five films; neat PLA, GLY-LAC 1:3, GLY-LAC 1:6, GLY-LAC 1:9 and GLY-LAC 1:12 with same loading rate (10wt%) for each, were prepared through solution casting method. The other films were prepared with different GLY-LAC loading rates, the same loading and annealing temperature but at different

annealing times as well as the same loading and different annealing temperature were prepared. PLA solution and GLY-LAC were mixed and stirred for 3 hr. to get a well dispersed and mixed solution, and then the mixed solutions were cast on a petri-dish and dried under room temperature through slow evaporation for 24 hr. After the sample dried peel off slowly from the petri-dish and annealing was do for it. Annealing was done at 110 ℃ temperature to select the best nucleating agent from GLY-LAC 1:3, GLY-LAC 1:6, GLY-LAC 1:9 and GLY-LAC 1:12 nucleating agents based on their nucleation impact (degree of crystallinity) on PLA (Yuan et al., 2016).

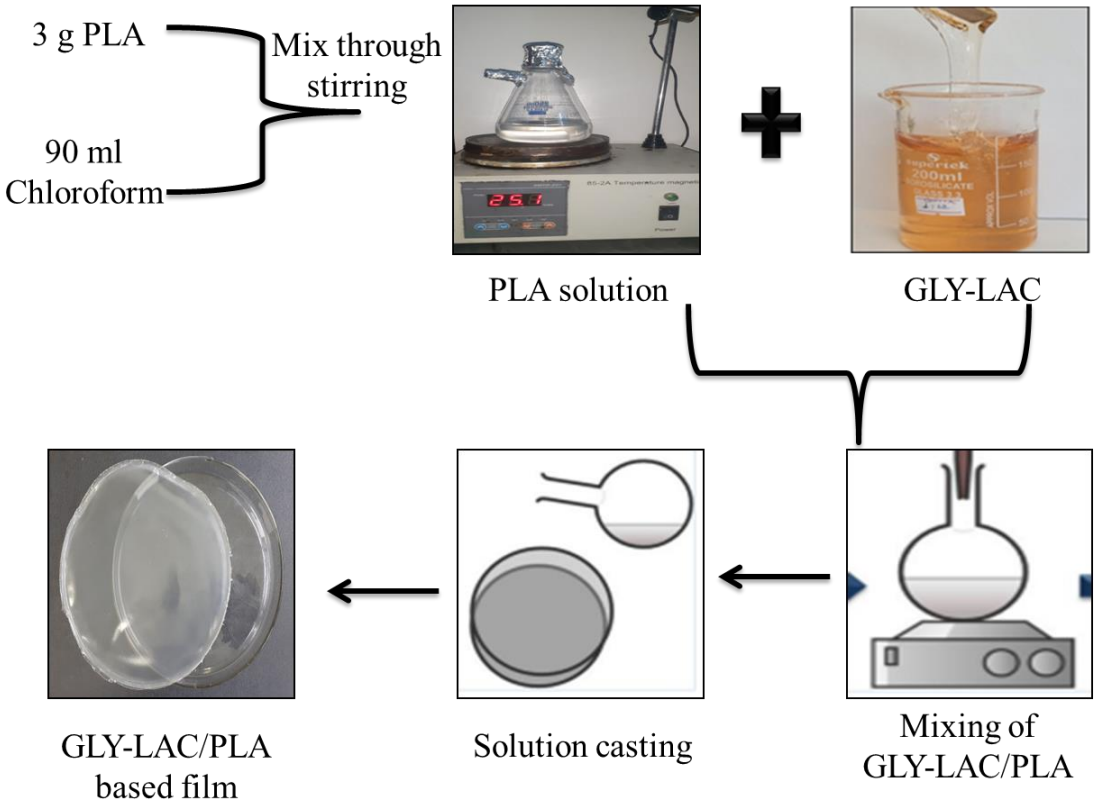

Figure 3-6: Preparation of GLY-LAC/PLA based biofilm

3.2.6.2 AgNPs/GLY-LAC/PLA based bio-polymer film

In the other film which was based on the presence of nanoparticles films, the preparation method was the same; here also solution casting method was applied. AgNPs/GLY-LAC/PLA films were prepared as discussed above in section 3.2.6.1, prepared AgNPs/GLY solution with different Ag concentrations (1wt%, 3wt%, 5wt%, 7wt%, and 10wt% of PLA AgNPs), and they were mixed with 3 g of PLA matrix as shown in figure 3-7.

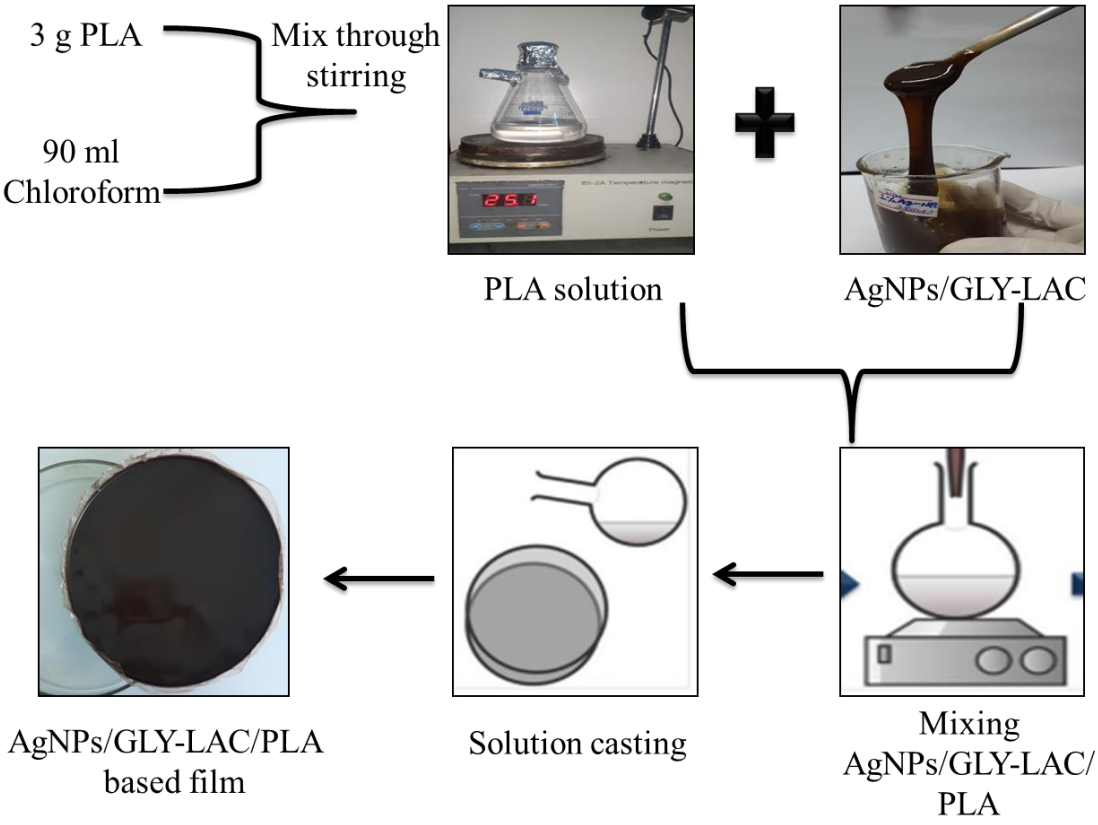

Figure 3-7: Preparation of AgNPs/GLY-LAC/PLA based biofilm

3.2.7 Annealing of PLA based films

To study the impact of annealing temperature, annealing time and loading rate on PLA crystallization, thermal and electrical conductivity based films, annealing was done for those prepared films. The same amount of base material (PLA) was used; then, the matrix with different loading rates of GLY-LAC 1:6 (0wt%, 1wt%, 3wt%, 5wt%, 7wt% and 10wt%), was mixed with PLA. Annealing was done at four different temperatures 90 ℃, 100 ℃, 110 ℃, and 120 ℃ for all NAs with different loading rates of the matrix and annealing time was 30, 90 and 150 minutes (J. Guo et al., 2021).

3.3 Characterization of synthesized and purified GLY-LAC

3.3.1 Acid value analysis:

This analysis was done for synthesised GLY-LAC before and after purification, to study the formation and to study effects of purification. The titration in this experiment was done according to the ASTM D974-12 method. In this case, l g of sample was measured and dissolved in 20 ml of chloroform. The solution was then titrated with 0.1 N KOH solutions in the presence of 10 droplets of phenolphthalein (indicator) solution. The acid value was calculated according to equation 3.1.

$$AV\left(\frac{mg}{g}\right) = \frac{(V - V_0) * NKOH * 56.1}{m} \ldots\ldots\ldots\ldots\ldots\ldots\ldots\ldots\ldots\ldots\ldots\ldots\ldots\ldots\ldots\ldots\ldots\ldots\ldots\ldots. (3.1)$$

Where; AV is the acid value (mg/g sample) of the conjugate, Vo is a volume of 0.1 N KOH solution used to titrate the blank solution, V is a volume of 0.1 N KOH solution used to titrate the sample, KOH – titre used for titration (0.1 N) and m is mass of the sample (1 g).

3.3.2 Viscosity Evaluation

The bio-conjugates viscosity was determined by VK 2000 viscometer type for both samples (before & after purification) based on the modified method of ASTM D562 and KREBS operating method (Akanksha et al., 2009). The sample to be tested was transferred to a clean and dry 250 ml beaker as shown in figure 3.8, and the viscosity of the sample was determined by using a spindle N° 5 at rotation speed of 25 rpm, near 100% torque.

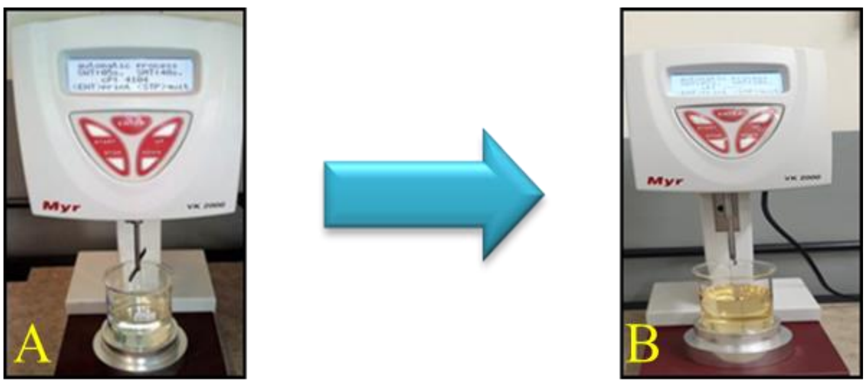

Figure 3-8: Viscosity measurement of the GLY-LAC bio-conjugate (A) before and (B) after purification

3.3.3 NMR Analysis

The idealized chemical structure and the expected LA chain length of the conjugates were investigated by ^{1}H NMR and ^{13}C-NMR characterizations with the incorporation of DEPT-135 analysis. The samples were dissolved in deuterated chloroform ($CDCl_3$), filtered with a 0.25 μm filter, and transferred to a 5 mm diameter NMR tube. For this case, the samples were completely dissolved in chloroform before the analysis. For ^{1}H NMR, chloroform (at 7.26 ppm) was used as the reference line.

3.3.4 FTIR Analysis

The existence of the expected functional groups and the expected interactions between the alcohol glycerol and the carboxylic acid in the synthesized and purified GLY-LAC were further confirmed by using FTIR, with model number FTIR-6600 type A FTIR spectroscopic machine with 2 mm/sec scanning speed and the spectrum was recorded from 400 cm^{-1} up to 4000 cm^{-1} range with 4 cm^{-1} resolution and 64 scan rates.

3.4 Characterization of *Vernonia amygdalina* (bitter leaf) plant leaf extract

3.4.1 Phytochemical screening of extract

Phytochemical screening for the extraction helps in the identification of bioactive compounds like phenolic, saponins, flavonoids, tannins, terpenoids, alkaloids, cardiac glycosides and anthraquione glycosides. Phytochemical screening tests of *V.amygdalina* leaf extract were carried out on the selected 40/60 (M/DW) plant extract. The phytochemical screening was done using the following standard procedures to identify the constituents (Gul et al., 2017; Usunomena et al., 2016).

Test for Phenolic Compounds: 1 ml of plant extract was transferred to the test tube and diluted to 2 ml of distilled water. To this, a few drops of neutral 10% ferric chloride solution were added. The dark green colour indicates the presence of phenolic compounds.

Test for Saponins: The test for the presence of saponins is known as the frothing test. About 5 ml of extract, a 5 ml of distilled water were added to the test tube and shaken while heating to boil. The appearance of foam-like, when frothing was mixed vigorously with a few drops of olive oil showed the presence of saponins.

Test for Flavonoids: The Phytochemical test for flavonoids was done by using alkaline reagent test. Here, 2 ml of 2.0% NaOH mixture was mixed with aqueous plant leaves extract. A concentrated yellow colour was produced, which became colourless when 2

drops of diluted acid was added to the mixture. This result showed the presence of flavonoids.

Test for Tannins: 1 ml of plant extract was transferred to the test tube by using a dropper. 2 mL of 5% ferric chloride was added. The formation of dark blue or greenish-black will be observed in the presence of tannins.

Test for Terpenoids: 5 ml of plant extract sample was transferred to a test tube and treated with 2ml of chloroform after and evaporated on the water bath then boiled with 3 ml of concentrated H_2SO_4. If a grey colour is formed, it shows the presence of terpenoids.

Test for alkaloids: 1 ml of the extract was stirred with 1% HCl on a water bath for 5min and filtered. This filtrate was divided into three equal parts. To one portion of filtrate, add 1 ml Mayer's reagent (the mercury (II) chloride solution was added by potassium iodide). The formation of an orange-coloured precipitate indicates the presence of alkaloids.

Test for glycosides: According to Salkowski's Test, 1 ml of plant extract sample was added to the test tube. Then added 2 ml concentrated H_2SO_4 to the whole aqueous plant extract. A formation of reddish-brown colour is an indication of the presence of steroidal aglycone part of the glycoside.

3.4.2 FT-IR analysis

The existence of the expected functional groups of pure GLY-LAC and the effect of incorporation of GLY-LAC on PLA's functional groups and their interactions were analysed using FTIR. The same condtions were used as in section 3.3.4. KBr pellets was used as a carrier.

3.4.3 Thermal degradation analysis of *Vernonia amygdalina* plant by TGA

The thermal degradation of bio-lubricant blends was investigated using TGA equipment (TGA-DTA (DTG-60H), Shimdazu, South Korea). A sample weighing ~8-10 mg was heated from 30 ℃ to 800 ℃ at the heating rate of 10 ℃/min under a nitrogen (N_2) atmosphere.

3.5 Characterization of the synthesised Nanoparticles

3.5.1 Ultraviolet-visible Spectroscopy

Synthesized Ag nanoparticles were analysed by using UV-Vis models Shimadzu UV–Vis spectrophotometer UV-1800. The UV-Vis absorbance and reflectance spectra of the samples were recorded in the range of 200-800 nm. The Ag nanoparticle solution was prepared by mixing the freshly prepared AgNPs with distilled water after appropriate dilution.

3.5.2 Particle size analyser (PSA)/Zetasizer Nano

The Zetasizer Nano series performs size measurements using a process called Dynamic Light Scattering (DLS). Zetasizer Nano instrument (Nano ZS (Red badge)) with the model number ZEN 3600 (Malvern Instrument Ltd. Worcestershire, UK) was used to measure particle size. The laser used in Malvern Zetasizers was a 4 mW He-Ne laser of 632.8 nm wavelength; the laser sources provide a stable beam of coherent monochromatic light. There is an attenuator available to alter the power of a laser. Sample concentration was within the range 0.1 mg/ml - 0.5 mg/ml as minimum concentration by considering density, clean, square and disposable sizing cuvette was used as sample holder.

3.5.3 X-RAY Diffraction

XRD instrument used for the analysis of crystallographic arrangement of AgNPs with model number XRD-700 X-RAY diffractometer, shimadzu Corporation (Japan) with a scanning rate of 3^{o}/min and from 10^{o} up to 80^{o}. XRD was a powerful technique that helps to identify the structure, phase purity, degree of crystallinity and unit cell parameters of a given sample. The XRD patterns were recorded by the measurements of the angles at which the X-ray beams were diffracted by the periodicity of the sample. The relation between the distance between two planes (d-spacing) and the angle of diffraction (2θ) was calculated using Bragg's equation (equation 3.2).

$$d = \frac{n\lambda}{2sin\theta} \dots\dots\dots\dots\dots\dots\dots\dots\dots\dots\dots\dots\dots\dots\dots\dots\dots\dots\dots\dots \text{(3.2)}$$

Where: d= Spacing, λ= wave length of incident X-ray (0.15406 nm), n= order of diffraction (1) and θ= diffraction angle.

The average crystalline or grain size of nanoparticle was calculated using scherrer equation (3.3)

$$D = \frac{K\lambda}{\beta cos\theta} \ldots \ldots \ldots \ldots \ldots \ldots \ldots \ldots \ldots \ldots \ldots \ldots \ldots \ldots \ldots \ldots \ldots \ldots \ldots \ldots \ldots \ldots \ldots \ldots \ldots \ldots \ldots \ldots \ldots . \ldots \ldots . (3.3)$$

Where, D= Crystallite size, K= shape factor (Scherrer constant) (0.9), λ= wave length of X-ray (0.15406 nm), β= Full width at half maximum (FWHM), θ= diffraction angle

3.5.4 FTIR

FTIR spectroscopy was used to analyse the macromolecular modification of the samples. The expected interaction between the silver and the components of plant leaf extract in the synthesized product was further confirmed using FTIR with the incorporation of KBr pellets.

3.6 Stability study analysis of AgNPs within GLY-LAC bio-conjugate

3.6.1 Surface charge determination by Zeta potential

Zetasizer Nano instrument (Nano ZS (Red badge)) with model number ZEN 3600 (Malvern Instrument Ltd. Worcestershire, UK) was used to measure zeta potential. Zetasizer Nano range options for zeta potential measurement were 3.8 nm to 100 µm size range for Zeta potential. A minimum concentration of between 0.1 and 1% w/v is required to obtain sufficient scattering from the solution to make a successful zeta potential measurement. Water was used as a dilution medium which is polar dispersant with a dielectric constant greater than 20.

3.6.2 Particle size analyser (PSA)/Zetasizer Nano

Zetasizer Nano instrument (Nano ZS (Red badge)) with a model number of ZEN 3600 which was used to measure particle size. Zetasizer nano range options for particle size measurement size range with maximum diameter 0.3 nm to 10 µm. Sample concentration was within the range 0.1-0.5 mg/ml as minimum concentration by considering density, cleanness, square and disposable sizing cuvette was used as sample holder.

3.6.3 FTIR

AgNPs/GLY-LAC was carried out to identify expected functional groups and their interaction. The effect of incorporation of AgNPs on the functional groups of the base matrix and the impacts of GLY-LAC on the stability of AgNPs was analysed. The functional groups coated AgNPs were examined using FTIR serial number A013861790.

3.6.4 Scanning Electron Microscopes (SEM) analysis

The surface morphology of the three films GLY-LAC/PLA, AgNPs/PLA and AgNPs/GLY-LAC/PLA was evaluated using BENCHTOP SEM (Model JCM-6000 PLUS) JEOL, JAPAN and their dispersions within the PLA matrix were computed. The samples were cut from those films by scissors into a rectangular form with 10 mm width and 40 mm length, with a magnification of 20 µm. The samples were placed on double-sided carbon tape and operated at an accelerating 1 kV voltage.

3.7 Characterization of PLA based films

3.7.1 GLY-LAC/PLA based film

3.7.1.1 Thermal property analysis

Differential scanning calorimeter (DSC) is a technique used to investigate the response of polymers to heating/cooling. Neat PLA and PLA with GLY-LAC matrix thermal properties were analysed by DSC on a DSC-60 Shimdazu, South Korea. 6-8 mg mass of samples were weighed and hermetically sealed in an aluminium pan; the samples were prepared carefully through cutting by scissors. Heating and cooling rate (k) were used at 10 ℃/min and -10 ℃/min, respectively, which were chosen according to ASTM D3418 standard. The samples were carefully cut with the size of the sample holder, and then heating from 25 ℃ to 200 ℃ and cooling from 200 ℃ to 0 ℃ were done to study the influence of different chain length GLY-LAC on PLA. An empty sealed aluminium crucible was used as a reference and dry nitrogen was used as purge gas at a rate of 50 ml/min. Finally, glass transition temperature (T_g), melting temperature (T_m) and ΔH_m were determined from the DSC thermogram. Degree of crystallinity (X_C) was calculated based on the heat of melting (fusion) according to equation (3.4):

$$X_C = \frac{\Delta H_m}{\Delta H_m^{\circ}} * 100\% \dots \dots \dots (3.4)$$

Where: X_C - degree of crystallinity, ΔH_m - melting enthalpy changes, ΔH_m° - melting enthalpy of 100% crystalline (93.7 J/g).

3.7.2 AgNPs/GLY-LAC/PLA based film

3.7.2.1 Thermal conductivity analysis

QTM-500 is a quick thermal conductivity meter through measuring methods of hot wire method or probe method, the probe consists of a single heater wire and thermocouple. When constant electric power (energy) was given to the heater, the temperature of the wire rises in exponential progression. The temperature rising curve is plotted in a linear line with a time axis scaled in logarithm. The measuring range was between 0.023 to 12 W m^{-1} k^{-1} with a sample, measuring time was standard 60 sec and dimension of 100 (W) × 50 (L). QTM-500 has three reference materials: Rl-2 Clear quartz inbox, R2-2 silicone rubber inbox, R3-2 polyethylene form inbox. The measurement was done after heating the machine for 30 minutes and 2 minutes for cooling of the heater was also required within each sample measurement. Finally, thermal conductivity was determined by using equation 3.5.

$$\lambda = \frac{Q * \ln(T2/T1)}{4 * \pi\ (T2 - T1)} \ldots\ldots\ldots\ldots\ldots\ldots\ldots\ldots\ldots\ldots\ldots\ldots\ldots\ldots\ldots\ldots\ldots\ldots (3.5)$$

3.7.2.2 Electrical conductivity analysis

Electrical conductivity was measured with SP-300 Potentiostat equipment with an integrated temperature sensor, up to 500 mS/cm and 0.01 μS/cm resolutions could be reached in the measured area. The temperature measurement range is between 20–120 °C with an accuracy of ± 0.2 °C (Chereches et al., 2019). After an electrically conductive (EC) solution was prepared, the sample was inserted into the solution through two methods, the first one was by preparing a solid sample in the form of film and inserting the sample into the solution and connecting it with the electrodes then the electrical conductivity of the sample was measured, the second one was by coating the sample on glass materials. In addition to the potentiostat, another electrical conductivity test was used, a digital multi-meter and probe station (Agilent B2902A precision Source/Measure Unit (SMU).

CHAPTER FOUR

4. RESULTS AND DISCUSSION

4.1 Synthesis and purification of GLY-LAC

A condensation reaction was conducted between glycerol and lactic acid. In this reaction, the three reactive "OH" groups of glycerol react with three molecules of lactic acid yielding the NAs GLY-LAC. However, there were impurities due to the possibility of side reactions between the hydroxyl group of glycerol and the carboxylic group of lactic acid or the hydroxyl group of one lactic acid with the carboxylic group of another lactic acid and also impurities from unreacted lactic acid and glycerol. To remove those impurities from crude GLY-LAC, solubility in two different miscible liquid methods was utilized with ethyl acetate and sodium chloride. Due to the better solubility of lactic acid in water than in ethyl acetate and the insolubility of glycerol in ethyl acetate. The synthesis and purity of GLY-LAC were examined through NMR, FTIR, colour changes, viscosity measurement as well as based on acid value (AV).

4.1.1 Acid value of GLY-LAC

In the condensation reaction, the ratio of reacted carboxylic acid to initial carboxylic groups was related to the degree of esterification and purification of the condensation reaction. Therefore, the degree of esterification and purification was estimated by the free acid value through the titration method. The AV of GLY-LAC 1:3, 1:6, 1:9, and 1:12 before and after purification are tabulated in table 4.1. These data give us information on the formation of esterification reaction, removal of unreacted lactic acid, unreacted glycerol and lactic acid oligomers. Due to the presence of carboxylic acid on lactic acid, as the amount of carboxylic acid decreased it indicates the consummation of the acid by glycerol and more ester bond was formed, which was why the amount of carboxylic acid decreased after purification. Again as the acid amount diminished it indicates the removal of lots of LAOLG and unreacted lactic acid, because large amount of carboxylic acid is available on both of them. This analysis was supported by the change in viscosity, as the chain length of the matrix increased after purification took place.

4.1.2 Viscosity and colour change

During the condensation reaction of glycerol with lactic acid, the insufficient reaction time, temperature and imbalance of reactive hydroxyl or carboxyl group to perform further reaction between the two reactants were leading to the formation of lower molecular weight molecules, which decreased the viscosity.

The viscosity of the conjugate was increased with the molar ratio; this was due to the availability of enough amounts of reactive groups in the system. The more the concentration of the reactant there was the more the reaction rate and the more product formation.

Table 4.1: Acid values of GLY-LAC before and after purification

Samples	**Acid value (mg/g)**		**Method**
	Before purification	After purification	
GLY-LAC 1:3	75.73	33.023	Titration
GLY-LAC 1:6	137.44	89	Titration
GLY-LAC 1:9	148.66	92.54	Titration
GLY-LAC 1:12	157.08	112.86	Titration

The viscosity of the conjugates was dependent on the chain length of the GLY-LAC arm before and after purification. The measured viscosity of the four different GLY-LAC matrixes (1:3, 1:6, 1:9, and 1:12) before purification was below 5,270 cP, which was 268, 298, 354, and 376 cP respectively. The lower viscosity was due to the higher amount of unreacted lactic acid monomers. But after purification, the viscosity of all GLY-LAC matrixes becomes more than 5,270 cP (maximum measurement by the instrument), because of the removal of unreacted lactic acid and lactic acid oligomers as well as due to having enough reaction time and temperature.

The other physical confirmation for the purification of the GLY-LAC was the colour change, as shown below in figure 4.1. The colour of GLY-LAC after purification became dark brown from a light yellowish colour. This was due to the removal of unreacted lactic acid, lactic acid oligomers and a change in macromolecular transformation. In addition to these, the detailed analysis regarding chain and structural analysis was done through proton and carbon NMR, which highly confirms the formation and purification of the matrix.

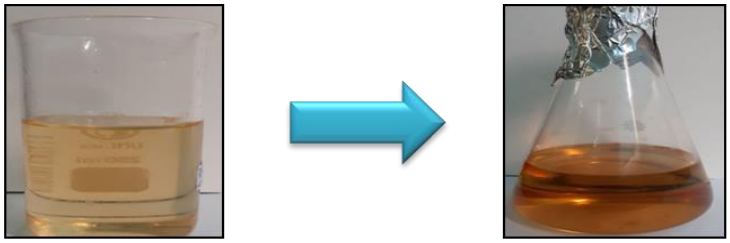

Before purification After purification

Figure 4-1: Colour change of GLY-LAC 1:6 during purification

4.1.3 Structural analysis of purified GLY-LAC 1:6 bio-conjugate/NMR

The proton NMR (^{1}H NMR) spectra and carbon NMR (^{13}C NMR) are particularly useful in identifying differences between the four glyceryl lactate matrix (1:3, 1:6, 1:9, and 1:12) before and after purification, to find out the impacts of purification on those matrices. From that matrix, GLY-LAC 1:6 matrix was selected for the next detailed NMR structural analysis due to its higher improvement on degree of crystallinity (X_c= 85.2%). Due to the complexity of NMR analysis for each of the GLY-LAC bio-conjugate, therefore for the simplicity of discussion, the next detailed explanation focuses on GLY-LAC 1:6. The rest of NMR data for the other GLY-LAC was attached to the appendix part (Appendix 2-Appendix 8), but the explanation method was similar for all of GLY-LAC. The removal of free lactic acid, free glycerol and lactic acid oligomers from the glyceryl lactate matrix were analysed before and after the purification.

The removal efficiency was obtained from the analysis of Lactic Acid Oligomer NMR (LAOLG), GLY-LAC 1:6 matrixes NMR before and GLY-LAC 1:6 matrixes after purification. Comparison was done based on the removal of existing peaks, formation of new peaks, increase or decrease in intensity, and change in chemical shift values of the spectrum. The difference in intensities for the three NMR spectra and the position of peaks was very crucial as shown in Scheme 1.1 and 1.2. The reason behind focusing on the NMR spectra of LAOLG was the availability of the excess amount of lactic acid during the production of glyceryl lactate. It was possible to expect lactic acid as free unreacted lactic acid and lactic acid oligomer.

4.1.3.1 Structural analysis of LAOLG

Proton NMR (^{1}H NMR) of Lactic acid; it is known that 90% of lactic acid aqueous solutions contain a series of oligomers at equilibrium with lactic acid. The latter is the predominant species that contain the smallest monomer up to the tetramer oligomers. As

shown in Scheme 1.2 presence of methine (CH) and methyl groups (CH_3) on LAOLG monomer, dimmer, trimmer, and tetramer, occurred in four distinct positions of the (CH) and (CH_3). These were in the free LA monomer, terminal position near COOH group or OH end groups and in the middle chain. These were further confirmed by H-NMR spectra of LAOLG as shown figure in 4.2 and the peak position is also tabulated in table 4.2. As the chain length of the LAOLG increases, the chemical shifting values of the chemicals became greater or move to the left for all hydrogen types.

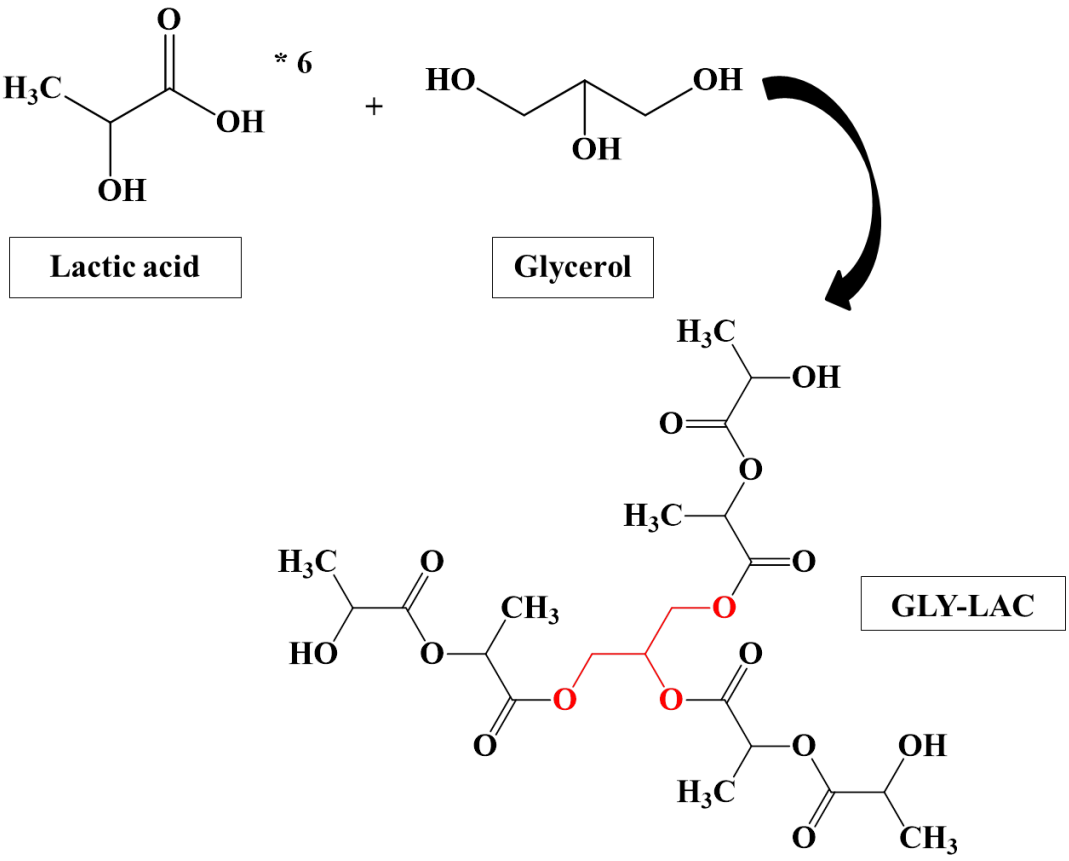

Scheme 1-1: Reaction Scheme for the synthesis of GLY-LAC 1:6 bio-conjugate

In general, most of the chemical shift values of the purified GLY-LAC 1:6 conjugate were shifted to the lower, as shown in figure 4.4 when compared with LAOLG (figure 4.2) and non-purified GLY-LAC (figure 4.3). This implies confirmation of the removal of free and oligomerized lactic acid from the system. When LAOLG and other impurities were removed the peak intensity of the purified GLY-LAC 1:6 was increased. Because the protons on the pure GLY-LAC had a chance of becoming intense this is previously masked by impurities.

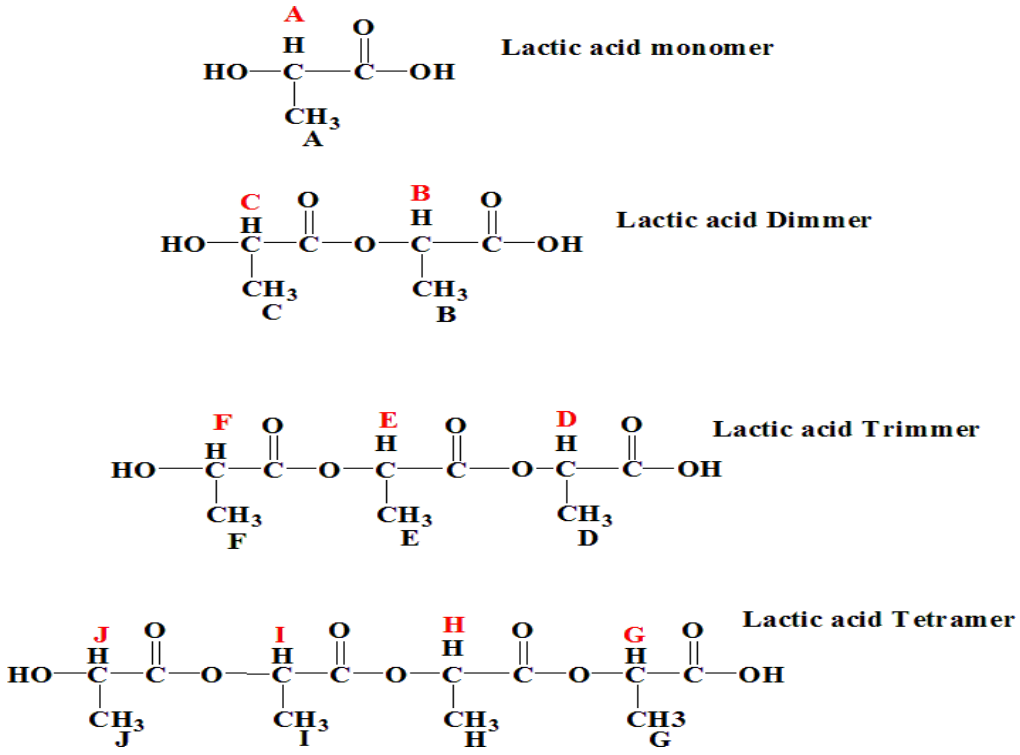

Scheme 1-2: Peak position for the synthesis of Lactic Acid Oligomer (LAOLG)

Table 4.2: NMR chemical shifts (in ppm) of CH and CH_3 protons in A-T units of L- Lactic Acid Oligomer

Hydrogen type	Monomer	Dimmer		Trimmer		Tetramer		Polymer
	A	B	C	D	F	G	J	
CH_3	1.27	1.38	1.27	1.44	1.40	1.40	1.27	1.46
CH	4.03	4.92	4.19	4.20	4.98	4.99	4.20	5.1

For example, the internal chain (4.18-4.27 ppm) was increased after purification took place, which indicates the removal of a mass of bonds of free lactic acid as well as oligomerized lactic acid (Borowicz et al., 2019).

There are new and less intense multiplet peaks at 1.12-1.14 ppm which resembles triplet peaks during expansion. Those peaks were not available on both the non-purified and LAOLG NMR spectrum. These triplet's peaks occurred likely due to -CH_3 groups

connected to -CH_2 methyl functionalities of residual ethyl acetate that was not removed during purification. This explanation could be supported by Distortionless Enhancement by Polarization Transfer (DEPT) analysis of ^{13}C NMR. DEPT analysis there were three downward peaks (-Ve), which resembled the presence of two carbon from CH_2 and also the other peak was for the impurity of ethyl acetate. Supported by the data on Chemical Book in which ethyl acetate was found at 0.9 (Beavers et al., 2009).

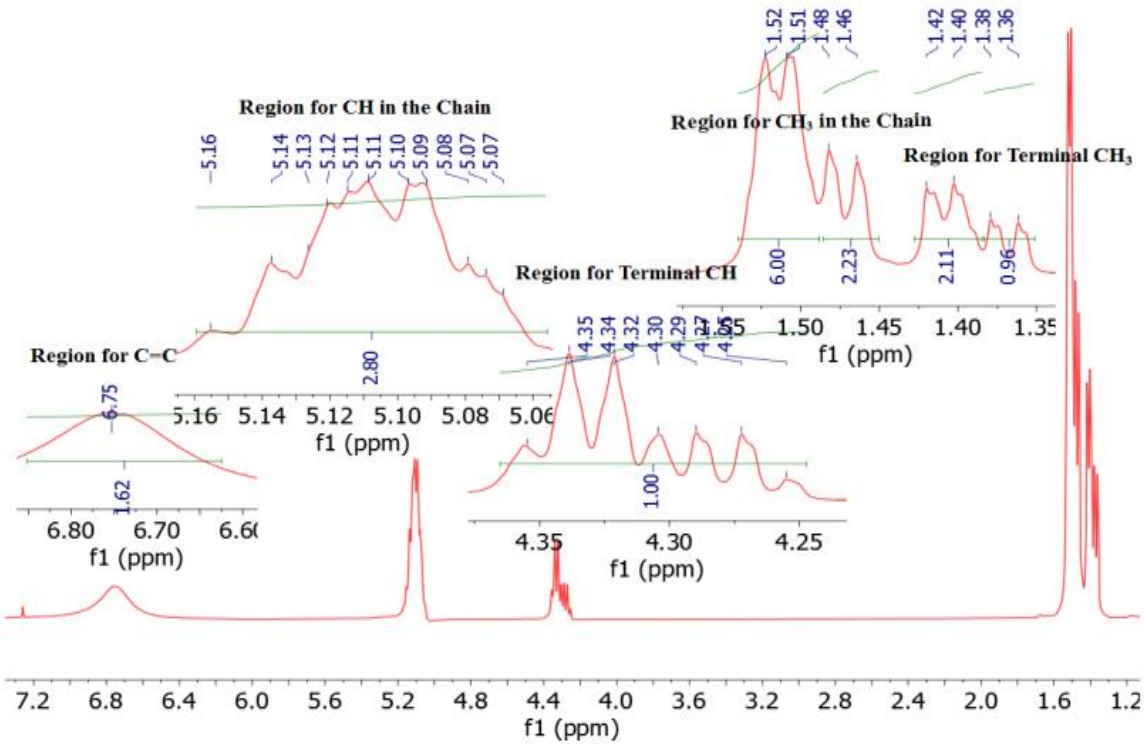

Figure 4-2: ^{1}H-NMR Spectra for LAOLG Bio-conjugate

The four different doublets peaks occurred at 1.28 ppm, 1.33 ppm, 1.38 ppm, and 1.43 ppm attributed to methyl group protons (CH_3). The presence of hydroxylated doublet peak at 1.28-1.29 ppm was responsible for the unreacted methyl group of lactic acid of monomer, dimmer and trimmer chains and the doublets indicate that these methyl groups are near a –CH group which was more shielded, which shifted to up-field depending on the location of repeating units concerning chain ends. The other three doublet peaks which appear in the 1.33-1.34 ppm, 1.38-1.40 ppm, and 1.43-1.45 ppm range are responsible for esterified methyl group protons in the main chain. Those three doublets are attributed to six single CH_3 groups of the purified GLY-LAC 1:6 conjugate.

These results are in agreement with the reports in the literature (Beavers et al., 2009; Gross et al., 2018; Rashkov et al., 1996). Here those four doublets peaks were available for both

NMR (LAOLG and non-purified GLY-LAC 1:6), in figure 4.2 and figure 4.3 but with different intensity and peak positions. The area under the peaks which give rise to that signal was higher in purified GLY-LAC 1:6 conjugate due to the removal of the large chain of free and oligomer lactic acid. This created the chance for reacted glycerol and lactic acid to become shine sharply. The number of protons increased for the purified GLY-LAC 1:6 methyl group.

The removal of oligomerized lactic acid CH which is carboxylated within the internal main chain (methine group in the lactic acid), that occurred at the resonance of 5.07-5.16 ppm range was confirmed by the decrement of those multiplet peaks on the purified GLY-LAC 1:6 conjugate. It had only three peaks at a resonance range of 5.01 ppm and 5.06 ppm. A literature study also expected methine group in chemical shift environments of 5.09 - 5.21 ppm (Román-Ramírez et al., 2018).

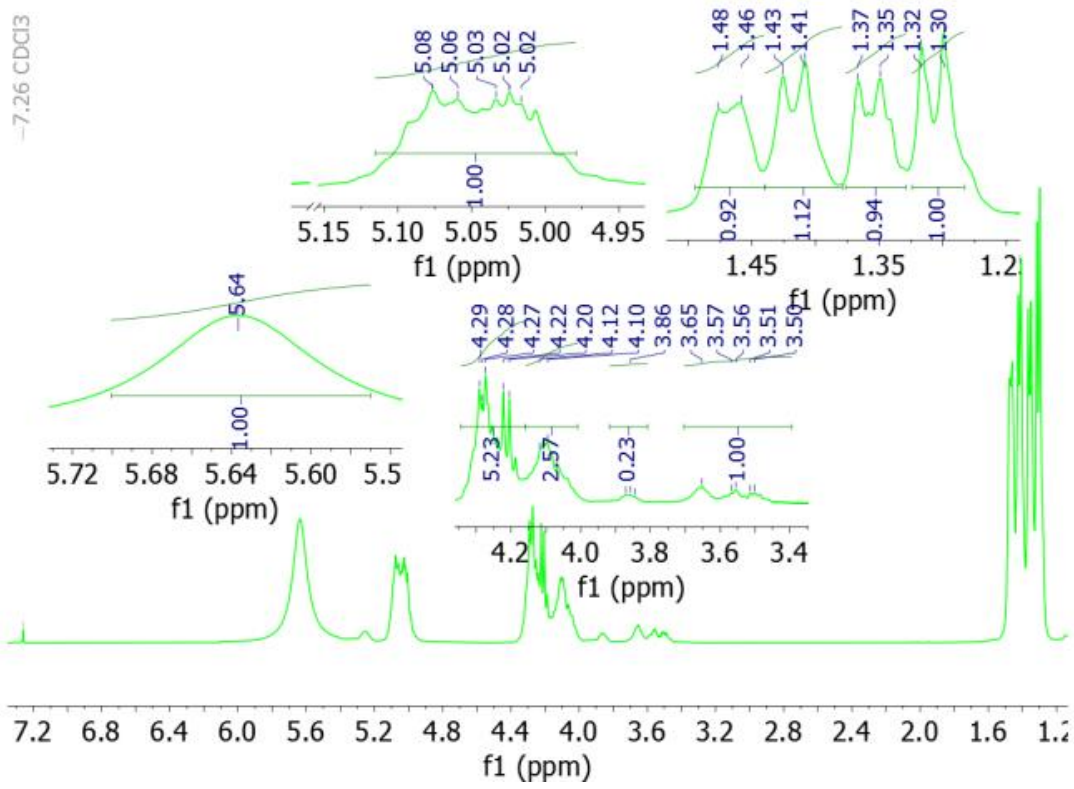

Figure 4-3: [1]H NMR spectra for non-purified GLY-LAC 1:6 bio-conjugate

The other evidence is the peak area, the area under peaks which directly indicates the number of equivalent protons that give rise to that signal. Regarding these when considering the methine (CH) group of LAOLG and purified GLY-LAC 1:6, the number of the proton was decreased by 64.3% after purification that indicating a mass of bonds was removed. In addition to these the chemical shift values of the purified matrix were

decreased to the lower values. Which resembled the indication of the removal of LAOLG, due to this electron from the pure product GLY-LAC hydroxyl end highly shielded (up-filed) the proton-nucleus and the proton experience a lower magnetic field. Therefore the proton resonance at a lower frequency had lower chemical shift values (Espartero et al., 1996; Rashkov et al., 1996).

Regarding methine group proton (CH) in the Tetramer of lactic acid, only proton which was OH free signal of internal ester bonds in CH existed at 4.20 ppm in the chain after purification. The other hydrogen in CH at 4.99 ppm was absent, which confirmed the reaction between the glycerol and lactic acid took place. On literature also reported the absence of the peak at this ppm (Rashkov et al., 1996).

These explanations also work for dimmer and trimmer lactic acid chains in which only shielded methine protons have occurred at 4.18 - 4.20 ppm of the chain. This result was supported by a study by (Rashkov et al., 1996), in which methine protons were considered to be in the range of 4.23-4.29 ppm. The de-shielded protons which were expected at 4.98-5.0 ppm were absent for the three of NMR spectrum, which was used as a supporter for the formation of glyceryl lactate. For monomer carboxylated free lactic acid end units whose methine protons should appear at 4.03 ppm in the terminal CH chain were also absent which indicates the absence of unreacted lactic acid monomer for the three (LAOLG, non-purified GLY-LAC 1:6 and purified GLY-LAC 1:6 conjugate) NMR spectrum, in which confirm this study (Rashkov et al., 1996).

A new singlet peak at 4.08 ppm methine group proton (CH) which is not found on the LAOLG resembled the internal ester bonds at the hydroxylic end chain of the purified GLY-LAC 1:6 conjugate as shown in figure 4.4. This peak was also found on non-purified GLY-LAC 1:6 with a higher chemical shift value (4.10 ppm) with a de-shielded proton nucleus. The doublet signal peaks at 4.25 - 4.27 ppm belong to the methylene group proton of the internal chain ester bonds of the reacted glycerol. This is not completely formed on the free and oligomer lactic acid.

The presence of OH ended a group of the conjugate was proofed by the occurrence of new small signals at 3.46-3.63 ppm. There was a singlet and less intense peak at 3.83 ppm for the indication of OH end functionalization of purified GLY-LAC 1:6 conjugate chains. This peak was also available for non-purified GLY-LAC 1:6 at 3.87 ppm, but it is not found on LAOLG (figure 4.2). This indicates the internal ester bond formation for the

conjugate. The other two singlet peaks that support the formation of the ester bond of the conjugate have occurred at 1.92 ppm and 2.0 ppm which are attributed to allylic hydrogen located on the carbon atom attached to the double bond of ethyl acetate and supported by the data of Chemical Book with CAS number of 141-78-6.

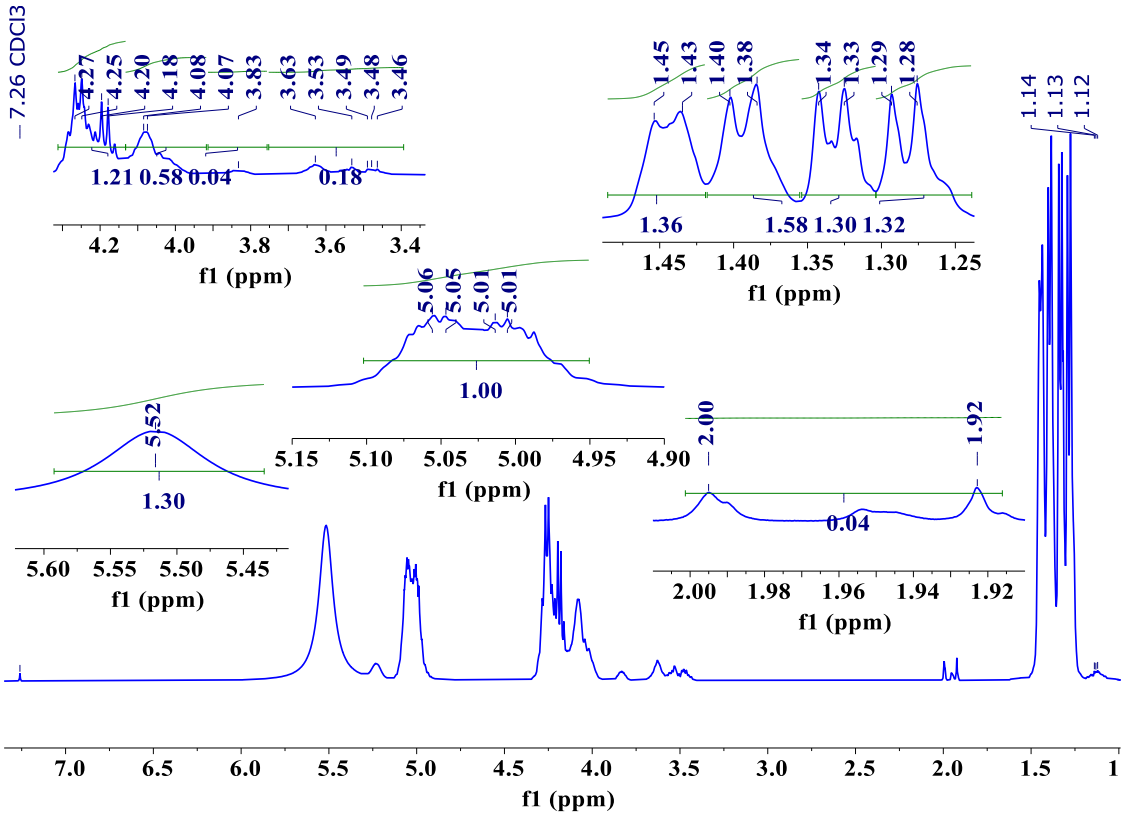

Figure 4-4: ^{1}H NMR spectra for purified GLY-LAC 1:6 bio-conjugate

That showed the proton NMR peak of ethyl acetate at 2.038 ppm chemical shift value that was adjacent to the methyl group. The two peaks were not found on both non-purified GLY-LAC 1:6 matrix and LAOLG NMR. The peak at 5.52 ppm on purified GLY-LAC 1:6 conjugate is attributed to the double bond formation during the reaction in which vinylic hydrogen, which hydrogen was directly attached to C=C-H (H was attached to alkene C). This might be become from oxidation reaction with the external oxygen. This vinylic hydrogen also occurred on LAOLG at 6.75 ppm, which was very di-shielded, indicating the more electronegativity of the hydrogen, but on non-purified GLY-LAC 1:6 (figure 4.3) vinylic hydrogen presented at 5.64 ppm (Faller et al., 1989). Besides to the proton NMR analysis for the confirmation of synthesis and purification of the GLY-LAC matrix was done using carbon NMR (^{13}C NMR) analysis to know the removal of different carbon components from the GLY-LAC matrix.

Table 4.3: ^{1}H NMR Chemical shifts (ppm) value of purified GLY-LAC 1:6 conjugate

Chemical shift values (ppm)				
	Free lactic acid	**Oligomer lactic acid**	**Reacted LA within the chain**	**Peak type**
CH_3			1.14 - 1.12 Purified 1:6 GLY-LAC	Triplet (New peak)
			Absent on non-Purified 1:6 GLY-LAC	
	1.28 - 1.29 Purified			Doublet
	1.30 - 1.32 non-Purified			
			1.33 - 1.34 Purified	Doublet
			1.35 - 1.37 non-Purified	
			1.38 - 1.40 Purified	Doublet
			1.41 - 1.43 non-Purified	
			1.43 - 1.45 Purified	Doublet
			1.46 - 1.48 non-Purified	
OH			3.63 - 3.46 Purified	Multiplet
			3.50 - 3.67 non-Purified	
			3.83 Purified	Singlet
			3.87 non-Purified	
CH_2			4.27 - 4.25 Purified	Multiplet
			4.28 - 4.29 non-Purified	
CH	4.03 (absent)			-
			4.08 Purified	Singlet
			Absent for non-Purified	
		4.20 - 4.18 Purified		Multiplet
		4.27 - 4.20 non-Purified		

		5.0 - 4.98 (absent)		-
		5.06 -5.01 Purified		Multiplet
		5.08 -5.02 non-Purified		
Allylic hydrogen (C=C-C-H_3)			1.92 Purified 1:6 GLY-LAC (New peak)	Singlet
			Absent for Non-Purified	
			2.0 Purified 1:6 GLY-LAC (New peak)	Singlet
			Absent for Non-Purified	
Vinylic hydrogen (C=C-H)			5.52 Purified 1:6 GLY-LAC	Singlet
			5.64 for non-Purified	

4.1.4 Chain Length Analysis

From the ^{13}C-NMR spectrum in figure 4.6 and table 4.4, it is possible to find out the carbonyl bonds within CO, CH, CH_2, and CH_3 carbons that are present in the structure of GLY-LAC macromolecules, resembled the purified GLY-LAC 1:6 conjugate, which was determined with the incorporation of carbon peaks on Distortion less Enhancement by Polarization Transfer (DEPT-135) NMR (Baran et al., 2018). The comparisons of the spectra of the three ^{13}C-NMR were done based on the same criteria of the ^{1}H NMR analysis for the three matrixes. In ^{13}C-NMR spectrum analysis, the intense peaks at characteristic chemical shifts of 16.44 – 19.77 ppm resembled the two carbons of methyl groups (CH_3). In which they associated for unreacted free lactic acid on monomer and reacted lactic acid within the core of the chain respectively.

The other carbons shifted to the higher chemical shift values are due to the attachments to the hydroxyl group at the end of the lactic acid oligomer chain located at 66.32 – 68.89 ppm in figure 4.5. The peak was attributed to the α methine group (-CH-OH), the carbon at

the peak of 66.85 ppm resembled the methine group (CH) of free lactic acid. Whereas the other carbons belong to the conjugate chain as well as lactic acid within the internal chain and the methine group that de-shielded to the downfield of the higher chemical shift values.

Due to the presence of ester bond (-C(O)-O-CH(CH_3)-) attachment at 68.89 ppm carbons of the α-methine group at the ester group. The presence of methylene carbons in the main chain was supported by evidence from DEPT-135 NMR analysis (Appendix 6). DEPT-135 was used to check the nature of these carbon peaks. From the DEPT-135 spectrum two methylene carbons reactions (-CH_2-CH-CH_2 -), shown by two downward peaks (-Ve peaks) at 62.74 ppm and 65.26 ppm attributed to the methylene group in the product, gave evidence for the presence of significant reaction (Rashkov et al., 1996).

As shown in figure 4.6, the peak areas of the carbonyl group on the conjugate in the ^{13}C-NMR spectra were found between 160 and 180 ppm. From the figure 4.6 letter "D" belongs to the free lactic acid monomer carbonyl group in carboxyl groups (C=O)-OH) at 177.61 ppm. Whereas this signal is at a lower intensity on LAOLG (figure 4.5), due to the oligomerization reaction, that was why it increased after purification. Because the reaction between glycerol and lactic acid took place, which decrease the chance of oligomerization reaction.

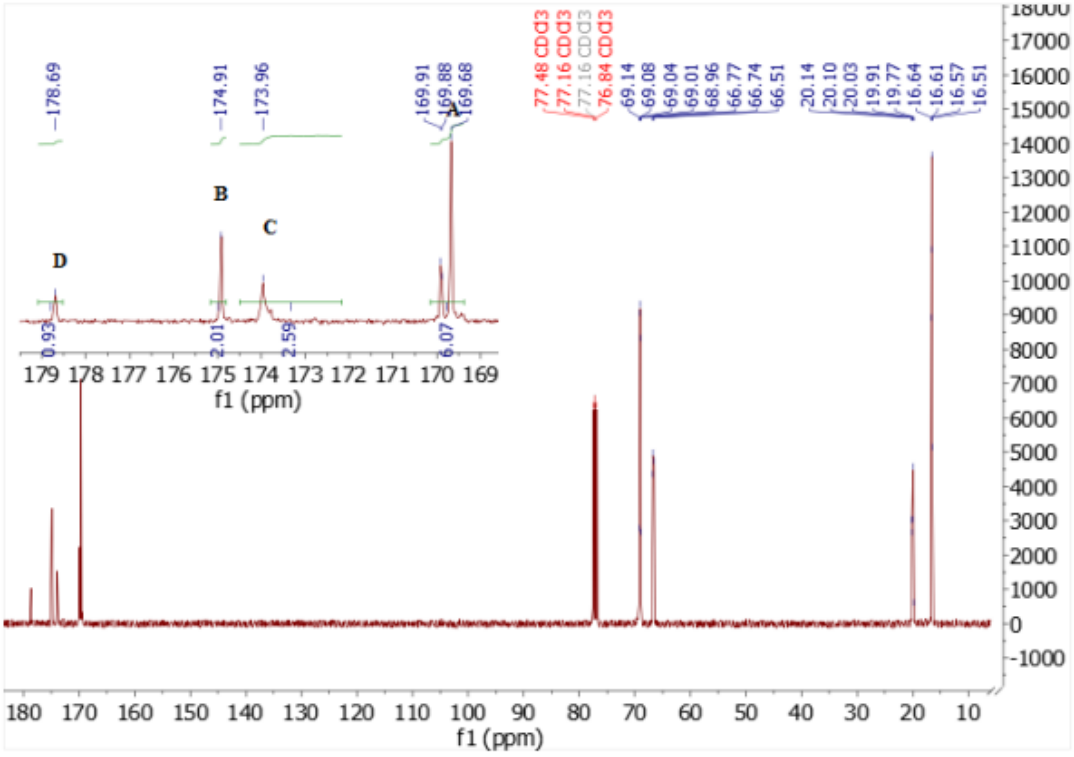

Figure 4-5: ^{13}C-NMR Spectra for LAOLG bio-conjugate

In figure 4.6, carbons of the carbonyl groups in ester groups (-C=O)-O-) that were adjacent to the hydroxyl group show two sharp peaks at 172.84 and 172.8 ppm symbolized by “C”. This was the main evidence for the occurrence of the reaction between glycerol and lactic acid. Only one peak was found on the NMR of LAOLG (figure 4.5) which was also evident for the esterification reaction for the formation of product GLY-LAC. In figure 4.7 these signals had lower intensity on non-purified GLY-LAC 1:6, but after the purification, those signals become very intense due to the removal of impurities (free lactic acid and oligomer of lactic acid) (Espartero et al., 1996).

Again from figure 4.6, the carbonyl signal of the lactic acid end group that was on an area of letter “B” is observed at 174.58 -175.01 ppm. This signal was from the carbonyl group adjacent to the ester oxygen for glycerol-based and lactic acid oligomer. But here it cannot distinguish between the LA oligomers reacted and not reacted with glycerol. Only a single peak was observed on the NMR of LAOLG (Figure 4.5).

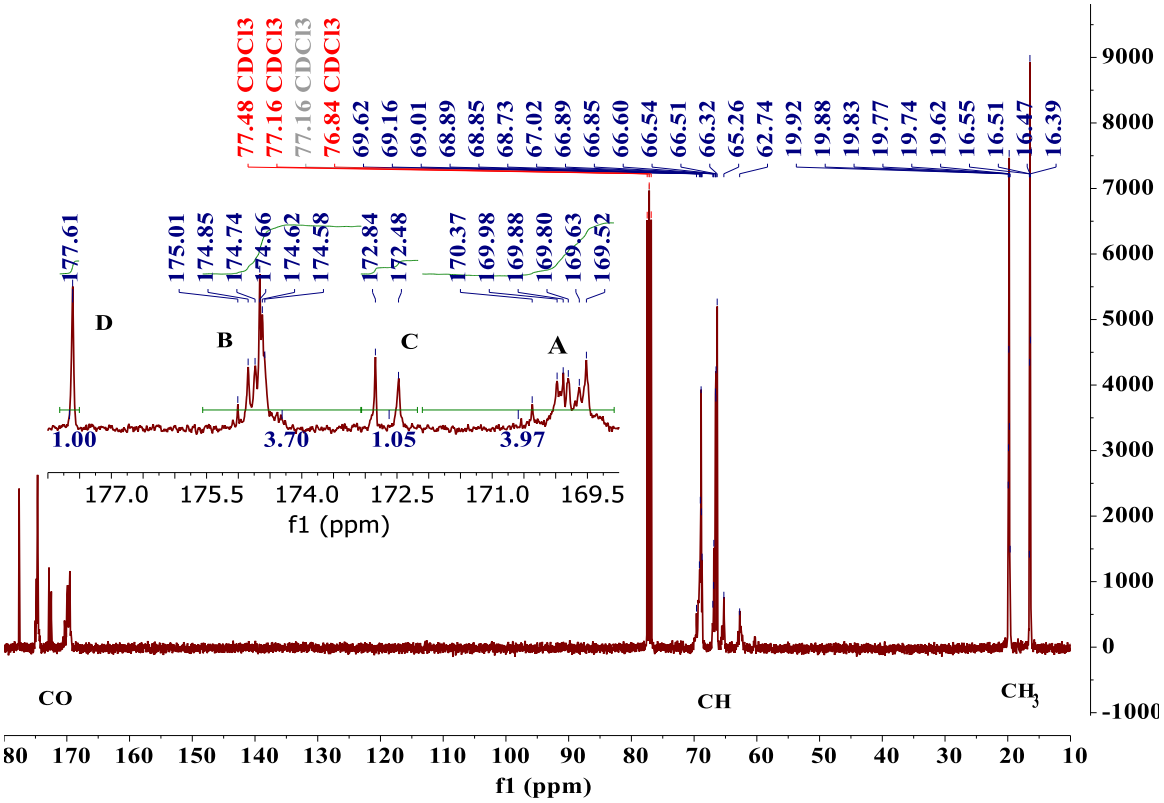

Figure 4-6: ^{13}C-NMR Spectra for purified GLY-LAC 1:6 bio-conjugate

Carbonyls which were assigned by the letter “A”, the two signals resembled carbons in the lactic acid branch and the lactic acid oligomer at 169.52 -170.37 ppm. On figure 4.5 LAOLG NMR analyses were very intense peaks, due to the absence of the main reaction, only oligomerization reaction took place. But the NMR of the non-purified conjugate in

figure 4.7 peaks was almost the same as with purified GLY-LAC 1:6 conjugate. There was only a little intensity difference. The other signal were due carbons from solvent at 76.84 - 77.48 ppm of Deuterated chloroform ($CDCl_3$) (Borowicz et al., 2019; Paciorek-Sadowska et al., 2019).

Furthermore, the synthesis and purification were confirmed and supported by the FTIR analysis for the GLY-LAC 1:6 before and after purification, there were peaks in which their intensity increased or decreases due to the removal of unwanted impurities.

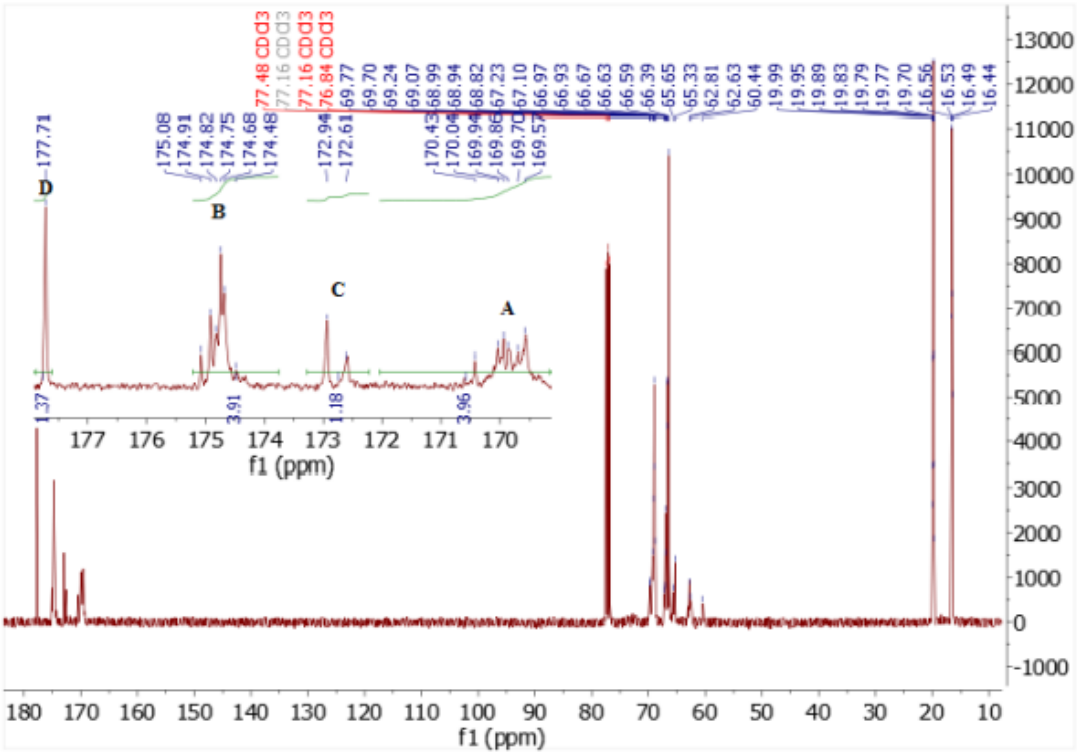

Figure 4-7: ^{13}C-NMR Spectra for non-purified GLY-LAC 1:6 bio-conjugate

4.1.5 Macromolecular arrangements of purified and non-purified GLY-LAC 1:6 bio-conjugate

The other supporting information for the purification of GLY-LAC 1:6 is the analysis of the FTIR spectrum of purified and non-purified GLY-LAC bio-conjugates through a comparison of their response for IR as shown in figure 4.8. On both bio-conjugates, all necessary characteristics of transmittance peaks have existed. The presence of the OH functional group was evidenced by a broad peak found at 3415 cm^{-1} in non-purified bio-conjugates. This broad peak was found on the purified bio-conjugate with a slightly sharp and shifted peak position, and also the intensity of the peak on the non-purified bio-conjugates was lower than that of the purified matrix.

On both bio-conjugate, there was stretching of CH_3 at 2929 cm^{-1}, but the peak found on the purified conjugate was highly intense than on the non-purified conjugate. The main indicator for the formation of the GLY-LAC matrix was the existence of a carbonyl group (ester functional group). The ester bond occurred for both bio-conjugate at 1743 cm^{-1}. As a result of the purification process, unreacted lactic acid and glycerol, oligomerized lactic acid and other impurities were removed from the bio-conjugate. These phenomena were confirmed by the formation of a highly intense and very sharp peak on purified conjugate.

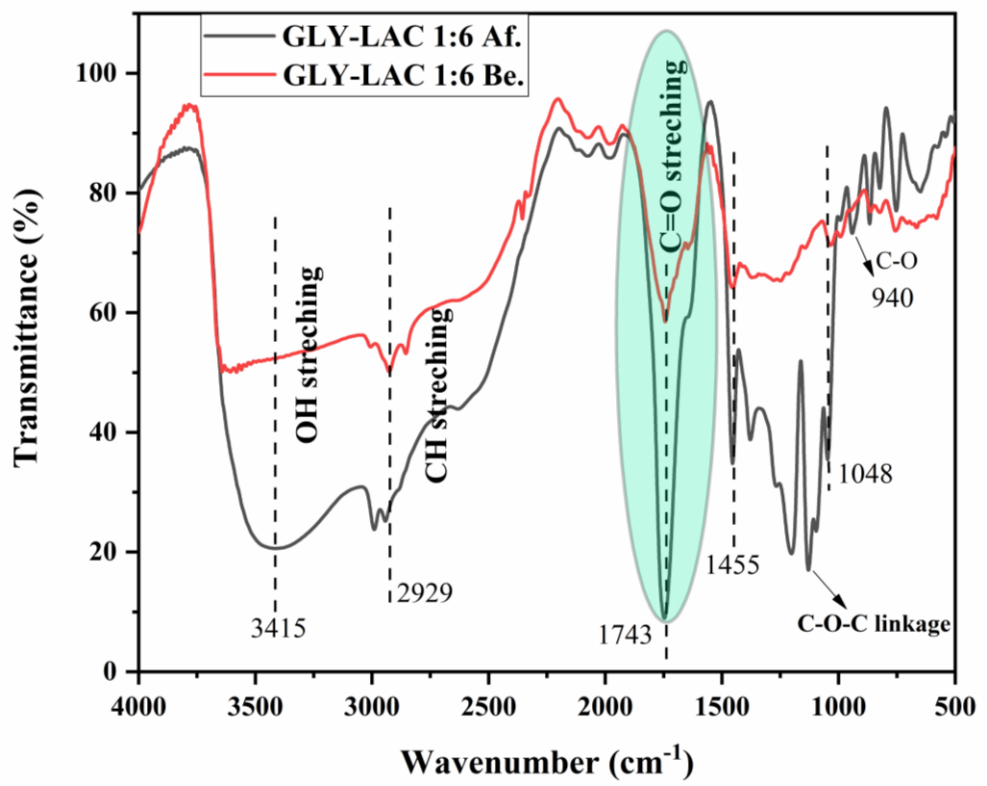

Figure 4-8: Functional group analysis for GLY-LAC 1:6 before and after purification

But on a non-purified matrix, this peak was less intense and their intensity also lowers due to the presence of unreacted lactic acid and glycerol. This shields the ester bond from becoming intense. In another case, a transmittance peak was observed at 940 cm^{-1} for the C-O stretching of the primary hydroxyl group from glycerol. This peak was observed in GLY-LAC bio-conjugates. The other peak found at 1048 cm^{-1} was attributed to C-O stretching in the secondary OH group of glycerol. Therefore, it was possible to confirm the formation of GLY-LAC and also the removal of unwanted impurities. Therefore, FTIR analyses supported the NMR analysis.

4.2 Analysis of Plant Leaves Extract

The components of the *V. amygdalina* (bitter leaf) plant leaf were analysed by using phytochemical screening, FTIR and TGA.

4.2.1 Phytochemical screening Analysis

Phytochemical screening tests were done to determine the class of compounds present in the extract. Phytochemicals were a large number of secondary metabolites or bioactive compounds found in plants. Phytochemical screening of methanol with distilled water (M/DW) based extracts followed standard protocols are described in table 4.4. The phytochemical screening gives positive results within the ferric chloride test of phenols, frothing test, an alkaline test of flavonoids, and Tannin preliminary phytochemical tests.

Table 4.4: Phytochemical screening of *V. amygdalina* plant leaves extract

No.	Phytochemical Compounds	Results	Methods of Tests
1.	Alkaloids	+	Meyers reagent test
2.	Saponins	+	Frothing test
3.	Flavonoids	+	Alkaline test
4.	Tannins	+	Ferric chloride test
5.	Terpenoids	-	Salkowski's test
6.	Phenolic	+	Ferric chloride test
7.	Glycosides	-	Salkowski's Test

Where: "+" indicates the presence and "-" indicates the absence

The phytochemical screen for secondary metabolites revealed the presence of phenolics, saponins, flavonoids, and tannins in the M/DW extract. The phenolic compounds which are tabulated in table 4-4, which were split into phenolic acids and polyphenols were the major class of secondary metabolites. These molecules can be discovered in combination with mono and polysaccharides, connected to one or more phenolic groups, or as derivatives such as ester or methyl esters (Minatel et al., 2017). Ogdid and his co-workers also show phenolic phytochemical components in *vernonina amygdalina*. Saponins were a

complex and chemically diverse group of bitter-tasting surface-active agents (surfactants) that may cause a lot of foaming activity in aqueous solutions (Ogidi et al., 2019).

Saponins are starch glycosides with three hydroxyl groups connected to complicated sugar components. Flavonoids are a class of natural chemicals with a phenolic structure that varies. Flavonoids occurring in *V. amygdalina* have been identified with luteolin, luteoiin 7-O- β glucuronoside, and luteolin 7-O-β glucoside (Igile et al., 1995). Tannins are commonly denoted as tannic acids, they were derived from phenolic acid. Tannins are water-soluble polyphenols that were present in *V. amygdalina* (Ali et al., 2020). Methanol-based extract of *V.amygdalina* shows positive results for phenolic, saponins, flavonoids, tannins, and alkaloids which were fitted with the literature (Ekam et al., 2010).

4.2.2 Macromolecular arrangements of *V.amygdalina* plant

Furthermore, the phytochemical screening was supported by FTIR analysis of bitter leaf powder; the organic compounds were clearly shown. The main target for FTIR analysis was to check the compositions of *V.amygdalina* plant leaf extract. As shown in figure 4.9, the presence of saponins (O-H stretching and N-H group of amide) within the *V.amygdalina* plant was identified through the occurrence of the peaks at 3387 cm^{-1} and the peak at 2932 cm^{-1}. The peaks are indicating the presence of C-H stretching of the alkanes, which is supported by a phytochemical screening of frothing test. The stretching of the carbonyl group (C=O) from proteins of plants existed at the spectrum of 1600 cm^{-1} indicates the presence of flavonoid compounds (Aisida et al., 2019).

Carbohydrates of the plant extract existed at a peak of 1338.55 cm^{-1} indicating the CH_3 group. The fingerprint region of the spectra (1268 cm^{-1}) accounts for the presence of OH (phenolic hydroxyl group stretching) and the peak at 1076 cm^{-1} indicates absorption spectra alkaloid compounds of the C-N group. The existing peak at 824 cm^{-1} area was related to the C=H stretch. FTIR of result confirmed the presence of phytochemical components, phenol, saponins, flavonoids, and tannins, which are stabilizing, capping and reducing agents (Liu et al., 2020).

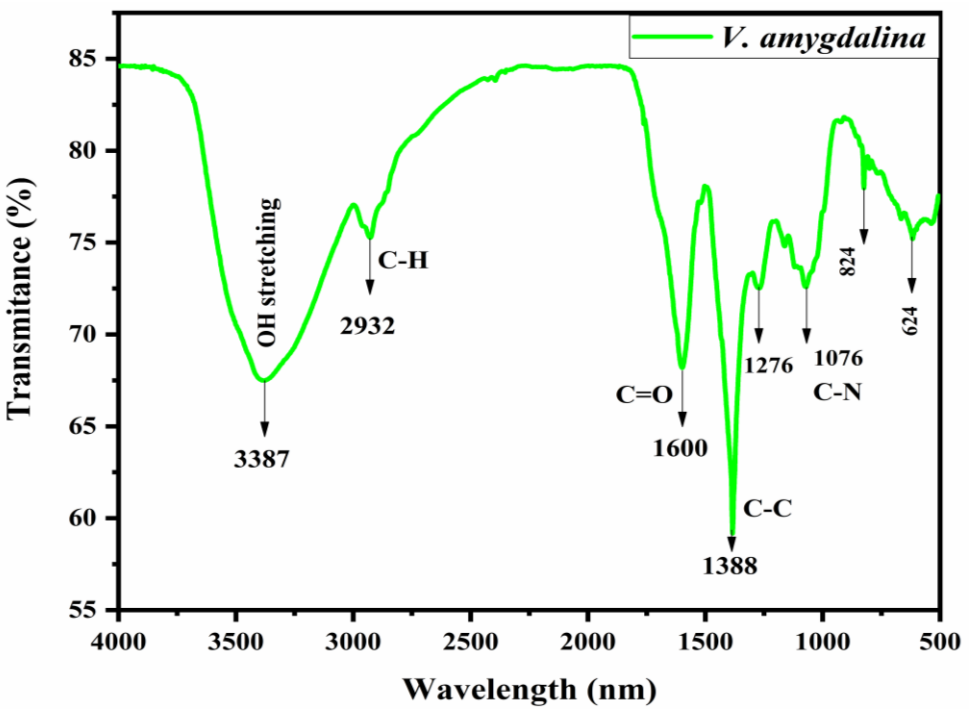

Figure 4-9: Functional group analysis for *V.amygdalina* plant leaf extract

The degradation temperature of the plant was found by the analysis of TGA and also TGA supported the presence of the phytochemical components when the temperature of the system increased the specific components at each temperature were identified.

4.2.3 Thermal degradation analysis of *Vernonia amygdalina* by TGA

Thermal stability analysis of the plant leaves (*Vernonia amygdalina* (bitter leaf) or Girawa) was investigated by using TGA (Thermal Gravimetric Analyser). TGA thermo-grams plotted through recording of weight loss of the leaves sample as the temperature increased, through the temperature increments. It was possible to determine the maximum temperature that the plant could resist (for calcination purpose the plant from of AgNPs), as well as the derivative of TGA also plotted on the same thermo-gram. As shown in figure 4.10 the maximum temperature at which the leaf's maximum amount of degradation occurred was 680-700 ℃. Due to the presence of water, the initial decomposition of the plant leaves started at around 133 ℃.

Four stages of DTG curves were observed for *Vernonia amygdalina* plant leaf in figure 4.10. The first stage occurred from 30 ℃ to 187.77 °C, which is caused by the 25.95 % loss of water molecules and Saponins of *Vernonia amygdalina.* The second stage curve occurred at the temperature starting from 187.77 ℃ to 234 ℃, here around 8.7 % flavonoids contained in lignin parts, then the DTG curve broadly increases on the third

stage of the curve. This indicates that large weight loss occurred around 47.18 % of polysaccharides and glucose was removed at a temperature of 234 ℃ to 431.11 ℃ in which the DTG curve occurred.

The last degradation step in which 16.4 % loss has occurred at 541.8 ℃ to 666.38 ℃ temperatures. This corresponds to the loss of lignin-containing tannins composites at high temperatures; due to its complex aromatic structure of tannin this is the reason why it resists degradation at high temperatures. Around 680 ℃ complete degradations of the plant occurred in which the organic compound of the plant was completely converted to ashes (Lisperguer et al., 2016).

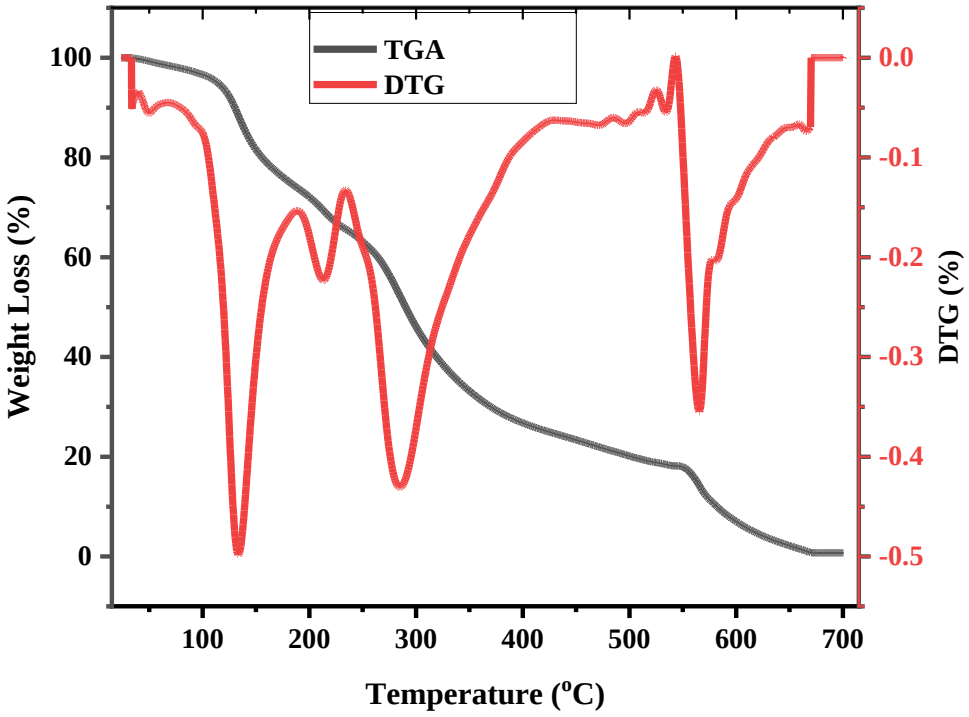

Figure 4-10: TGA and DTG Graph of the *Vernonia amygdalina* plant leaf

4.3 Analysis of Green Synthesized AgNPs

4.3.1 UV-Vis analysis of AgNPs

The reduction of silver ions (Ag^{+}) to the silver nanoparticle (Ag^{0}) through the green synthesis method by adding *V. amygdalina* leaf extract into silver nitrate solution was confirmed using a UV-Visible spectrophotometer within range of 200–800 nm. The bio-organic compounds present in *V. amygdalina* were responsible for the mediated synthesis

of metal salt into Ag^{+} and finally into Ag^{0}. This was confirmed by colour change due to the availability of free electrons on metal nanoparticles giving surface plasmon resonance absorption band.

The peak of AgNPs occurred at 415 nm and 423 nm in figure 4.11, resembling for absorption spectrum during the synthesis stage of silver ions. At an aqueous solution of silver nitrate during the reaction with *Vernonia amygdalina* leaf extract. The other maximum absorption spectrum which occurred at 423 nm was observed after completion of the reaction (after 6 hours). Therefore wavelength of AgNPs stabilizes at 423 nm, which confirmed the formation of the cluster stage by the addition of plant extract which is acting as a reducing agent, capping and stabilizing agent due to its phytochemical components (E. Abbasi et al., 2016). AgNPs are synthesized through three stages: reduction of silver nitrate, formation of cluster and growth of AgNPs (I. Khan et al., 2019).

The synthesised AgNPs were characterized after five months with and without calcination, to check the capping efficiency of the *V. amygdalina* leaves extract. The UV-Vis response of AgNPs without calcination occurred at 418 nm which indicates very high capping as well as stabilizing efficiency of *V.* amygdalina extract. The absorption spectrum obtained was within the range of AgNPs. The colour changed from colourless to brownish colour also indicators for AgNPs formation, first the reddish-brown colour was observed, and as the reaction precede reddish-brown colour was changed to dark brown. This strongly indicated the formation of silver nanoparticles as shown in figure 4-12.

Different scholars reported that due to the surface plasmon resonance of AgNPs, the absorption peak of AgNPs occurred at about 400-450 nm. Confirming the formation of AgNPs (Huq, 2020).

The Ag^{+} was reduced into Ag^{0} by the process of binding on the bulk surface of Ag^{+} by the bio-organic and bioactive compounds present in the *Vernonia amygdalina* plant extract, which have hydroxyl and ketonic groups. The reaction mixture has an absorption maximum of 415-423 nm suggesting the formation of Ag nanoparticles.

$$Ag^{+} + e^{-}(bio - organci\ compounds) \rightarrow Ag^{0}$$

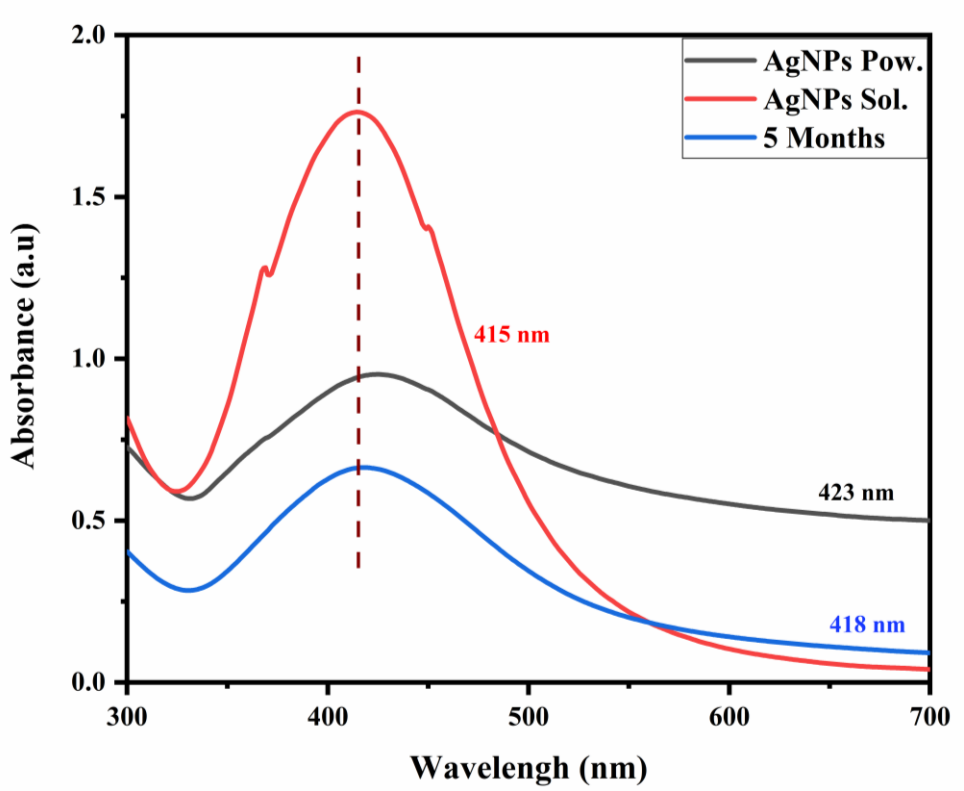

Figure 4-11: UV-Vis absorption spectrum of biosynthesised of Ag-NPs after 6 hr, 24 hr, and 5 months

Figure 4-12: Colour change during bio-synthesis of AgNPs, (A) Silver nitrate solution (B) Plant extract and (C) Mixture of both solutions.

Figure 4-13 shows calcined AgNPs spectra; there were two bands at the wavelength of 381 nm and 271 nm, which were attributed to Ag nanoparticles and Ag oxide respectively. Due to the removal of *V. amygdalina* plant extract, AgNPs became pure metal. This pure AgNPs metal gets the freedom of reacting with external air and also due to its high

hygroscopic properties it absorbs moisture from the atmosphere, that was why two peaks were observed on calcined AgNPs (T. Xu et al., 2022).

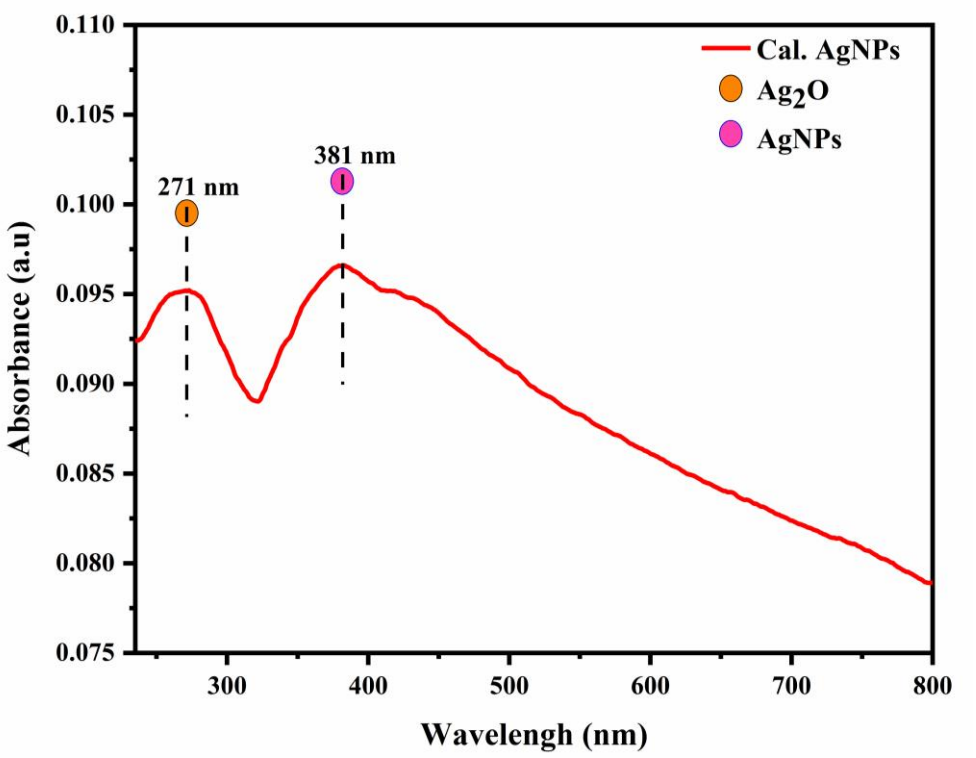

Figure 4-13: UV-Vis absorption spectrum of calcined AgNPs after 5 months

The main issue of the nanoparticle synthesis was their size, because they are nanoparticles, therefore in this research; the size of AgNPs was determined using PSA.

4.3.2 Particle size distribution of AgNPs

As shown in figure 4.14, the Particle size distribution (PSD) of AgNPs was recorded by PSA. A polydispersity of two peaks, peak-1 had 56.45 nm particle sizes with 66.5% intensity and the second peak was recorded with a very lower particle size of 3.05 nm with 33.5% intensity. The reason for the small AgNPs size was probably due to the negative charges of the particles (-27.2) as shown in figure 4-18 in section 4.4.1. That led to an additional force for the Ag particles to repeal each other and the surface charge of AgNPs (Dieckmann et al., 2009).

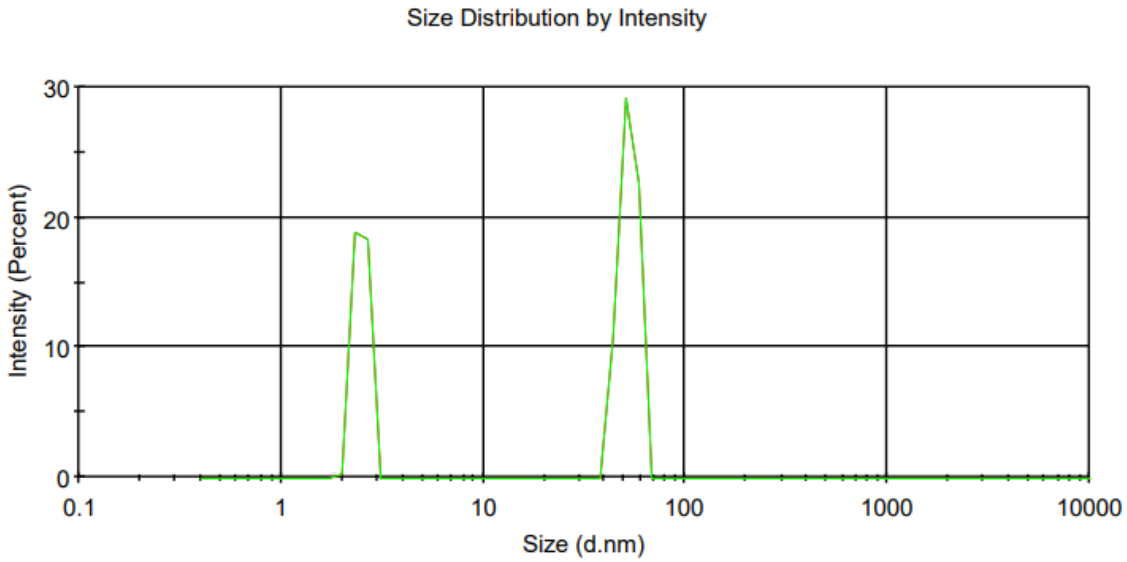

Figure 4-14: Particle size distribution (PSD) of AgNPs

4.3.3 Crystallographic arrangements of AgNPs analysis

The crystalline structure of AgNPs with and without calcination was identified by using XRD as shown in figure 4-15. The XRD pattern of AgNPs without calcination was characterized by six intense peaks. This is attributed to Ag nanoparticles and bio-organic phase in the whole spectrum of 2θ values ranging from 23 to 80 degrees that were synthesized by using Vernonia amygdalina plant leaves extract. From the two XRD patterns, AgNPs with and without calcination was compared targeting to analyse the impacts of *V. amygdalina* plant leaves extract on AgNPs synthesis.

The peaks position of 2θ values 38.23°, 44.42°, 64.58°, and 77.51° are attributed to calcined AgNPs and 38.18°, 44.19°, 64.58°, and 77.33° resembled AgNPs without calcination respectively. This indicates that the formation of silver nanoparticles (Desalegn et al., 2021).

These results of 2θ value are in good agreement with the data of JCPDS/ICPD file card no. 00-004-7383 (Fm-3m) (Sadeghi et al., 2015).

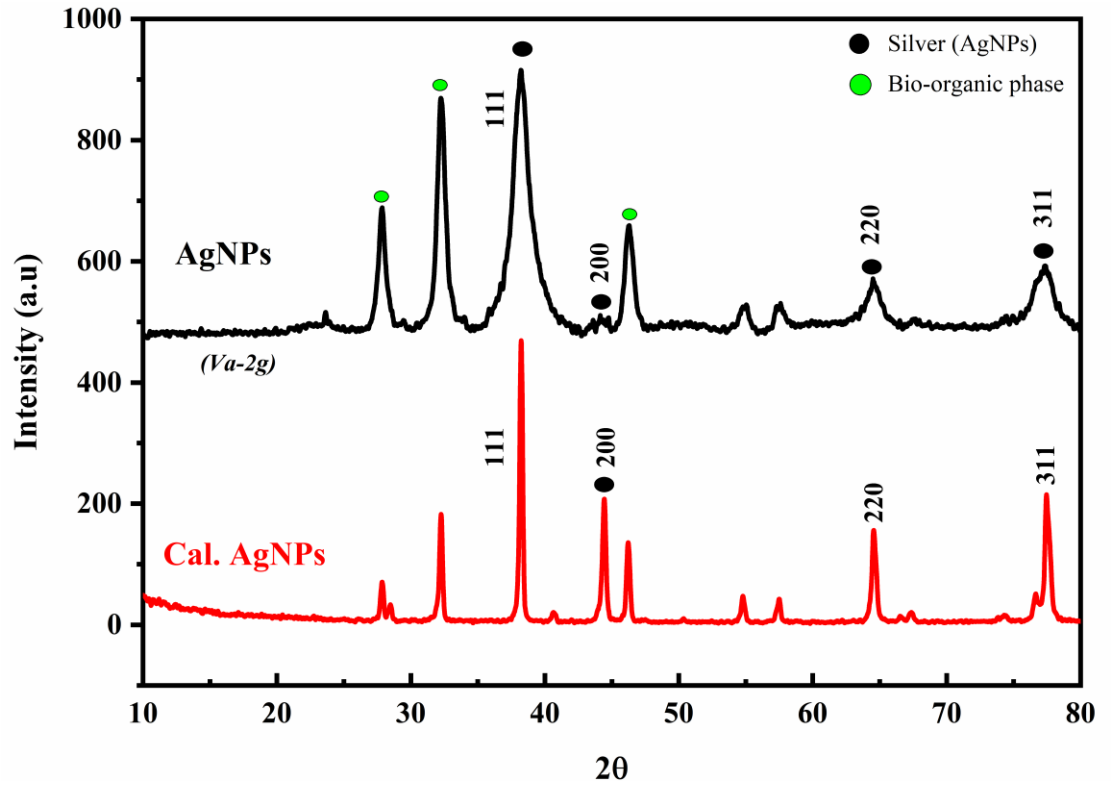

Figure 4-15: XRD of AgNPs without calcination (black) and Calcined. AgNPs (red)

In addition, the XRD results of AgNPs agreed well with the literature on the green synthesis of AgNPs using *Vernonia amygdalina* plant extract (Aisida et al., 2019). The other peaks were attributed to the formation of the bio-organic phase from organic compounds present in the *Vernonia amygdalina* plant extract. This was responsible for reducing Ag ions, stabilizing and capping agent of synthesized nanoparticles. Those peaks have occurred at 27.82°, 32.23°, and 46.36° peak positions. The other small impurity peaks may be due to the coupling reaction with the polyphenolic (OH) group and due to the highly hygroscopic nature of Ag nanoparticles (Aisida et al., 2019).

The comparison of the two XRD results for calcined AgNPs and AgNPs without calcination was done based on the shifting of 2θ values, crystallite size, and d-spacing of AgNPs. The average crystallite size of AgNPs with and without calcination calculated Scherrer equation is 26.71 nm and 30.48 nm, respectively, as shown in table 4-5. The crystallite size values are in good agreement with the study in the literature (Yazdanshenas et al., 2012), in which they reported the crystallite size of Ag 21.33 nm, 26.66 nm and 53.32 nm with different alkali pre-treatment.

The details of crystallite size are calculated and tabulated in appendix 11 and 12. The major 2θ values of AgNPs without calcination were shifted to the lower 2θ values due to

the presence of *Vernonia amygdalina* plant leaves extract. As shown in figure 4.16 the plant extract enters into the inner part of AgNPs grain with a different spatial arrangement, then forces the nanoparticles to expand or to increase in diameter. That is the reason for the occurrence of broadening peaks (black line in figure 4-15).

Whereas when the nanoparticles were passed through the calcination process to remove the organic components that come from the plant, the crystallite size of the AgNPs was decreased. It was possible to understand the influence of the plant leaves extract on the synthesis of AgNPs. The indications for the removal of plant leaf extract during calcination were that some intense peaks on AgNPs without calcination were partially removed and for some of them, there was a decrease in intensity also during calcination. The removal of plant extract gave a chance for AgNPs to become highly intense and exposed (peak at 44.19°).

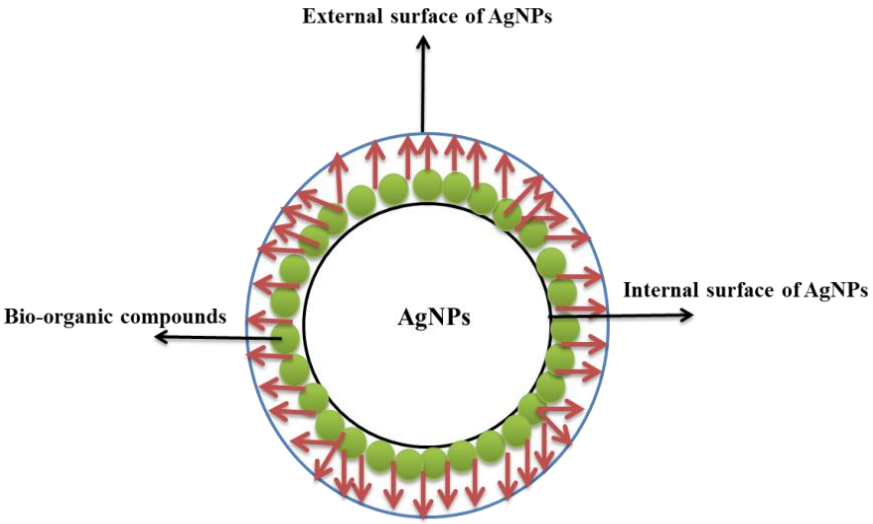

Figure 4-16: Effects of bio-organic compounds on AgNPs

The d-spacing calculated by using Bragg's equation of AgNPs with and without calcination, the results became 0.203 nm and 0.220 nm respectively. The details of the d-spacing calculation are tabulated in appendix 13 and 14. From the above three results (2θ values, crystallite size and d-spacing of AgNPs), it could be concluded that the addition of *Vernonia amygdalina* plant leaves extract increases the d-spacing of AgNPs and caused the shifting of 2θ values to the lower.

This indicates the *amygdalina* plant leaves extract was placed in the inner parts of AgNPs, due to that, the pressure from plant extract AgNPs tends to expand and causes the increasing (broadenings of peaks) of the d-spacing, shifting 2θ to the lower values for

AgNPs without calcination. The d-spacing of AgNPs is agreed with the values reported in the literature (Krithiga et al., 2015). The crystallite size of AgNPs without calcination also increases, it was understandable that the great impacts of plant leaf extract on the AgNPs synthesis, stabilizing and capping agent, which is supported by literature (Nzekekwu et al., 2019).

4.3.4 Macromolecular arrangements of greenly synthesized AgNPs

The functional group for the formed AgNPs and the presence of the plant components on the AgNPs were examined by using FTIR analysis, with the comparison of calcined AgNPs, FTIR of plant and AgNPs without calcination. As shown in figure 4-17, the functional groups of pure plant extract, the interaction between green synthesised AgNPs and plant extract and calcined AgNPs were analysed by FTIR spectroscopy. During the synthesis of AgNPs, reactions took place between silver nitrate and *Vernonia amygdalina* leaf extract. *V. amygdalina* act as reducing, capping, and stabilizing agents, therefore, FTIR measurements were carried out to identify the possible impacts of biomolecules before and after bio-reduction, which showed significant changes.

The presence of a capping agent on AgNPs or the presence of bio-organic functional groups that were responsible for bio-reduction was confirmed by the FTIR spectrum and showed peaks at 3303 cm^{-1}, 1588 $cm^{-1,}$ and 1110 cm^{-1}, the spectrum at 3303 cm^{-1} is due to the existence of OH stretching from phenolic compounds, it bonded directly to an intense aromatic hydrocarbon group at 1110 cm^{-1}. The availability of a peak at 1588 cm^{-1} which was attributed to amide protein supported the above discussion. The availability of the FTIR spectrum peaks at 3303 cm^{-1}, 2932 cm^{-1}, 1588 cm^{-1}, 1385 $cm^{-1,}$ and 1116 cm^{-1} indicating the presence of a capping agent within the AgNPs.

Generally, on the calcined AgNPs some of the bio-organic compounds of the plant extract were completely removed and some of them are decreased in intensity on the calcined AgNPs of the fingerprint region. However, the peak areas of pure AgNPs and Ag oxide bond were highly shined which were masked by plant extract. This discussion is supported by XRD the peak at 44.19^0, which shined during calcination. From figure 4-17 in the calcined AgNPs and plant leaf, there were sharp peaks around 3420 cm^{-1} and 3380 cm^{-1} respectively. There are shifted and a highly broad peak in calcined AgNPs, indicating hydroxyl groups OH stretching (Karthik et al., 2020).

Because the wavenumber in the calcined AgNPs is less than (larger wavelength) that of AgNPs without calcination, a broad OH peak occurred. Whereas a very weak peak was

created on the AgNPs without calcination. This implies that the peak difference between the two materials was due to the presence of plant leaf extract on AgNPs without calcination and the removal of plant leaf extract during calcination (Cal. AgNPs). Our discussion is supported by the study of the green synthesis and characterization of AgNPs using bitter and Neem leaf extract by Nzekekwu Ak. et al. (Nzekekwu et al., 2019).

In calcined AgNPs the stretching vibrations of OH bonds were observed at 3488 cm^{-1}-3420 cm^{-1}, because of the availability of the -CH (CH_3)-OH functional group, this was due to the removal of *V. amygdalina* leaf extract, the bonds between the AgNPs are free to stretch in all directions. There was a peak at 2078 cm^{-1} which is attributed to CH_3 (Aisida et al., 2019; Huq, 2020).

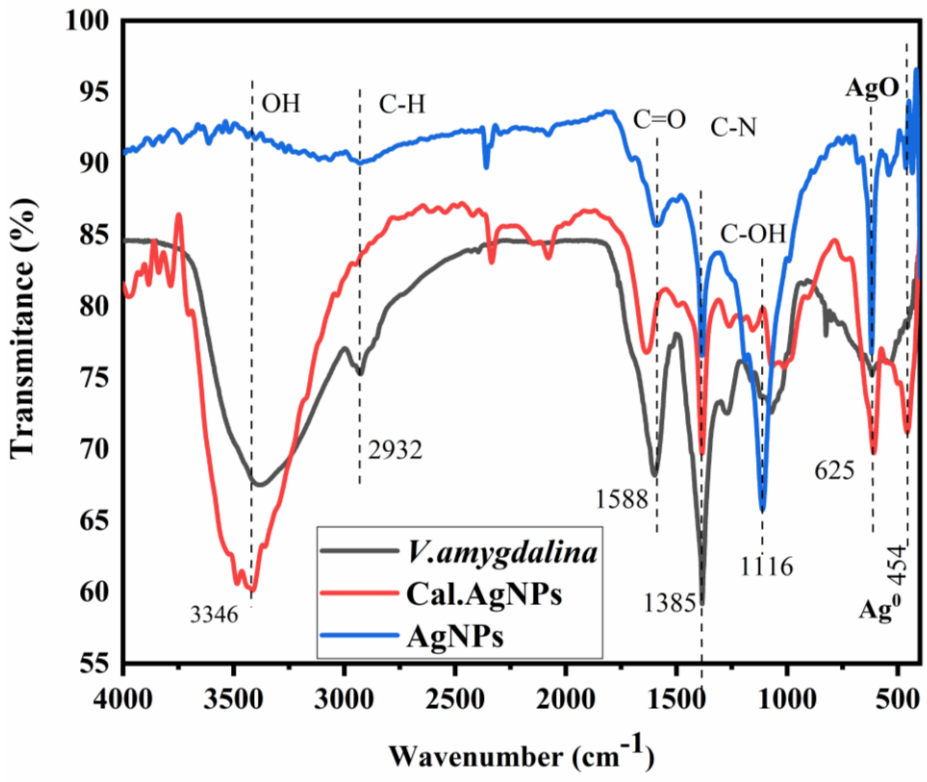

Figure 4-17: FTIR spectra of synthesized AgNPs (blue line), calcined AgNPs (red line), and *V. amygdalina* plant extract (black).

The peaks which occurred at shifted peak 1588 cm^{-1} were attributed to the stretching vibration of C=O (carbonyl group) in AgNPs due to the presence of –CH CO-O- functional group, which was shifted on Cal. AgNPs (1633 cm^{-1}) from the plant spectrum.

In the fingerprint regions of the FTIR, the stretching vibration of C-N bonds (alkane) was at the same wavenumber around 1385 cm^{-1} for three of them (AgNPs, calcined AgNPs, and *Vernonia amygdalina* plant) due to the availability of aromatic amines functional group.

However, the intensity of this functional group decreased on the calcined AgNPs spectrum, which indicates the removal of bio-organic compounds in some amount from the nanoparticles. The bending vibrations of Ag-O-H bonds were represented by a peak at 625 cm^{-1} for AgNPs, without calcination which was shifted to 611 cm^{-1} for calcined AgNPs, which was attributed to the presence of the Ag-O bond. The pure metal Ag^{o} (AgNPs) occurred at 454 cm^{-1}. This discussion is in good agreement with the study of (Aisida et al., 2019) in which they found the Ag-O bond at 682 peaks.

4.4 Stability of AgNPs within GLY-LAC matrix

4.4.1 The effects of surface charge on dispersions and stability of AgNPs

The stability and uniform distribution of AgNPs within GLY-LAC were described with zeta potential, SEM, FTIR and particle size distribution. The magnitude of the zeta potential indicates the potential stability of the colloidal system; a colloidal system is a system when a solid is dispersed within a liquid. According to the Malvern user manual (MAN0485 Issue 1.1 April 2013) and a lot of works of literature, particles with zeta potentials more positive than 30 mV or more negative than -30 mV are normally considered stable. This is related to the charge density on the surface. Zero becomes the least stable point (Isoelectric point), and a less negative and less positive number indicates unstable suspensions. Based on these, when referring to the zeta potential values of the AgNPs in colloidal nature as shown in figure 4.18, the value became -27.2 mV which is close to -30 mV.

Because of the availability of the plant extract on the surface or within the AgNPs as stabilizing and capping agent, gave the nanoparticles different properties such as long term stability, colloidal nature, and high dispersity of green synthesized Ag nanoparticles within the GLY-LAC (Ahmadi et al., 2020), (P. Kumar et al., 2013), (Jemilugba et al., 2019). When comparing our result with those literature values, the zeta potential value which we get is very large, therefore, the stability of AgNPs with *V. amygdalina* leaf extract was high.

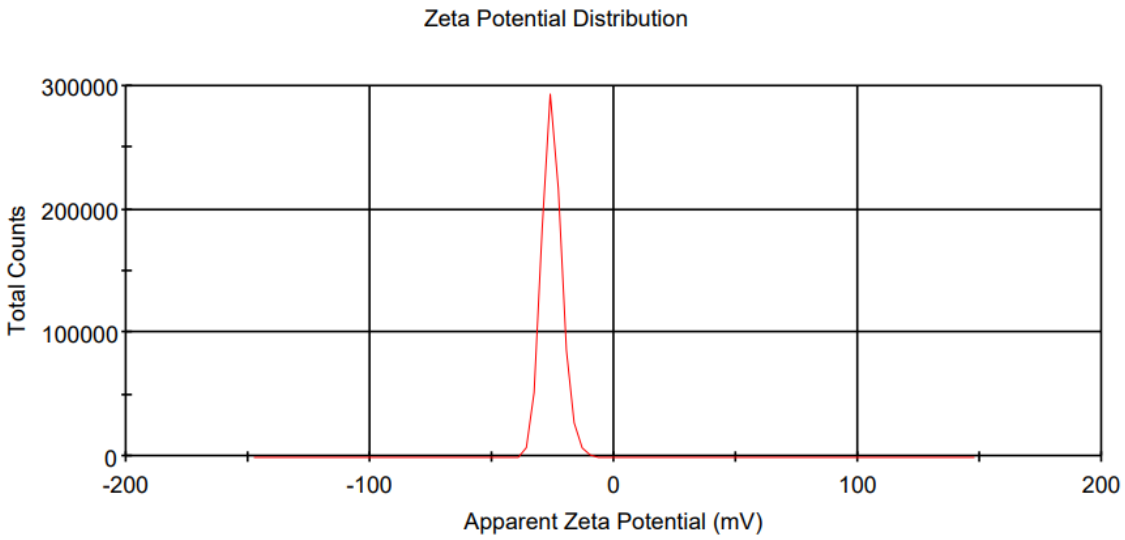

Figure 4-18: Zeta potential of synthesized AgNPs with calcination

The negative sign on zeta potential values indicates the net charge on the surface of AgNPs including up to the slipping plane, therefore, it had the potential of attracting positively charged particles from the external surface (dispersed solution). As shown in figure 4.19, due to the surface charge on AgNPs the positively charged particles were highly accumulated and attached to AgNPs.

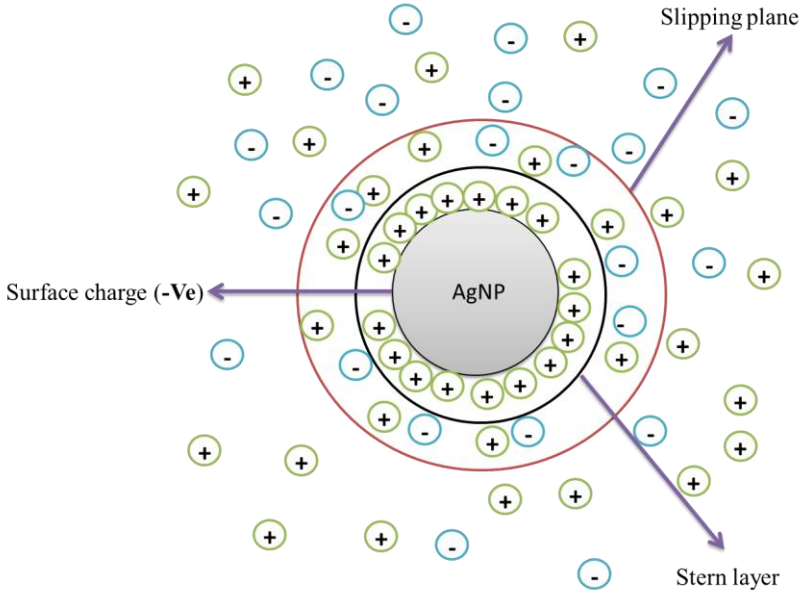

Figure 4-19: Colloidal dispersion of AgNPs (zeta potential)

The AgNPs particles in GLY-LAC suspension had a large negative zeta potential (-27.2 mV), which indicates the degree of electrostatic repulsion with similarly charged other AgNPs atoms adjacent to it within the dispersion. Therefore those nanoparticles tended to

repel each other and there was a big tendency for AgNPs to be well dispersed within the solution. This means that the AgNPs were neither flocculated nor agglomerated and settled down; the AgNPs resisted aggregation. The details of zeta potential measured data by the Malvern instrument were attached to the appendix part (Appendix 10).

From the data, the zeta potential of AgNPs is large; therefore there is no force to prevent the particles from well dispersed, as shown in figure 4.20. The synthesized Ag nanoparticles were well dispersed and stable even at room temperature, which means it was electrically stabilized. The stability of AgNPs within the GLY-LAC matrix is supported by a PSA analysis of the AgNPs dispersed matrix below.

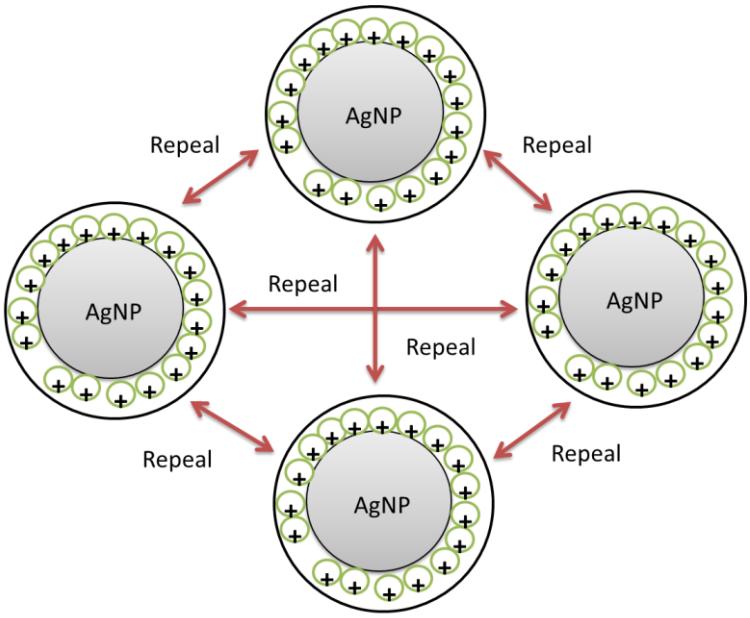

Figure 4-20: Resistance of AgNPs from the formation of agglomeration through repulsion

The surface charge of the AgNPs which was dispersed in the GLY-LAC highly affects the size of AgNPs as it is dispersed in the matrix, therefore the particle size of AgNPs/GLY-LAC was analysed by using PSA.

4.4.2 Particle size distribution of AgNPs within GLY-LAC

As shown below in figure 4-21, the particle size distribution of the nano-silver particles prepared was mono-dispersed within GLY-LAC. The particle size distribution was uniform which was confirmed by PSA analysis. It was obvious that uniform and stable dispersion of nanoparticles depend on the particle size of the particles. As the size of the particle become smaller its specific surface area to volume ratio became larger. Finally, the dispersion became stable because the higher the surface energy there was the greater the intermolecular force between those particles.

As shown in figure 4.14, the Particle size distribution (PSD) of AgNPs without dispersion within GLY-LAC was recorded with poly-dispersity of two peaks; peak-1 had 56.45 nm particle sizes with 66.5% intensity. The second peak was recorded with very lower particle size 3.05 nm with 33.5% intensity. But when the particle size distributions of AgNPs dispersed GLY-LAC was measured, as shown in figure 4-21 the size was increased to 33 nm, due to the availability of GLY-LAC matrix which is used as a carrier matrix and prevents the migration of nano-silver particles by carrying through its OH end functional group as well as due to the presence of GLY-LAC (Dong et al., 2019). The details of PSA measured data by Malvern instrument were attached in the appendix part (Appendix 1).

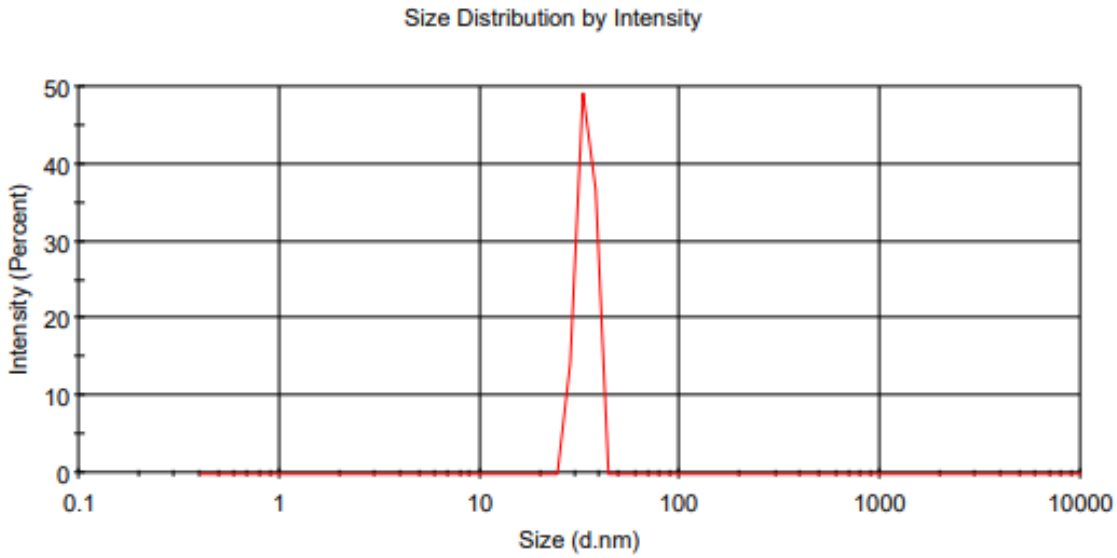

Figure 4-21: Particle size distribution of AgNPs within GLY-LAC matrix

The macromolecular arrangement of AgNPs dispersion within the GLY-LAC was analysed with different drying times to study the effects of drying time on the dispersion of AgNPs into GLY-LAC.

4.4.3 Macromolecular arrangements of AgNPs within GLY-LAC

FT-IR spectroscopy was used to characterize the chemical structure between the AgNPs and GLY-LAC at different drying times (12 hr., 24 hr., and 36 hr.). The strong absorption peak at 3462 cm^{-1} corresponds to the stretching vibration of the hydroxyl group of water. The functional group of GLY-LAC was analysed in figure 4.8 in section 4.1.5, in which the main indicator for the formation of the GLY-LAC matrix was the existence of an ester functional group or a carbonyl group. The ester bond occurred for both bio-conjugate at 1743 cm^{-1} and this peak was slightly shifted to 1748 cm^{-1} after AgNPs were incorporated as shown in figure 4.22. The presence of the OH functional group was evidenced by a broad

peak found at 3415 cm^{-1} on the FTIR spectrum of GLY-LAC conjugate, whereas when the bio-conjugate was incorporated with AgNPs, this peak was shifted to the higher position to 3465 cm^{-1} due to stretching by a huge OH functional group from AgNPs.

During drying of the matrix, for 36 hr., these OH peaks had very lower intensity relative to 12 hr. and 24 hr. drying time. This was very important for the dispersions and stability of AgNPs within GLY-LAC. Whereas during 12 hr. drying of the matrix, the OH functional group was at a very broad and intense peak which indicates that there was a large amount of OH functional group within the matrix, which did not interact with AgNPs. In another case, a transmittance peak was observed at 940 cm^{-1} that was for the C-O on GLY-LAC but during the mixing of AgNPs with GLY-LAC, there was a slight shifting of peak position, and the peak was found at 1048 cm^{-1} due to C-O stretching in secondary OH group of glycerol.

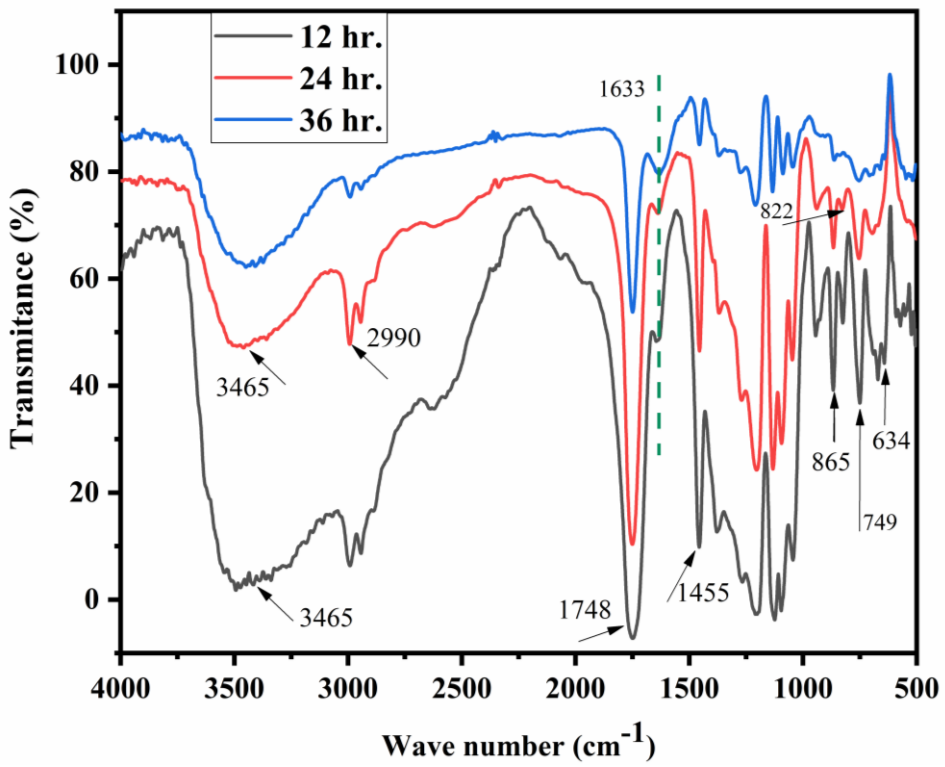

Figure 4-22: Functional group analysis for synthesized AgNPs with 12 hr., 24 hr., and 36 hr. drying time

The stretching of CH_3 at 2929 cm^{-1} for GLY-LAC was changed position to 2990 cm^{-1} due to the presence of nanoparticles. All the transmittance peaks attributed to pure GLY-LAC macromolecules were found on the FTIR spectrum of the AgNPs/GLY-LAC matrix. In the FTIR spectrum of AgNPs which was discussed in section 4.3.4, the formation of silver

nanoparticles was confirmed by the bending vibrations of Ag-OH bonds represented by the peak at 634 cm^{-1} for AgNPs. This was attributed to the presence of the Ag-O bond as shown in figure 4.22. Due to the presence of AgNPs and due to the hygroscopic nature of the silver, the OH group circled the nanoparticles there was a suppressed interaction between C=O and OH bond, which is why those peaks decreased in intensity.

Therefore for the dispersions as well as for stability issues of AgNPs within the GLY-LAC matrix, drying the mixtures (AgNPs/GLY-LAC) for 36 hr. is best to have more stable and uniform dispersions of nanoparticles within the bio-conjugate as shown in figure 4.23. It is easy to understand that physically there were uniform dispersions of nanoparticles, which were dried for 36 hr. in an air-drying oven from prepared film and supported by figure 4.22 FTIR spectrum analyses.

As wavenumber increases wavelength decrease but the energy and frequency also directly increase with wavenumber, this means that the interaction between C=O with Ag forms hydrogen bonding. Due to the formation of hydrogen bonding, the energy requirement of AgNPs stabilizes its dispersion within the base matrix (GLY-LAC) also increases. This is supported by the shifting of the wavenumber to higher as drying time increases from 12 hr. to 36 hr. The intensity ratio regarding the shoulder peak at 1643 cm^{-1} to the peak at 1748 cm^{-1} for 12 hr. drying was higher than those two peaks which means that the (C=O) major peak was bigger than the shoulder peak, but in the two peaks of 24 hr. and 36 hr. drying time. This explanation became reversed, as the drying time increased the major peak (C=O) intensity diminished, but the shoulder peak became increased in intensity.

This was due to the formation of stable point AgNPs with GLY-LAC matrix as the drying time gets increased, (C=O) and AgNPs get the chance to interact with each other, in which hydrogen bonding was formed between AgNPs and GLY-LAC. From the shifting of the (C=O) peak through increased drying time, the peak for 12 hr. drying was at 1748 cm^{-1} and for 24 hr. and 36 hr. drying time the peak was shifted to 1752 cm^{-1}. Therefore it is possible to conclude that the mass of the (C=O) molecule was reduced and the interaction of AgNPs and GLY-LAC was favoured. This discussion is supported by the green synthesis of silver nanoparticles by OT Jemilugba and they reported that the C=O ester bond shifted from 1713 cm^{-1} to 1705 cm^{-1} due to the incorporation of AgNPs with C=O (Jemilugba et al., 2019).

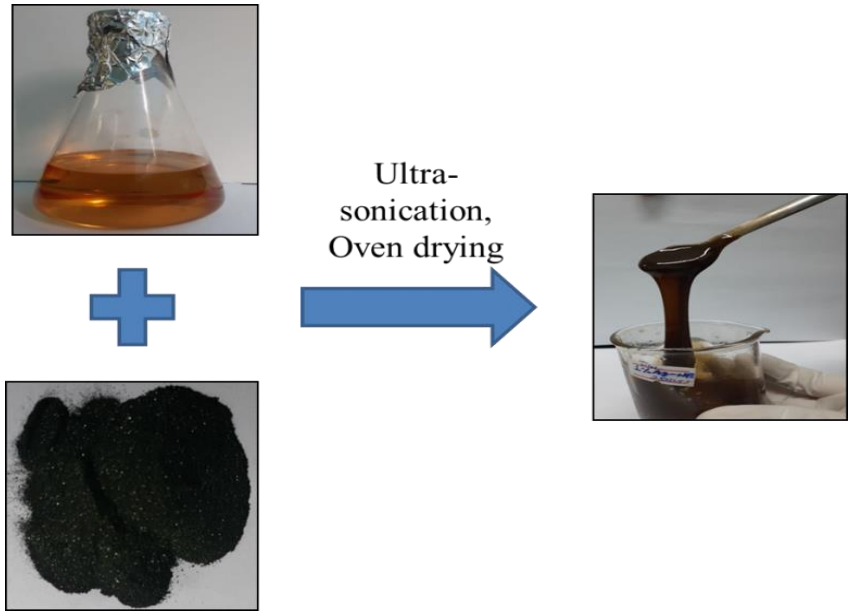

Figure 4-23: Dispersions of AgNPs into GLY-LAC bio-conjugate

Finally, the dispersions of AgNPs within GLY-LAC were confirmed by using SEM analysis for the three samples, GLY-LAC/PLA, AgNPs/PLA and AgNPs/GLY-LAC/PLA.

4.4.4 Morphological analysis of AgNPs/GLY-LAC

The dispersion of Ag nanoparticles within the GLY-LAC matrix was evaluated using SEM. Uniform and well dispersion of AgNPs was required for its effectiveness within the PLA matrix; there was a poor dispersion of AgNPs within the PLA when only pure Ag was dispersed, because of the agglomeration of the Ag nanoparticles. Due to this, the expected network within PLA was disrupted as shown in figure 4.24 (B). The comparison regarding dispersions was done for the three matrices, (A) SEM image of GLY-LAC/PLA, (B) SEM image of AgNPs/PLA here dispersions was done without the addition of GLY-LAC matrix, and (C) AgNPs/GLY-LAC/PLA, the fourth (D) was scanned at 5 µm with the same sample with (C) for magnification to show in detail.

Figure 4-24, (A) was used for the confirmation of the dispersions of pure GLY-LAC within PLA. The SEM image showed a clear structure of GLY-LAC. “B” shows the dispersion of AgNPs into PLA without GLY-LAC, the dispersions were not good because of the particles dispersed as apart to each other on some parts (as shown by arrows) of the PLA, due to the lack of GLY-LAC as a base matrix.

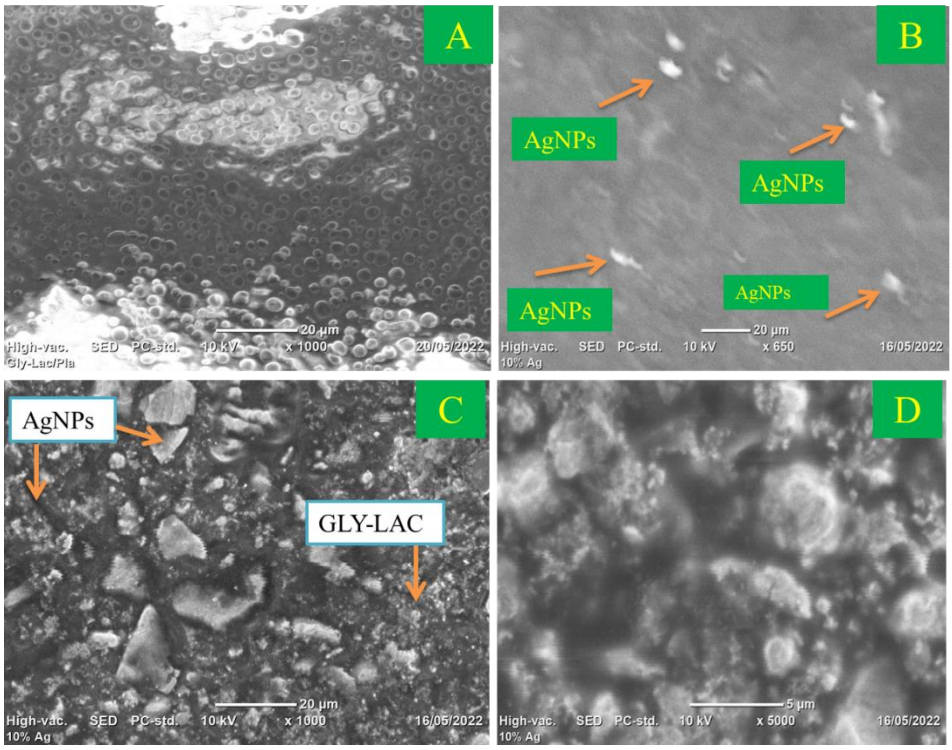

Figure 4-24: SEM images of (A) GLY-LAC/PLA film, (B) AgNPs/PLA film, (C) AgNPs/ GLY-LAC/PLA and (D) AgNPs/ GLY-LAC/PLA at 5 µm

As shown in (C) due to the presence of the GLY-LAC matrix as a carrier matrix the uniform AgNPs dispersion was occurred throughout the entire PLA surface, because of the base matrix the GLY-LAC has a long chain and OH end group which made it to act as a lubricant/carrier by creating a room for the nanoparticles, so that they slide one to another then no agglomeration was formed. A homogenous and stable dispersion was formed, here gives information on AgNPs embedded within PLA. As described in section 3.2.5 the dispersion was done by magnetically stirred solution and was passed through an ultra-sonication process. But when the base matrix which was GLY-LAC removed, the AgNPs were agglomerated within some parts of PLA (as shown by arrow on "B"). These stable dispersions of AgNPs showed in detail on a 5 µm image (Pinto et al., 2017).

After the confirmation of well, uniform and stable dispersions of AgNPs within the GLY-LAC, their individual as well as combined effects of the PLA were studied through preparing biopolymer film in the solution casting method.

4.5 Nucleation effect of GLY-LAC on the crystallization of PLA

DSC analysis was taken to study the effects of nucleating agents (GLY-LAC) on the crystallization behaviour of PLA. From the DSC plot (thermo-gram) it was possible to get the melting temperature (T_m), melting enthalpy (ΔH_m), glass transition temperature, crystallization temperature (T_C), crystallization enthalpy (ΔH_C) parameters, which were finally used to calculate the degree of crystallinity (X_C) of PLA. Below in figure 4.25, DSC curves of neat PLA and mixtures of PLA with 10wt% loading of GLY-LAC (1:3,1:6,1:9,1:12) were shown, and the annealing was taken place at 110 ℃ for 150 minutes. The calculated degree of crystallinity and other numerical values from the heating curve were summarized in table 4-5. The degree of crystallinity of PLA and PLA/GLY-LAC composite films were calculated using equation (3.5) (Farhoodi et al., 2012; Srithep et al., 2013).

From the existed solid NAs, GLY-LAC nucleating agents differ in their synergetic properties, which act as crystallizers as well as plasticizer agents within the PLA matrix. Because only the PLA matrix chains were going through crystallization, not the incorporated nucleating agent, therefore the nucleating agent could freely move within the PLA matrix. The main difference between those nucleating agents (GLY-LAC 1:3, GLY-LAC 1:6, GLY-LAC 1:9, and GLY-LAC 1:12) was their chain length, as the mixing ratio of lactic acid to glycerol increases, the chain length also increases. Depending on the chain length of GLY-LAC, the formation of the amorphous and crystalline structures formed also varied. By its nature, PLA is a semi-crystalline polymer that has an amorphous and crystalline region, in its amorphous state no crystallization occurs during fast cooling.

When the nucleating agent (GLY-LAC) was incorporated with PLA, the crystalline region of PLA become more crystallized by initiating its crystallization using GLY-LAC, so that the crystallization of the PLA became more improved and also in the amorphous region of PLA, the nucleating agent promotes or increases the tendency of amorphous state by acting as a plasticizer. During solution casting the previous thermal history of PLA was erased which means PLA's become completely amorphous from its semi-crystalline nature so that PLA starts crystallization after incorporation of the nucleating agent from zero (Aliotta et al., 2017).

The comparisons for those four nucleating agents were done based on their percentage of the degree of crystallinity on PLA and the values were used to quantify the effectiveness of

the four nucleating agents with constant parameters. During one variable at a time study (OVAT), the first two parameters (temperature and time) were taken as constant at 110 ℃ and 150 minutes, respectively.

Based on the neat PLA crystallization temperature and the requirement for a longer crystallization time due to its slow crystallization, literature reported that PLA starts crystallization at 110 ℃ (Bhandari et al., 2019; Simmons et al., 2019). The advantage of improving the degree of crystallinity of PLA is that there was a decrease in the PLA degradation rate: when PLA had semi-crystalline properties its degradation rate in 60 days was 30%, whereas amorphous samples reached 60% degradation in only 35 days (Pérez-Fonseca et al., 2016).

From the calculated degree of crystallinity of the neat PLA and PLA with the GLY-LAC nucleating agent, it was possible to conclude that the incorporation of the nucleating agent significantly enhanced the crystallization of PLA and GLY-LAC served as a nucleating agent. With the incorporation of GLY-LAC 1:3, GLY-LAC 1:6, and GLY-LAC 1:9 within PLA there was an increment in degree of crystallinity of 68.8%, 85.2%, and 71% respectively, when compared with the neat PLA which was 61.8%. However, for the GLY-LAC 1:12, the crystallinity was decreased even from the neat PLA as shown in figure 4-25.

Table 4.5: Calculated degree of crystallinity of annealed neat PLA and GLY-LAC /PLA

Sample	T_g(℃)	$\Delta H_m(J/g)$	T_m(℃)	X_c(%)
Neat PLA (with)	56.71	58	154.69	61.8
PLA/GLY-LAC 1:3	45.56	64.5	150.83	68.8
PLA/GLY-LAC 1:6	45.034	79.8	150.67	85.2
PLA/GLY-LAC 1:9	44.71	66.56	150.83	71
PLA/GLY-LAC 1:12	47.13	40.2	151.21	42.9

These results indicated that the crystallization degree of PLA was improved with the incorporation of the nucleating agent that had a medium chain length, but when the chain length of the nucleating agent becomes larger (as the chain extended highly), the nucleating agent (GLY-LAC) hinders the polymer from crystallization. It is possible to conclude that the nucleating agent (GLY-LAC 1:12) was attributed to the plasticizer instead of the crystallizer, the plasticity property of GLY-LAC 1:12 was also advantageous in improving the higher brittleness of PLA (Lule et al., 2018).

As the chain length becomes large the OH functional group of the 3-armed GLY-LAC become a lot and then those OH react, attached, and entangle the matrix of PLA which produce folding, which favours the increment of the amorphous part rather than forming a crystalline region. They also provide a large free volume within the PLA matrix then GLY-LAC 1:12 nucleating agent makes the PLA matrix become very flexible and slide one over another, which means that GLY-LAC 1:12 acts as a lubricant also. That was why the degree of crystallinity was becomes lower (42.9%). This analysis was supported by the increment of glass transition temperature from 44.71 ℃ to 47.13 ℃, which means that chain movement or the flexibility of PLA increased with the addition of GLY-LAC 1:12, in which it embedded itself between PLA chains and created a large free space to make the PLA move freely (Lule et al., 2018).

Therefore GLY-LAC 1:6 was selected for the next study among other NAs due to its higher degree of crystallinity (85.2%), to use it as the best NAs. These measurements were repeated three times to confirm the quality of the result and the averaged degree of crystallinity was taken for a GLY-LAC 1:6 film sample. This improvement was supported by the study which focuses on annealing, only by using annealing the degree of crystallinity of PLA was improved from 16.39% to 49.56% (Srithep et al., 2013).

The incorporation of GLY-LAC within the PLA matrix improves both the glass transition (decreased by GLY-LAC) and melting temperature of PLA; indicating that GLY-LAC acts as an efficient NAs. On the endothermic process during heating, a melting peak was observed for the entire matrix including neat PLA, those peaks occur at about 150-154 ℃, and the peaks occurred because of the enhanced crystallinity of PLA (melt crystallization).

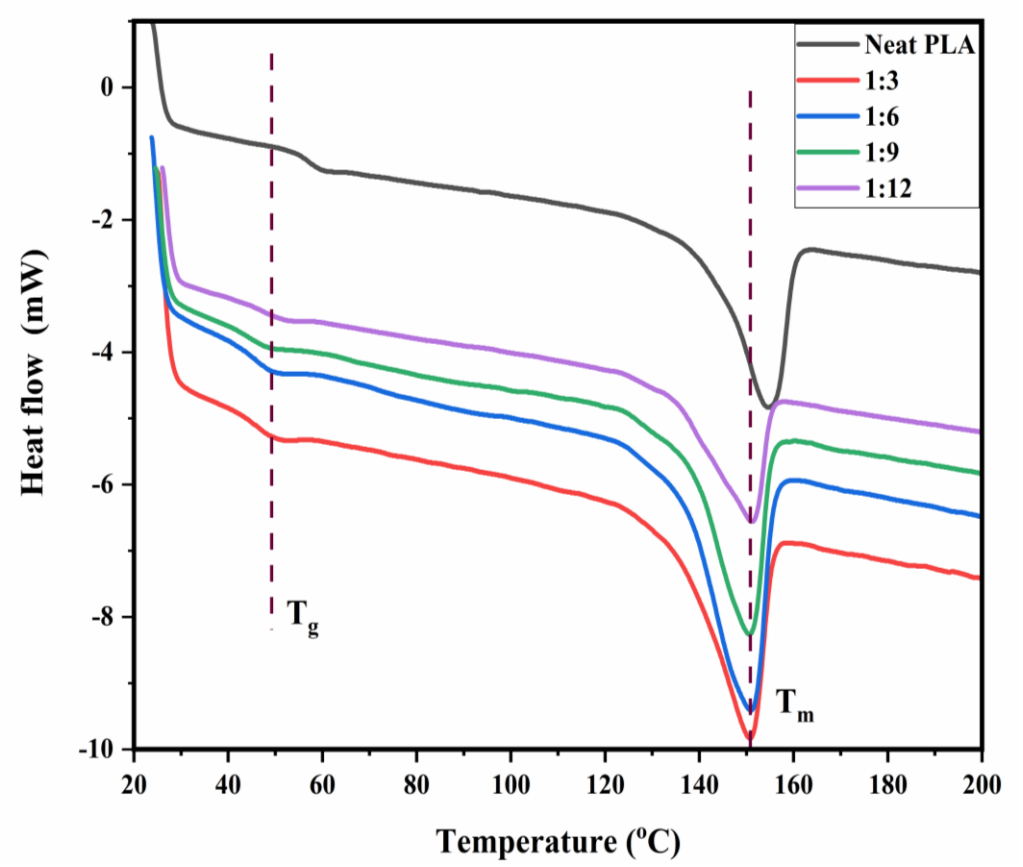

Figure 4-25: The heating cycle of neat PLA and PLA/GLY-LAC (GLY-LAC 1:3, 1:6 1:9, 1:12)

That was why the melting process requires a large amount of enthalpy as shown in table 4.9 to convert crystalline solid PLA into a liquid, 64.5 J/g, 79.8 J/g, 66.56 J/g were enthalpy for GLY-LAC 1:3, 1:6 and 1:9 respectively, however for the neat PLA and GLY-LAC 1:12 the melting enthalpy requirement was small, which indicate the neat PLA was in a semi-crystalline state, these are why requires less amount of melting enthalpy.

As glass transition temperature was decreased from 56.71 ℃ to 44.71 ℃ and the melting temperature also decreased from 154.69 ℃ to 150.83 ℃, due to the relaxation of the PLA matrix, it requires a lower temperature to melt, but as T_g increased for GLY-LAC 1:12 the T_m also increased. The observed melting peaks were used as evidence for the indication that all of the GLY-LAC nucleating agents expect the GLY-LAC 1:12 matrixes to promote the crystallization rate of PLA, whereas their nucleation capacity varied with their chain length. These discussions were supported by the study in which they examined the poly (lactide) stereo-complexes nucleating agent influence on the crystallization behaviour of poly (lactide), the four-armed PLA enhance the degree of crystallization, this was due to the chain length of four-armed PLA stereo-complexes (Ji et al., 2019). Therefore due to the

improvement of PLA crystallinity, its mechanical properties also improved its application area become expanded such as in the piping industry, 3D printing, and others.

From the thermo-gram plot in figure 4-25 of the heating curve, the T_g (glass transition temperature) of neat PLA was larger (56.71 ℃) than those PLA with a nucleating agent. This implies that without a nucleating agent PLA was in its rigid state (higher T_g) or higher T_g, the chain mobility of PLA was reduced, which means that it requires a large amount of energy to become flexible/soften from its rigid state property. However, after the addition of different nucleating agents (GLY-LAC), this rigid part of PLA shifted into the softened (flexible) state, which made the T_g of the PLA lower.

Here also the energy (enthalpy) requirement of the PLA changed from a rigidity state into a soft state was very low but in neat PLA this energy requirement was very high. Glass transition temperature is a temperature range in which polymer is transformed from a rigid state into a flexible state. The above discussion could be in good agreement with the study which was focused on the effects of alumina loading percentage on PLA properties, in which the incorporation of alumina there was a shifting in T_g of PLA to the lower temperature (Lule et al., 2018).

Due to GLY-LAC 1:12 having lower crystallization ability, the glass transition temperature becomes lower when compared with neat PLA. These analyses agree with the discussion which focuses on using DEET (N,N-diethyl-3-methylbenzamide) as a plasticizer for PLA, which efficiently decreases the glass transition temperature of the PLA from 62 ℃ to 50.5 ℃ (Du et al., 2020). The main advantage of the decrement in T_g was it provides a faster crystal growth rate because polymer chains are free to move and made easier the formation of ordered chains, but here it takes a longer nucleation time.

Effects of annealing on neat PLA

Treating materials, especially polymers with isothermal as well as non-isothermal temperatures completely had a great impact on the physical and chemical properties of the materials. As shown below in figure 4-26 and the tabulated numerical values, when the neat PLA was annealed at 110 ℃ isothermal temperatures for 2 hr. 30 minutes, during annealing the glass transition temperature was decreased from 61.6 ℃ to 56.71 ℃, which indicates the formation of regularly arranged crystals, therefore due to annealing, the T_g became lower which means that the PLA became soften at a lower temperature, which was very advantageous regarding energy cost.

As shown in table 4-6 the melting temperature was also increased from 143 ℃ to 154.69 ℃, in which a large amount of energy was required during the process of annealing PLA, because of the formation of a higher crystallized structure, a large amount of energy was required to melt the crystallized part. Annealing of PLA had improved the chain arrangement of polymer into the regularly ordered matrix, which was why the thermal properties of annealed PLA were improved. The crystallinity of neat PLA without annealing was lower than that of annealed PLA (33% to 61.8%).

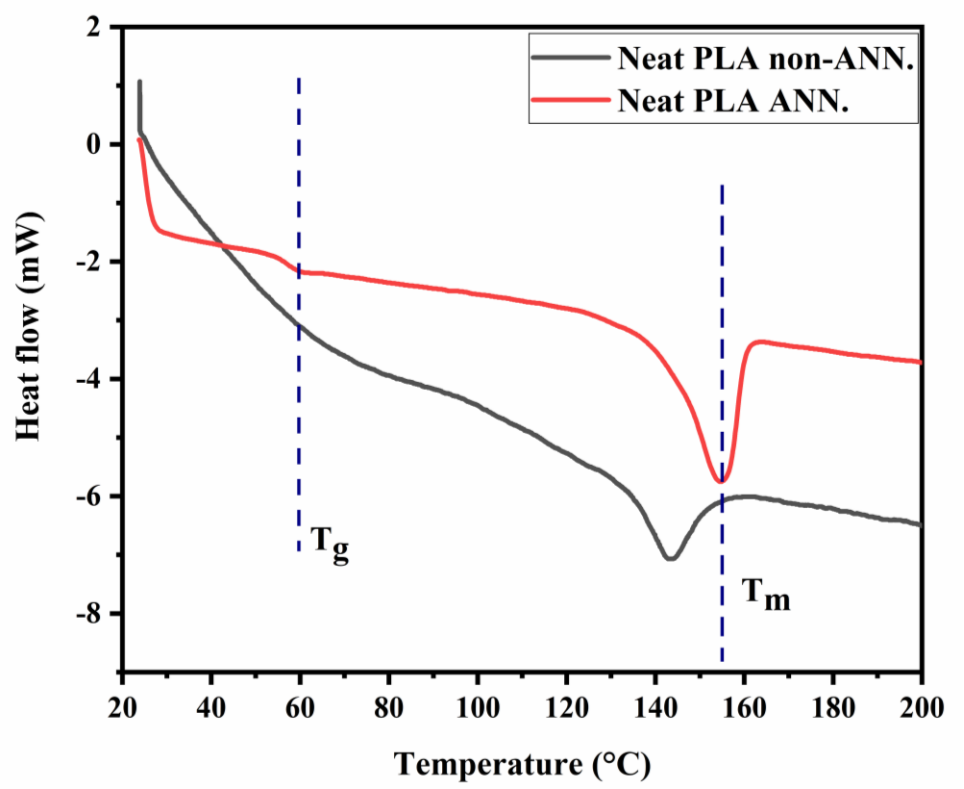

Figure 4-26: The heating cycle of neat PLA without and without annealing

Table 4.6: Calculated degree of crystallinity of neat PLA with and without annealing

Sample	T_g(℃)	$\Delta H_m(J/g)$	T_m(℃)	X_c(%)
Neat PLA (non-annealed)	61.6	31	143	33
Neat PLA (annealed)	56.71	58	154.69	61.8

Research that focuses on the study of the annealing effect on PLA properties by A. A. Perez-Fonseca, on their study they found that degree of crystallinity of neat PLA before

annealing was 47.7% and after annealing was done for the same neat PLA degree of crystallinity become 51.5% (Pérez-Fonseca et al., 2016). After the best nucleating agent was selected (GLY-LAC 1:6) from the four nucleating agents, the annealing effects at different time was examined.

4.5.1 Effects of annealing time on the degree of crystallinity of PLA

It was obvious that GLY-LAC improves the crystallization properties of PLA, but to achieve a high degree of crystallinity heat treatment was required, which was annealing. The tabulated data in table 4-7, showed that the increased degree of crystallinity of PLA is improved with the increasing annealing time; it gives a long cycle time for crystallization of PLA. Treating the sample with heat reduces the surface free energy (volume) and the boundary between PLA chains and gives a chance for nucleation and enables crystallization. During annealing as an indication for crystallinity, there was a change in colour of the PLA film from transparent white to slightly opaque and also changed from very soft to hard film.

When the annealing time increased from 30 minutes to 150 minutes, the degree of crystallinity also increased from 74.7% to 85.2%, as PLA gets enough time its slow crystallization properties changed to good crystallization, which strengthen its structure, and the details of the DSC data is plotted in figure 4-27. This discussion is supported by the study which focuses on annealing, in which the annealing time and temperature impacts were studied on poly (lactic acid), when the time reached 10 minutes the degree of crystallinity was 16.39% at 80 ℃. But this value was shifted to 49.56% at 30 minutes of annealing, on their research there was no nucleating agent used, this much improvement was achieved only through annealing (Srithep et al., 2013).

Table 4.7: Effects of annealing time on the degree of crystallinity of PLA

Sample	$Time$ (minutes)	$\Delta H_m(J/g)$	T_m(℃)	T_g(℃)	X_c(%)
PLA/GLY-LAC 1:6	30	70	149.4	42.8	74.7
PLA/GLY-LAC 1:6	90	75.4	150	45	80.46
PLA/GLY-LAC 1:6	150	77.22	150.67	45.034	85.2

Annealing has a great impact on the end application of PLA by influencing Tg, thermal conductivity, and others (Takayama et al., 2011).

By using one parameter at a time (OVAT), the effects of annealing temperature on the degree of crystallinity were examined in by making the loading rate and annealing time constant.

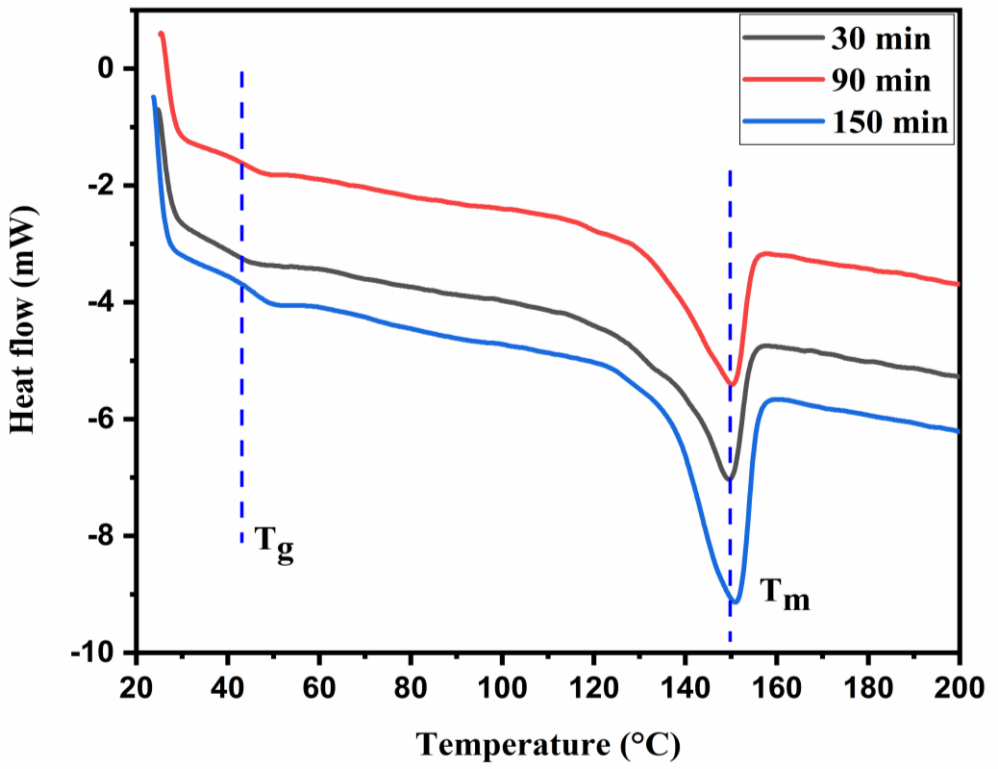

Figure 4-27: The heating cycle of PLA/10wt% GLY-LAC 1:6 at different annealing times

4.5.2 Effects of annealing temperature on the degree of crystallinity of PLA

The addition of a nucleating agent (GLY-LAC) well improved the degree of crystallinity, in addition to these the impacts of annealing the PLA at different temperatures were analysed here. As shown below in figure 4-28 the degrees of crystallinity were increased during annealing as the temperature increased from 90 ℃ to 110 ℃, all the calculated numerical values were tabulated in table 4-8.

The highest degree of crystallinity which was 85.2% achieved at 110 ℃ with the addition of 10wt% of GLY-LAC, but after annealing temperature of 110 ℃ the degree of crystallinity was decreased to 65.63%, because of the approaching of this annealing temperature (120 ℃) to the normal melting temperature of neat PLA which were around

140 - 150 ℃, therefore it degrades easily above this temperature. Annealing the PLA further above this temperature made it lose its physical as well as chemical properties (Simmons et al., 2019).

Table 4.8: Effects of annealing temperature on the degree of crystallinity of PLA

Sample	Temperature (℃)	T_g(℃)	$\Delta H_m(J/g)$	T_m(℃)	$Time$ (minutes)	X_c(%)
PLA/GLY-LAC 1:6	90	52	66.5	150.5	150	71
PLA/GLY-LAC 1:6	100	54	69.8	150.5	150	74.5
PLA/GLY-LAC 1:6	110	45.034	77.22	150.67	150	85.2
PLA/GLY-LAC 1:6	120	48.5	61.5	151.90	150	65.63

As the annealing temperature increased the nucleating agent (GLY-LAC) became more flexible within the PLA matrix and it act as a nucleation initiator. The crystallinity of PLA becomes improved. Whereas beyond 120 ℃ of the annealing temperature, the GLY-LAC became highly flexible and also loses its physical properties, then it becomes a plasticizer than a crystallizer. Because the PLA matrix started to move freely due to the temperature that it annealed was approached the melting temperature of PLA. The added GLY-LAC also became movable which is why the decrement in crystallinity above 120 ℃ occurred. This discussion is supported by the study on the annealing impacts of blends of poly(lactic acid) (PLA) and poly(ε-caprolactone) (PCL), and the degree of crystallinity is shifted from 11.4% to 45.6% (Takayama et al., 2011).

Beyond the effects of annealing temperature on the degree of crystallinity, another factor that needs to be taken into consideration for the degree of crystallinity of PLA is the loading rate of GLY-LAC. The percentage of nucleating agents on PLA properties had a great impact directly or indirectly.

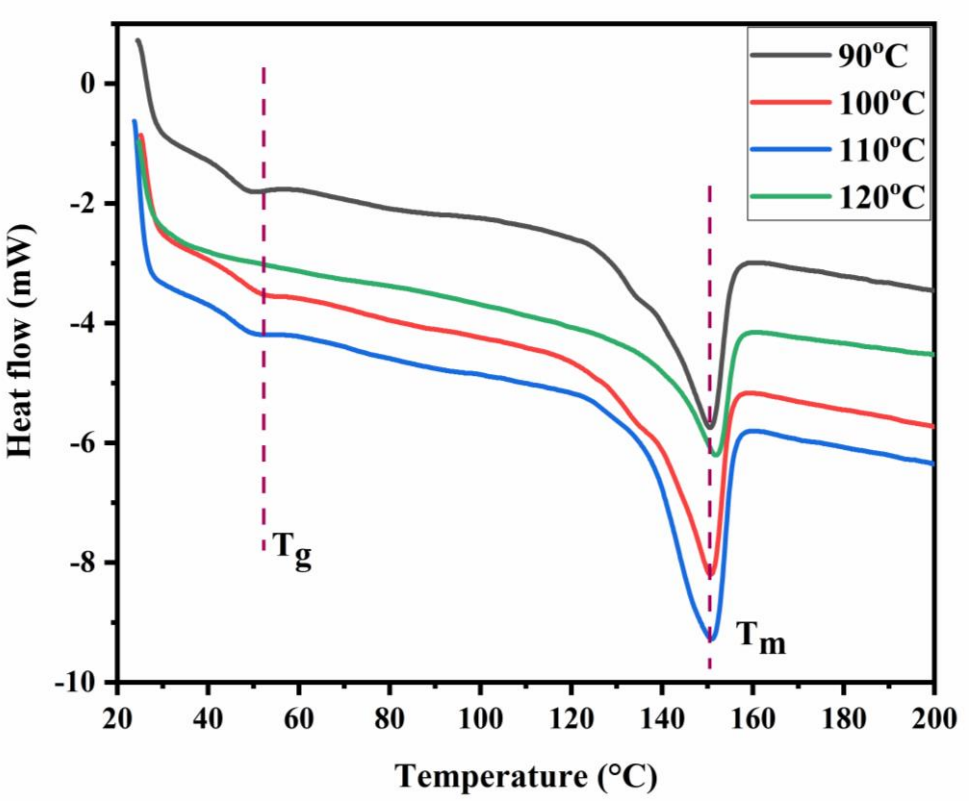

Figure 4-28: The heating cycle of PLA/10wt% GLY-LAC 1:6 at the different annealing temperature

4.5.3 Effects of loading rate of GLY-LAC on the degree of crystallinity of PLA

The loading amount of GLY-LAC on crystallinity percentage was studied at constant annealing time (150 minutes) and constant annealing temperature (110 ℃). As shown in figure 4-29 and table 4-9**,** the addition of 1wt% of GLY-LAC leads to the increment in crystallinity to 62.9%, in which the percentage of increment is 1.74% concerning neat PLA, in which its degree of crystallinity was 61.8% (see table 4-6 and figure 4-26). The melting temperature was shifted from 154.69 ℃ to 145℃, which improve the energy requirement of PLA to melt it; indirectly the reprocessing of PLA became very easy. Yu et al. reported that as the talc loading rate was increased from 3wt% to 6wt% the degree of crystallinity was also shifted from 3.6% to 11.4% (Yu et al., 2019).

Table 4-9: Effects of loading rate of GLY-LAC on the degree of crystallinity of PLA

Sample	Loading rate (wt%)	T_g(℃)	$\Delta H_m(J/g)$	T_m(℃)	X_c(%)
PLA/GLY-LAC 1:6	1	57.2	59	145	62.9
PLA/GLY-LAC 1:6	3	53	61	142.5	65.1
PLA/GLY-LAC 1:6	5	55.5	62.9	145.4	67.18
PLA/GLY-LAC 1:6	10	45.034	79.8	150.67	85.2

The increment of the concentration of the GLY-LAC increases the degree of crystallinity due to the higher chain mobility of GLY-LAC within the PLA matrix. As the GLY-LAC get the chance of free movement within the PLA, they are directly attached to the PLA matrix and become initiators for nucleation and made fast propagation as well as nucleation growth. Finally, the overall crystallinity becomes improved as NAs additions increased, but due to the cost of the NAs, the highest effects or impact with small loading of NAs were always required. The highest degree of crystallinity occurred with 10wt% loading of GLY-LAC (Lule et al., 2018).

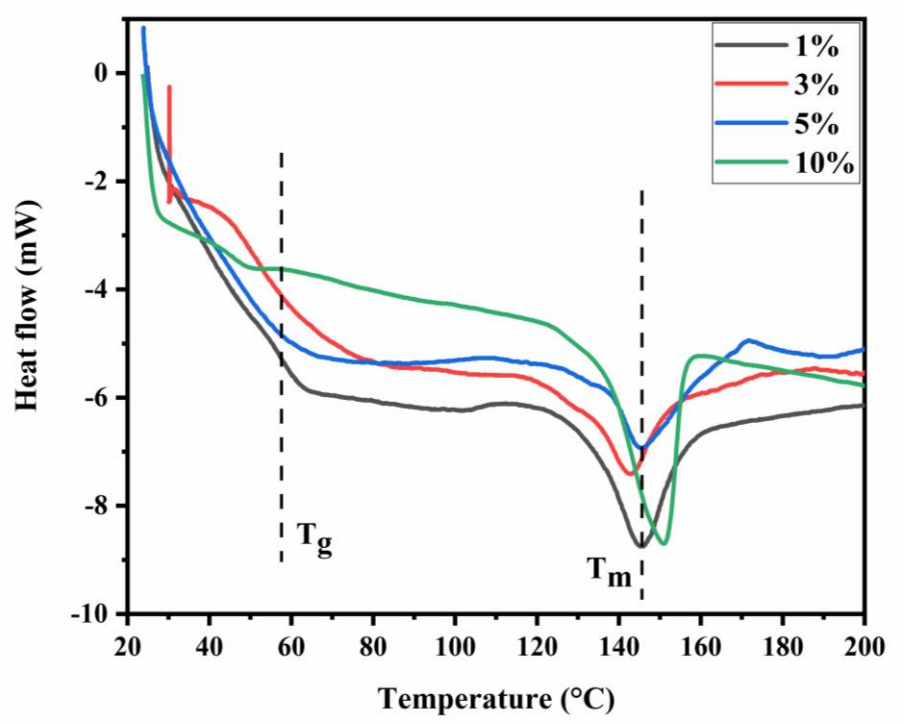

Figure 4-29: The heating cycle of PLA/10wt% GLY-LAC 1:6 at different loading rates

4.6 Thermal and Electrical conductivity of AgNPs/GLY-LAC/PLA based films

4.6.1 Thermal conductivity analysis

By their nature many polymers are thermal insulators, however, after the addition of different conductive fillers such as AgNPs, their insulating properties changed into conductors. Here the nano-particles serve as energy carriers (phonons) which were useful in energy transport (heat transfer). When an electrical current was passed through the heater probe, there was a temperature drop (dT) on the film during heating (Q). In our case, the supplied current was I^2 = 0.6250 ampere. The thermal conductivity (λ) of PLA is initially increased from 0.2059 W/m K to 0.7 W/m K with AgNPs loading up to 5%, but beyond these limitations, the thermal conductivity decreased to 0.6220 W/m K with 7% AgNPs loading.

This was because of the formation of agglomeration within the AgNPs (thermally conductive filler), because of these the conductive network chain becomes distracted. Therefore, its thermal conductivity becomes lower or lower heat flow took place within PLA. However, when the AgNPs amount becomes small the thermal conductivity also becomes lower, due to the difficulty of the formation of a thermal conductive network, which became difficult for the fillers to contact and form a network with each other, (A. Li et al., 2017) also reported in their review of graphene polymer composites paper that to have thermal conductive materials, there must be a thermal conductive network between those fillers as well as polymer. If there is a mismatch between graphene and the polymer the conduction was disrupted or there was phonon scattering (A. Li et al., 2017).

These improvements in thermal conductivity were reached due to the improvements in the degree of crystallinity of PLA and also because the polymer which becomes an orderly arranged the chance of having a conductive network was very high. The literature study reported that the crystallinity of polymers had a great impact on the conductivity of polymers; they reported that as the thermal conductivity of PLA increases, the degree of crystallinity also increased (L. Bai et al., 2018).

In our thermal conductivity study of PLA, there were significant improvements when compared with the neat PLA. The increments in thermal conductivity through the AgNPs loading were not linear, as the loading of AgNPs was low there was a rapid increment of thermal conductivity around 65.8wt% with 1wt% AgNPs loading.

Whereas when the loading becomes 3wt% the slope of thermal conductivity slightly increased slightly then decreased to 4.2%, this was due to the formation of agglomeration between the fillers. Again the thermal conductivity rose when the AgNPs content increased, due to the good formation of a heat conduction network.

This discussion is supported by the study of (Tessema et al., 2017), in their study, they tried to find the effect of silica filler loading, as an initial step when the filler amount was lower the thermal conductivity was also increased by 35% with 2wt% silica loading and then loading percentage rose into 4wt% the thermal conductivity decreased to 14% and finally increased when the amount of loading reached 6wt%.

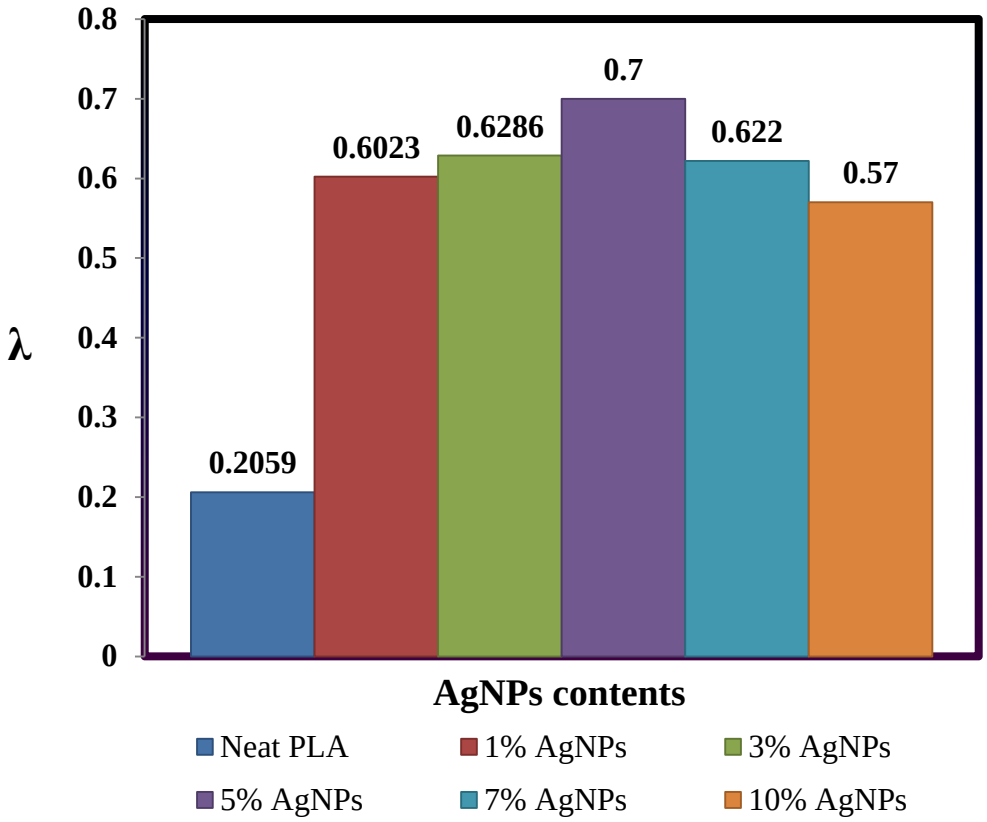

Figure 4-30: Thermal conductivity (**λ**) of AgNPs/GLY-LAC/PLA at a different loading rate

Due to the formation of a conductive network within the PLA matrix, the heat flow was conducted, and the electrical conductivity also requires this conductive network between the polymers, the final result of AgNPs as filler was discussed below.

4.6.2 Electrical conductivity analysis

Polylactic acid (PLA) is an excellent electrical insulator, but with the addition of different conductive fillers, this property changed into more electrical conductive properties. In this research, the impact of greenly synthesized AgNPs on the electrical conductivity of PLA was studied. The samples were prepared through different methods, 1) solution casting for the digital multi-meter test,2) coating on ITO (Indium Tin Oxide) glass for electrochemical impedance spectroscopy (EIS) test and 3) coating on insulator glasses for probe and station (Agilent B2902A precision Source/Measure Unit) test. With these testing machines the electrical conductivity was not improved (the prepared samples were not conductors).

During testing through a digital multi-meter (DL-2080) with power supply (DL 1013T1 DE LORENZO) for checking continuity test with different DC supply (from 5 volts up to 100 volts), no reading for voltages as well as the current was detected with open as well as short circuit methods, as shown below in figure 4-31.

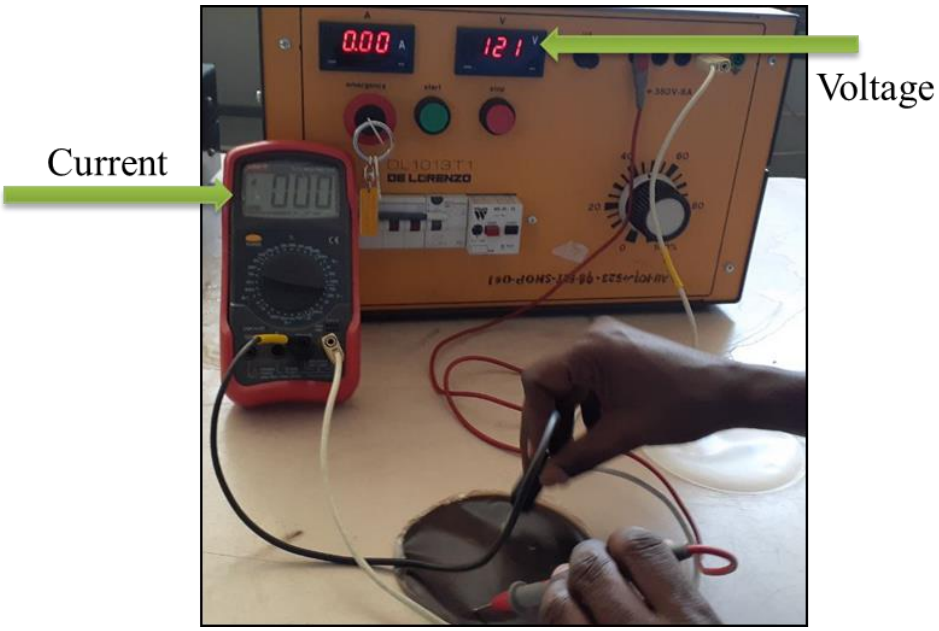

Figure 4-31: Continuity test of AgNPs/GLY-LAC/PLA biofilm by digital multi-meter

Measurement for EIS was performed in two ways, the first one was by coating the powder on ITO glass, which was conductive on one side as shown in figure 4.32 and the second method was done by preparing biopolymer film (AgNPs/GLY-LAC/PLA), again here also a meaningless signal for resistivity were detected for both samples as shown on figure 4.33. The other testing method was using a mini digital multi-meter (DT-9205A) for continuity checking purposes, here also no meaningful signal was observed.

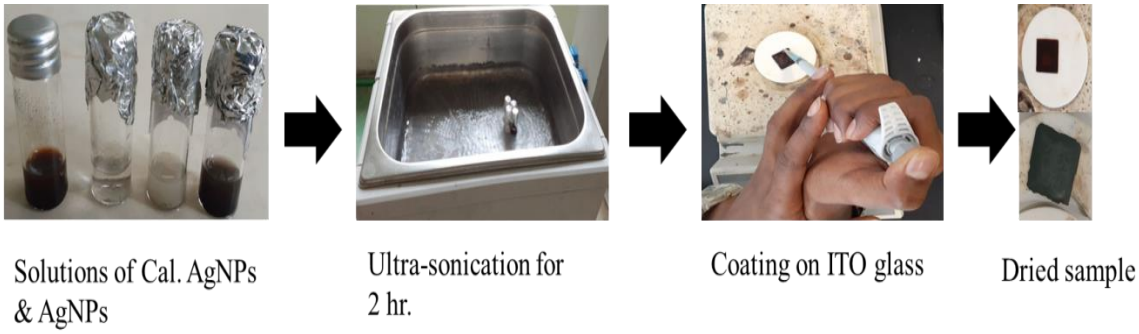

Figure 4-32: Sample preparation for EIS test (coating process on ITO glass)

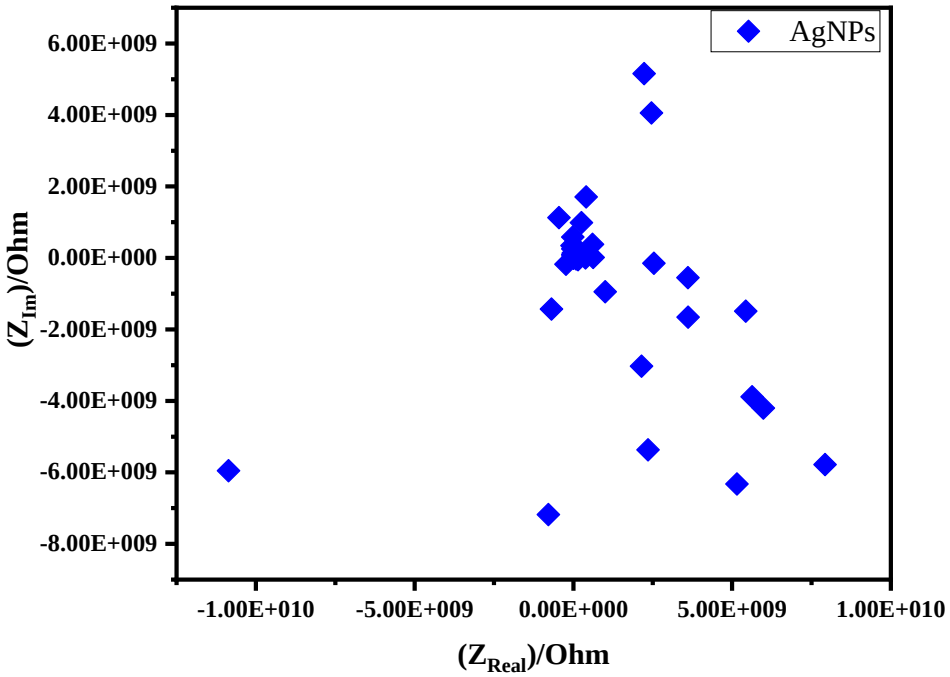

Figure 4-33: Electro impendency spectroscopy (EIS) testing

Finally, a conductivity test for the raw material (AgNPs) itself was performed. Then when the continuity test was done for the powder AgNPs through a mini digital multi-meter (DT-9205A) as shown in figure 4.34, no continuity signal was observed; therefore, now the main problem was reached out. The next step was testing the continuity of calcined AgNPs powder at 700 ℃ to remove the encircled or encapsulated plant leaves extract from AgNPs. The result showed us there was a continuity signal as well as there was a numerical value reading and also there was a beep sound for the indication of the continuity test for calcined AgNPs. But there was no numerical value reading as well as a beep sound for AgNPs without calcination, which indicates AgNPs were an insulator when the plant leaves extract was incorporated within it. The numerical value one (1) as shown

in figure 4.34 (a) on the digital multi-meter was an indicator for open system (non-conductor) instead of conductivity.

For conformity, the conductivity test was done for both calcined AgNPs as well as AgNPs by using a probe station (Agilent B2902A precision Source/Measure Unit) instrument. For these measurements, the samples were prepared by coating on insulator glass as shown in figure 4.32 (the same step was also used here, the only difference was the glass, here insulator glass was used). There was a linear relationship between supplied voltage and measured current for calcined AgNPs, which was without plant extract (black line in figure 4.35).

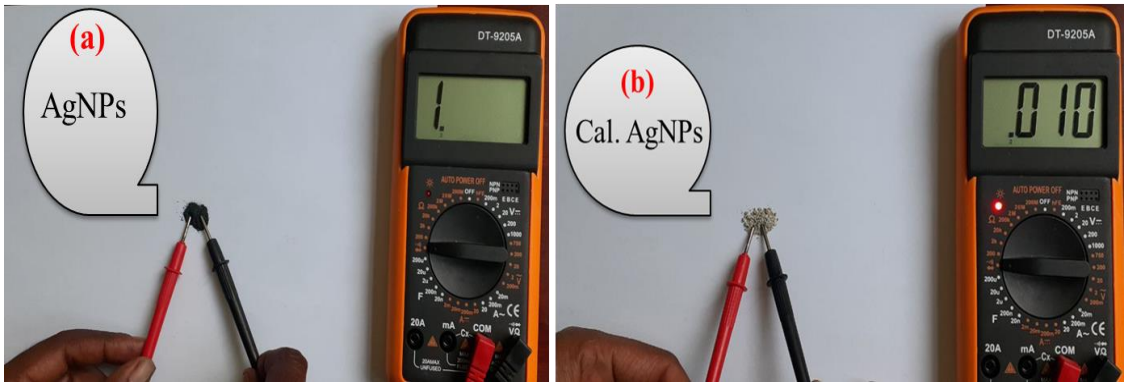

Figure 4-34: Continuity test of (a) AgNPs without calcination (b) Calcined AgNPs by digital multi-meter

But for green synthesized AgNPs without calcination, there was a deviation of signal (no reading for current conductivity, red line) from the expected linear graph as shown in figure 4-35; literature reported that the increment of current was the result of increased voltage.

The main reason for the non-conductivity of greenly synthesized AgNPs was due to the hole or gap formation between those nano-particles, because of the presence of plant leaf extract within the AgNPs. The charge which was supplied doesn't have a network to fellow through the PLA matrix, which indicates that the conductive network was not formed, due to the discontinuity of the electric charge. The formed hole was due to the capping ability of plant extract, AgNPs were shielded by the plant extract during the green synthesis of nanoparticles and therefore it can't conduct the supplied electric current. But after the calcination process took place to remove those plant leaves extract from powder

AgNPs, there was the conduction of electric current between those particles as shown in figure 4-35**.**

As far as our knowledge no literature was found regarding greenly synthesized AgNPs for the application of electrical conductivity improvements, but there were a lot of research papers regarding green synthesized AgNPs for other applications such as antimicrobial study, drug carriers, thermal stability study, drug carriers, and others (Garibo et al., 2020).

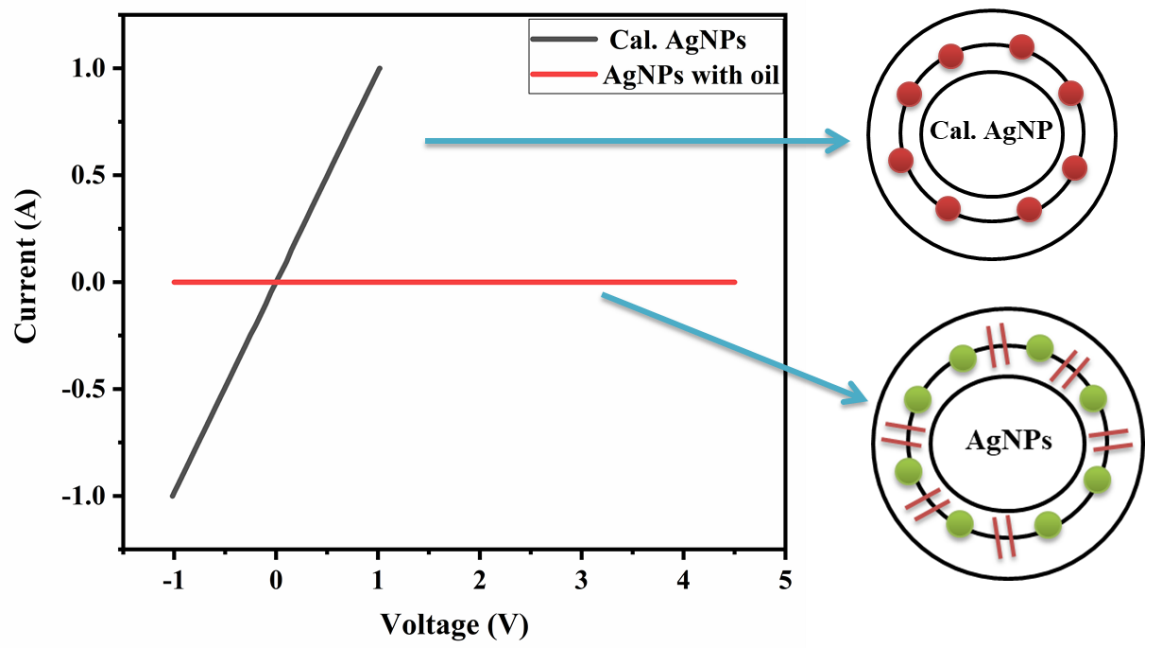

Figure 4-35: I-V Curve of AgNPs with and without calcination

It is possible to use AgNPs/GLY-LAC/PLA films in thermal conductive but electrically insulator application areas such as electronic packing, thermal management, Printed circuited boards (PCBs) and integrated circuits (Lin et al., 2017; Zhang et al., 2018).

CHAPTER FIVE

5. CONCLUSION AND RECOMMENDATIONS

5.1 Conclusion

From these research work interesting impacts of GLY-LAC on degree of crystallinity as well as conductive filler (AgNPs) on thermal conductivity was archived. The general ideas of this research work are summarized below:

- ✓ A 3-armed bio-based NAs GLY-LAC was perfectly synthesized through the condensation reaction between lactic acid and glycerol at 190 ℃ and 8 hr. NMR showed that the formation of GLY-LAC bio conjugates.
- ✓ Through purification, LAOLG, free lactic acid and unreacted glycerol impurities were removed and the removal was confirmed by decrement in AV and viscosity as well as NMR and FTIR analysis showed their removal.
- ✓ AgNPs was synthesized through biological method using *V. amygdalina* plant leaves extract for capping, stabilizing, and reducing agent, due to its phytochemical components. UV-Vis analysis showed the formation of AgNPs between 415-423 nm absorption peaks.
- ✓ FTIR spectrum also showed the formation and interaction of AgNPs and plant extract. During XRD analysis four peaks were shown for AgNPs at 38.18°, 44.19°, 64.58°, and 77.33°.
- ✓ Stable dispersion of AgNPs into GLY-LAC was studied using zeta potential analysis (-27.2 mV), SEM and FTIR analysis also showed uniform dispersion of AgNPs. The size of AgNPs was confirmed by PSA which was 3 nm and 56 nm.
- ✓ The impacts of GLY-LAC on the crystallization of PLA were studied with a DSC instrument. GLY-LAC 1:6 was selected as the best NAs due to its higher degree of crystallinity (X_C = 85.2%) relative to neat PLA. Effects of annealing time, annealing temperature and loading rate of GLY-LAC were optimized using GLY-LAC 1:6 and 150 minutes, 110 ℃ and 10wt% loading rate were optimized parameters, respectively.
- ✓ AgNPs/GLY-LAC/PLA biopolymer film was prepared and the thermal conductivity of PLA was improved from 0.2 W/m K to 0.7 W m^{-1} k^{-1} with 5wt% AgNPs loading. Whereas, the AgNPs don't enhance the electrical conductivity of PLA, because of the presence of phytochemical components on AgNPs surface, which shield the EC conductivity properties of AgNPs.

5.2 Recommendations

In this research work, both products (3-armed GLY-LAC and AgNPs) were synthesized with a green synthesis method. Glyceral lactate has biodegradability and biocompatibility properties, due to its synthesis from organic materials. It was used as a nucleating agent (crystallizer) to solve the poor crystallinity properties of PLA and also it was used as a host matrix for AgNPs. AgNPs were used as conductive fillers in the PLA matrix to study their effects on thermal and electrical conductivity. Both products had multi-functional properties, interesting physical and chemical properties and good compatibility with each other, due to this awesome property below are recommendations for future work:

- Due to the good heat-conducting property of green synthesized AgNPs, it will be good if research is conducted in detail regarding the electrical conductivity property of AgNPs with another synthesis method.
- Due to the biocompatibility of AgNPs with GLY-LAC, using the matrix as a thermic fluid (heating oil) will be a good research area, especially on an industrial scale.
- Besides the thermal conductivity properties of AgNPs, it also has good magnetic properties, but a detailed study will be required.
- Dispersions and stability issue of AgNPs within GLY-LAC was physically very attractive but needs to be supported by TEM, and SEM on the nano level.
- There was an indication for the improvement in mechanical tests (elongation at break from 2.935 mm to 4.264 mm) wih10wt% AgNPsGLY-LAC loading, but detail research will be required on individual effects of AgNPs.
- The effects of AgNPs on the degree of crystallinity of PLA require detailed investigation there was an indication of improvement (Appendix 9).

REFERENCES

Abbasi, A. M. R., Marsalkova, M., & Militky, J. (2013). Conductometry and size characterization of polypyrrole nanoparticles produced by ball milling. *Journal of Nanoparticles, 2013*.

Abbasi, E., Milani, M., Fekri Aval, S., Kouhi, M., Akbarzadeh, A., Tayefi Nasrabadi, H., . . . Nejati-Koshki, K. (2016). Silver nanoparticles: synthesis methods, bio-applications and properties. *Critical reviews in microbiology, 42*(2), 173-180.

Aghebati-Maleki, A., Dolati, S., Ahmadi, M., Baghbanzhadeh, A., Asadi, M., Fotouhi, A., . . . Aghebati-Maleki, L. (2020). Nanoparticles and cancer therapy: Perspectives for application of nanoparticles in the treatment of cancers. *Journal of cellular physiology, 235*(3), 1962-1972.

Ahmadi, S., Fazilati, M., Mousavi, S. M., & Nazem, H. (2020). Anti-bacterial/fungal and anti-cancer performance of green synthesized Ag nanoparticles using summer savory extract. *Journal of Experimental Nanoscience, 15*(1), 363-380.

Aisida, S. O., Ugwu, K., Akpa, P. A., Nwanya, A. C., Nwankwo, U., Botha, S. S., . . . Ezema, F. I. (2019). Biosynthesis of silver nanoparticles using bitter leave (Veronica amygdalina) for antibacterial activities. *Surfaces and Interfaces, 17*, 100359.

Akande, I. G., Ajayi, S., Fajobi, M. A., Oluwole, O. O., & Fayomi, O. S. I. (2021). *Advancement in the Production and Applications of Conductive Polymers (CPs).* Paper presented at the Key Engineering Materials.

Akanksha, D., Vikas, G., Neetesh, K., Shailendra, S., Neelam, B., & Dinesh, K. (2009). Formulation and evaluation of neomycin sulphate ointment containing natural wound healing agent Curcuma longa. *Int J Pharm Sci Drug Res, 1*, 116-118.

Aliotta, L., Cinelli, P., Coltelli, M. B., Righetti, M. C., Gazzano, M., & Lazzeri, A. (2017). Effect of nucleating agents on crystallinity and properties of poly (lactic acid)(PLA). *European polymer journal, 93*, 822-832.

Althues, H., Henle, J., & Kaskel, S. (2007). Functional inorganic nanofillers for transparent polymers. *Chemical Society Reviews, 36*(9), 1454-1465.

Ambaye, T. G., Vaccari, M., Castro, F. D., Prasad, S., & Rtimi, S. (2020). Emerging technologies for the recovery of rare earth elements (REEs) from the end-of-life electronic wastes: a review on progress, challenges, and perspectives. *Environmental Science and Pollution Research*, 1-23.

Amechi, M. (2018). *Green synthesis of silver nanoparticles using leaf (vernonia amygdalina) extracts in selected solvents and it's characterization by spectrocopic methods and scanning electron microscopy.* Godfrey Okoye University, Enugu.

Anis, B., El Fllah, H., Ismail, T., Fathallah, W. M., Khalil, A., Hemeda, O., & Badr, Y. A. (2020). Preparation, characterization, and thermal conductivity of polyvinyl-formaldehyde/MWCNTs foam: A low cost heat sink substrate. *Journal of Materials Research and Technology, 9*(3), 2934-2945.

Arif, R., & Uddin, R. (2021). A review on recent developments in the biosynthesis of silver nanoparticles and its biomedical applications. *Medical Devices & Sensors, 4*(1), e10158.

Arroyo, J., & Ryan, C. (2018). Incorporation of carbon nanofillers tunes mechanical and electrical percolation in PHBV: PLA blends. *Polymers, 10*(12), 1371.

Azizi, S., Azizi, M., & Sabetzadeh, M. (2019). The role of multiwalled carbon nanotubes in the mechanical, thermal, rheological, and electrical properties of PP/PLA/MWCNTs nanocomposites. *Journal of Composites Science, 3*(3), 64.

Bai, H., Huang, C., Xiu, H., Zhang, Q., & Fu, Q. (2014). Enhancing mechanical performance of polylactide by tailoring crystal morphology and lamellae orientation with the aid of nucleating agent. *Polymer, 55*(26), 6924-6934.

Bai, L., Zhao, X., Bao, R.-Y., Liu, Z.-Y., Yang, M.-B., & Yang, W. (2018). Effect of temperature, crystallinity and molecular chain orientation on the thermal conductivity of polymers: a case study of PLLA. *Journal of materials science, 53*(14), 10543-10553.

Baig, N., Kammakakam, I., & Falath, W. (2021). Nanomaterials: A review of synthesis methods, properties, recent progress, and challenges. *Materials Advances, 2*(6), 1821-1871.

Baran, A., Vrábel, P., Olčák, D., & Chodák, I. (2018). Solid state 13C-NMR study of a plasticized PLA/PHB polymer blend. *Journal of Applied Polymer Science, 135*(21), 46296.

Beavers, E. M., Klabunde, K. J., Wang, B., & Sun, S. (2009). Lactic acid–magnesium oxide nanocrystal interactions: how nanoparticle size and shape affect chemistry and template oligomerization. *New Journal of Chemistry, 33*(9), 1951-1959.

Bertuoli, P. T., Ordoño, J., Armelin, E., Pérez-Amodio, S., Baldissera, A. F., Ferreira, C. A., . . . Aleman, C. (2019). Electrospun conducting and biocompatible uniaxial and

Core–Shell fibers having poly (lactic acid), poly (ethylene glycol), and polyaniline for cardiac tissue engineering. *ACS omega*, *4*(2), 3660-3672.

Bhandari, S., Lopez-Anido, R. A., & Gardner, D. J. (2019). Enhancing the interlayer tensile strength of 3D printed short carbon fiber reinforced PETG and PLA composites via annealing. *Additive Manufacturing*, *30*, 100922.

Bhateria, R., & Singh, R. (2019). A review on nanotechnological application of magnetic iron oxides for heavy metal removal. *Journal of Water Process Engineering*, *31*, 100845.

Borowicz, M., Paciorek-Sadowska, J., Isbrandt, M., Grzybowski, Ł., & Czupryński, B. (2019). Glycerolysis of Poly (lactic acid) as a Way to Extend the "Life Cycle" of This Material. *Polymers*, *11*(12), 1963.

Botkin, J. H., Dunski, N., & Maeder, D. (2002). Improving molding productivity and enhancing mechanical properties of polypropylene with nucleating agents. *Kwinana: Ciba Speciality Chemicals*.

Brighenti, R., Li, Y., & Vernerey, F. J. (2020). Smart polymers for advanced applications: a mechanical perspective review. *Frontiers in Materials*, *7*, 196.

Carbone, M. J., Vanhalle, M., Goderis, B., & Van Puyvelde, P. (2015). Amino acids and poly (amino acids) as nucleating agents for poly (lactic acid). *Journal of Polymer Engineering*, *35*(2), 169-180.

Ceregatti, T., Pecharki, P., Pachekoski, W. M., Becker, D., & Dalmolin, C. (2017). Electrical and thermal properties of PLA/CNT composite films. *Matéria (Rio de Janeiro)*, *22*.

Chen, H., Ginzburg, V. V., Yang, J., Yang, Y., Liu, W., Huang, Y., . . . Chen, B. (2016). Thermal conductivity of polymer-based composites: Fundamentals and applications. *Progress in Polymer Science*, *59*, 41-85.

Chen, J., Yu, Q., Cui, X., Dong, M., Zhang, J., Wang, C., . . . Guo, Z. (2019). An overview of stretchable strain sensors from conductive polymer nanocomposites. *Journal of Materials Chemistry C*, *7*(38), 11710-11730.

Chen, Z., Zhang, X., & Pei, Y. (2018). Manipulation of phonon transport in thermoelectrics. *Advanced Materials*, *30*(17), 1705617.

Chereches, E. I., & Minea, A. A. (2019). Electrical conductivity of new nanoparticle enhanced fluids: An experimental study. *Nanomaterials*, *9*(9), 1228.

Demirci, S., Sutekin, S. D., & Sahiner, N. (2020). Polymeric Composites Based on Carboxymethyl Cellulose Cryogel and Conductive Polymers: Synthesis and Characterization. *Journal of Composites Science, 4*(2), 33.

Desalegn, T., Murthy, H. A., & Limeneh, Y. A. (2021). Medicinal plant Syzygium guineense (willd.) DC leaf extract mediated green synthesis of Ag nanoparticles: investigation of their antibacterial activity. *Ethiopian Journal of Sciences and Sustainable Development, 8*(1), 1-12.

Dev, S., Sachan, A., Dehghani, F., Ghosh, T., Briggs, B. R., & Aggarwal, S. (2020). Mechanisms of biological recovery of rare-earth elements from industrial and electronic wastes: A review. *Chemical engineering journal, 397*, 124596.

Diantoro, M., Hidayati, N. N. S., Latifah, R., Fuad, A., Nasikhudin, Sujito, & Hidayat, A. (2016). *Electrical conductivity modification using silver nano particles of Jatropha Multifida L. and Pterocarpus Indicus w. extracts films.* Paper presented at the AIP Conference Proceedings.

Dieckmann, Y., Cölfen, H., Hofmann, H., & Petri-Fink, A. (2009). Particle size distribution measurements of manganese-doped ZnS nanoparticles. *Analytical chemistry, 81*(10), 3889-3895.

Ding, Y., Zhang, C., Luo, C., Chen, Y., Zhou, Y., Yao, B., . . . Ji, J. (2021). Effect of talc and diatomite on compatible, morphological, and mechanical behavior of PLA/PBAT blends. *e-Polymers, 21*(1), 234-243.

Dong, Y., Zhu, H., Shen, Y., Zhang, W., & Zhang, L. (2019). Antibacterial activity of silver nanoparticles of different particle size against Vibrio Natriegens. *PloS one, 14*(9), e0222322.

Du, F., Schick, C., & Androsch, R. (2020). Full-composition-range glass transition behavior of the polymer/solvent system poly (lactic acid)/ethyl butylacetylaminopropionate (PLA/IR3535®). *Polymer, 209*, 123058.

Dulińska-Litewka, J., Łazarczyk, A., Hałubiec, P., Szafrański, O., Karnas, K., & Karewicz, A. (2019). Superparamagnetic iron oxide nanoparticles—Current and prospective medical applications. *Materials, 12*(4), 617.

El-Taweel, S. H., & Abboudi, M. (2020). Nonisothermal crystallization kinetics of PLA/nanosized YVO4 composites as a novel nucleating agent. *Journal of Applied Polymer Science, 137*(5), 48340.

Espartero, J., Rashkov, I., Li, S., Manolova, N., & Vert, M. (1996). NMR analysis of low molecular weight poly (lactic acid) s. *Macromolecules, 29*(10), 3535-3539.

Evgin, T., Koca, H. D., Horny, N., Turgut, A., Tavman, I. H., Chirtoc, M., . . . Novak, I. (2016). Effect of aspect ratio on thermal conductivity of high density polyethylene/multi-walled carbon nanotubes nanocomposites. *Composites Part A: Applied Science and Manufacturing, 82*, 208-213.

Fallahi, H., Azizi, H., Ghasemi, I., & Karrabi, M. (2017). Preparation and properties of electrically conductive, flexible and transparent silver nanowire/poly (lactic acid) nanocomposites. *Organic Electronics, 44*, 74-84.

Faller, J., & Smart, C. (1989). Stereoselective vinylic carbon-hydrogen activation by a homogeneous iridium catalyst. *Organometallics, 8*(3), 602-609.

Farhoodi, M., Dadashi, S., Mousavi, S. M. A., Sotudeh-Gharebagh, R., Emam-Djomeh, Z., Oromiehie, A., & Hemmati, F. (2012). Influence of TiO 2 nanoparticle filler on the properties of PET and PLA nanocomposites. *Polymer (Korea), 36*(6), 745-755.

Gahlawat, G., & Choudhury, A. R. (2019). A review on the biosynthesis of metal and metal salt nanoparticles by microbes. *Rsc Advances, 9*(23), 12944-12967.

Garibo, D., Borbón-Nuñez, H. A., de León, J. N. D., García Mendoza, E., Estrada, I., Toledano-Magaña, Y., Blanco, A. (2020). Green synthesis of silver nanoparticles using Lysiloma acapulcensis exhibit high-antimicrobial activity. *Scientific Reports, 10*(1), 1-11.

Ghosh, S., Kaushik, R., Nagalakshmi, K., Hoti, S., Menezes, G., Harish, B., & Vasan, H. (2010). Antimicrobial activity of highly stable silver nanoparticles embedded in agar–agar matrix as a thin film. *Carbohydrate Research, 345*(15), 2220-2227.

Giner-Casares, J. J., Henriksen-Lacey, M., Coronado-Puchau, M., & Liz-Marzán, L. M. (2016). Inorganic nanoparticles for biomedicine: where materials scientists meet medical research. *Materials Today, 19*(1), 19-28.

Grancarić, A. M., Jerković, I., Koncar, V., Cochrane, C., Kelly, F. M., Soulat, D., & Legrand, X. (2018). Conductive polymers for smart textile applications. *Journal of Industrial Textiles, 48*(3), 612-642.

Gross, I. P., Schneider, F. S., Caro, M. S., da Conceicao, T. F., Caramori, G. F., & Pires, A. T. (2018). Polylactic acid, maleic anhydride and dicumyl peroxide: NMR study of the free-radical melt reaction product. *Polymer Degradation and Stability, 155*, 1-8.

Gul, R., Jan, S. U., Faridullah, S., Sherani, S., & Jahan, N. (2017). Preliminary phytochemical screening, quantitative analysis of alkaloids, and antioxidant activity of crude plant extracts from Ephedra intermedia indigenous to Balochistan. *The Scientific World Journal, 2017*.

Guo, J., Tsou, C.-H., Yu, Y., Wu, C.-S., Zhang, X., Chen, Z., . . . Guzman, M. R. D. (2021). Conductivity and mechanical properties of carbon black-reinforced poly (lactic acid)(PLA/CB) composites. *Iranian Polymer Journal*, 1-12.

Guo, R., Ren, Z., Bi, H., Xu, M., & Cai, L. (2019). Electrical and thermal conductivity of polylactic acid (PLA)-based biocomposites by incorporation of nano-graphite fabricated with fused deposition modeling. *Polymers, 11*(3), 549.

Guo, Y., Ruan, K., Shi, X., Yang, X., & Gu, J. (2020). Factors affecting thermal conductivities of the polymers and polymer composites: A review. *Composites science and technology, 193*, 108134.

Guo, Y., Zuo, X., Xue, Y., Tang, J., Gouzman, M., Fang, Y., . . . Rafailovich, M. H. (2020). Engineering thermally and electrically conductive biodegradable polymer nanocomposites. *Composites Part B: Engineering, 189*, 107905.

Halvaee, M., Didehban, K., Goodarzi, V., Ghaffari, M., Ehsani, M., & Saeb, M. R. (2017). Comparison of pristine and polyaniline-grafted MWCNT s as conductive sensor elements for phase change materials: Thermal conductivity trend analysis. *Journal of Applied Polymer Science, 134*(47), 45389.

He, S., Zhou, C., Chen, H., Liu, X., Li, H., Ma, W., . . . Han, T. (2020). Super soft conductors based on liquid metal/cotton composites. *Journal of Materials Chemistry C, 8*(10), 3553-3561.

Herizchi, R., Abbasi, E., Milani, M., & Akbarzadeh, A. (2016). Current methods for synthesis of gold nanoparticles. *Artificial cells, nanomedicine, and biotechnology, 44*(2), 596-602.

Horst, D. J., & de Andrade Junior, P. P. (2020). Evaluating the Electrical Conductivity and Resistivity of Carbon Nanostructures Embedded in the PLA Matrix. *Letters in Applied NanoBioScience, 9*, 1141-1146.

Huang, K., Yu, H., Xie, M., Liu, S., & Wu, F. (2019). Effects of poly (ethylene glycol)-grafted graphene on the electrical properties of poly (lactic acid) nanocomposites. *Rsc Advances, 9*(19), 10599-10605.

Huang, Y., Ellingford, C., Bowen, C., McNally, T., Wu, D., & Wan, C. (2020). Tailoring the electrical and thermal conductivity of multi-component and multi-phase polymer composites. *International Materials Reviews, 65*(3), 129-163.

Huq, M. (2020). Green synthesis of silver nanoparticles using Pseudoduganella eburnea MAHUQ-39 and their antimicrobial mechanisms investigation against drug

resistant human pathogens. *International journal of molecular sciences, 21*(4), 1510.

Inzelt, G. (2012). *Conducting polymers: a new era in electrochemistry*: Springer Science & Business Media.

Ivanov, E., Kotsilkova, R., Xia, H., Chen, Y., Donato, R. K., Donato, K., . . . Cimmino, S. (2019). PLA/Graphene/MWCNT composites with improved electrical and thermal properties suitable for FDM 3D printing applications. *Applied Sciences, 9*(6), 1209.

Jain, D., Daima, H. K., Kachhwaha, S., & Kothari, S. (2009). Synthesis of plant-mediated silver nanoparticles using papaya fruit extract and evaluation of their anti microbial activities. *Digest journal of nanomaterials and biostructures, 4*(3), 557-563.

Jamkhande, P. G., Ghule, N. W., Bamer, A. H., & Kalaskar, M. G. (2019). Metal nanoparticles synthesis: An overview on methods of preparation, advantages and disadvantages, and applications. *Journal of drug delivery science and technology, 53*, 101174.

Jemilugba, O. T., Parani, S., Mavumengwana, V., & Oluwafemi, O. S. (2019). Green synthesis of silver nanoparticles using Combretum erythrophyllum leaves and its antibacterial activities. *Colloid and Interface Science Communications, 31*, 100191.

Ji, N., Hu, G., Li, J., & Ren, J. (2019). Influence of poly (lactide) stereocomplexes as nucleating agents on the crystallization behavior of poly (lactide) s. *Rsc Advances, 9*(11), 6221-6227.

Jiang, J., Yang, S., Li, L., & Bai, S. (2020). High thermal conductivity polylactic acid composite for 3D printing: Synergistic effect of graphene and alumina. *Polymers for advanced technologies, 31*(6), 1291-1299.

Jin, F.-L., Hu, R.-R., & Park, S.-J. (2019). Improvement of thermal behaviors of biodegradable poly (lactic acid) polymer: A review. *Composites Part B: Engineering, 164*, 287-296.

Jing, Y., Quan, C., Liu, B., Jiang, Q., & Zhang, C. (2016). A mini review on the functional biomaterials based on poly (lactic acid) stereocomplex. *Polymer Reviews, 56*(2), 262-286.

Karthik, C., Suresh, S., Sneha, M., & Kavitha, S. (2020). A FTIR approach of green synthesized silver nanoparticles by Ocimum sanctum and Ocimum gratissimum on mung bean seeds. Inorg. Nano-Met. Chem. 50 (8): 606-612.

Khan, I., Saeed, K., & Khan, I. (2019). Nanoparticles: Properties, applications and toxicities. *Arabian journal of chemistry, 12*(7), 908-931.

Khan, S. A., Noreen, F., Kanwal, S., Iqbal, A., & Hussain, G. (2018). Green synthesis of ZnO and Cu-doped ZnO nanoparticles from leaf extracts of Abutilon indicum, Clerodendrum infortunatum, Clerodendrum inerme and investigation of their biological and photocatalytic activities. *Materials Science and Engineering: C, 82*, 46-59.

Kim, J. H., Hong, J. S., & Ahn, K. H. (2020). Design of electrical conductive poly (lactic acid)/carbon black composites by induced particle aggregation. *Journal of Applied Polymer Science, 137*(42), 49295.

Ko, J. A., & Lim, H. (2016). Metal-doped inorganic nanoparticles for multiplex detection of biomarkers by a sandwich-type ICP-MS immunoassay. *Analytica Chimica Acta, 938*, 1-6.

Kotsilkova, R., Petrova-Doycheva, I., Menseidov, D., Ivanov, E., Paddubskaya, A., & Kuzhir, P. (2019). Exploring thermal annealing and graphene-carbon nanotube additives to enhance crystallinity, thermal, electrical and tensile properties of aged poly (lactic) acid-based filament for 3D printing. *Composites science and technology, 181*, 107712.

Krithiga, N., Rajalakshmi, A., & Jayachitra, A. (2015). Green synthesis of silver nanoparticles using leaf extracts of Clitoria ternatea and Solanum nigrum and study of its antibacterial effect against common nosocomial pathogens. *Journal of Nanoscience, 2015*.

Kumar, P., Govindaraju, M., Senthamilselvi, S., & Premkumar, K. (2013). Photocatalytic degradation of methyl orange dye using silver (Ag) nanoparticles synthesized from Ulva lactuca. *Colloids and Surfaces B: biointerfaces, 103*, 658-661.

Kumar, R., Singh, S., & Yadav, B. (2015). Conducting polymers: synthesis, properties and applications. *International Advanced Research Journal in Science, Engineering and Technology, 2*(11), 110-124.

Kumar, S., Singh, R., Singh, T., & Batish, A. (2021). Investigations for magnetic properties of PLA-PVC-Fe3O4-wood dust blend for self-assembly applications. *Journal of Thermoplastic Composite Materials, 34*(7), 929-951.

Lakatos, Á. (2018). Thermal conductivity of insulations approached from a new aspect. *Journal of Thermal Analysis and Calorimetry, 133*(1), 329-335.

Lebedev, S., Gefle, O., Amitov, E., Berchuk, D. Y., & Zhuravlev, D. (2017). Poly (lactic acid)-based polymer composites with high electric and thermal conductivity and their characterization. *Polymer Testing, 58*, 241-248.

Lee, S. L., & Chang, C.-J. (2019). Recent developments about conductive polymer based composite photocatalysts. *Polymers, 11*(2), 206.

Li, A., Zhang, C., & Zhang, Y.-F. (2017). Thermal conductivity of graphene-polymer composites: Mechanisms, properties, and applications. *Polymers, 9*(9), 437.

Li, J., Zhang, Y., Liang, T., Bai, X., Pang, Y., Zeng, X., . . . Du, G. (2021). Thermal Interface Materials with Both High Through-Plane Thermal Conductivity and Excellent Elastic Compliance. *Chemistry of Materials, 33*(22), 8926-8937.

Li, K., Bian, S., Zhen, W., Li, H., & Zhao, L. (2021). Performance, crystallization and rheological behavior of poly (lactic acid)/N-(2-hydroxyl) propyl-3-trimethyl ammonium chitosan chloride intercalated vermiculite grafted poly (acrylamide) nanocomposites. *Reactive and Functional Polymers, 158*, 104791.

Li, Y., Han, C., Yu, Y., Xiao, L., & Shao, Y. (2018). Isothermal and nonisothermal cold crystallization kinetics of poly (l-lactide)/functionalized eggshell powder composites. *Journal of Thermal Analysis and Calorimetry, 131*(3), 2213-2223.

Lim, L.-T., Auras, R., & Rubino, M. (2008). Processing technologies for poly (lactic acid). *Progress in Polymer Science, 33*(8), 820-852.

Lin, Y., Huang, X., Chen, J., & Jiang, P. (2017). Epoxy thermoset resins with high pristine thermal conductivity. *High Voltage, 2*(3), 139-146.

Lisperguer, J., Saravia, Y., & Vergara, E. (2016). Structure and thermal behavior of tannins from Acacia dealbata bark and their reactivity toward formaldehyde. *Journal of the Chilean Chemical Society, 61*(4), 3188-3190.

Liu, H., Kang, P., Liu, Y., An, Y., Hu, Y., Jin, X., . . . Wang, X. (2020). Zinc oxide nanoparticles synthesised from the Vernonia amygdalina shows the anti-inflammatory and antinociceptive activities in the mice model. *Artificial cells, nanomedicine, and biotechnology, 48*(1), 1068-1078.

Lule, Z., Ju, H., & Kim, J. (2018). Thermomechanical properties of alumina-filled plasticized polylactic acid: Effect of alumina loading percentage. *Ceramics International, 44*(18), 22767-22776.

Lule, Z., & Kim, J. (2019). Thermally conductive and highly rigid polylactic acid (PLA) hybrid composite filled with surface treated alumina/nano-sized aluminum nitride. *Composites Part A: Applied Science and Manufacturing, 124*, 105506.

Luo, J., Wang, H., Zuo, D., Ji, A., & Liu, Y. (2018). Research on the application of MWCNTs/PLA composite material in the manufacturing of conductive composite products in 3D printing. *Micromachines, 9*(12), 635.

Malik, P., Shankar, R., Malik, V., Sharma, N., & Mukherjee, T. K. (2014). Green chemistry based benign routes for nanoparticle synthesis. *Journal of Nanoparticles, 2014*.

Margulis-Goshen, K., & Magdassi, S. (2012). Organic nanoparticles from microemulsions: Formation and applications. *Current Opinion in Colloid & Interface Science, 17*(5), 290-296.

Mármol, G., Sanivada, U. K., & Fangueiro, R. (2021). Effect of GNPs on the Piezoresistive, Electrical and Mechanical Properties of PHA and PLA Films. *Fibers, 9*(12), 86.

Mekonnen, M. M., & Hoekstra, A. Y. (2016). Four billion people facing severe water scarcity. *Science advances, 2*(2), e1500323.

Miranzo, P., Belmonte, M., & Osendi, M. I. (2017). From bulk to cellular structures: A review on ceramic/graphene filler composites. *Journal of the European Ceramic Society, 37*(12), 3649-3672.

Mishra, A. K. (2018). Conducting polymers: concepts and applications. *Journal of Atomic, Molecular, Condensed Matter and Nano Physics, 5*(2), 159-193.

Mishra, S., Panda, S., Akcil, A., Dembele, S., & Agcasulu, I. (2021). A Review on Chemical versus Microbial Leaching of Electronic Wastes with Emphasis on Base Metal Dissolution. *Minerals, 11*(11), 1255.

Moradi, F., Sedaghat, S., Moradi, O., & Arab Salmanabadi, S. (2021). Review on green nano-biosynthesis of silver nanoparticles and their biological activities: With an emphasis on medicinal plants. *Inorganic and Nano-Metal Chemistry, 51*(1), 133-142.

Murthy, H. A., Zeleke, T. D., Tan, K., Ghotekar, S., Alam, M. W., Balachandran, R., . . . Ravikumar, C. (2021). Enhanced multifunctionality of CuO nanoparticles synthesized using aqueous leaf extract of Vernonia amygdalina plant. *Results in Chemistry, 3*, 100141.

Nakamura, S., Sato, M., Sato, Y., Ando, N., Takayama, T., Fujita, M., & Ishihara, M. (2019). Synthesis and application of silver nanoparticles (Ag NPs) for the prevention of infection in healthcare workers. *International journal of molecular sciences, 20*(15), 3620.

Namsheer, K., & Rout, C. S. (2021). Conducting polymers: A comprehensive review on recent advances in synthesis, properties and applications. *Rsc Advances, 11*(10), 5659-5697.

Nezakati, T., Seifalian, A., Tan, A., & Seifalian, A. M. (2018). Conductive polymers: opportunities and challenges in biomedical applications. *Chemical Reviews, 118*(14), 6766-6843.

Núñez, C., Estévez, S. V., & del Pilar Chantada, M. (2018). Inorganic nanoparticles in diagnosis and treatment of breast cancer. *JBIC Journal of Biological Inorganic Chemistry, 23*(3), 331-345.

Nzekekwu, A., & Abosede, O. (2019). Green synthesis and characterization of silver nanoparticles using leaves extracts of neem (Azadirachta indica) and bitter leaf (Vernonia amygdalina). *Journal of Applied Sciences and Environmental Management, 23*(4), 695-699.

Oluwaniyi, O. O., Adegoke, H. I., Adesuji, E. T., Alabi, A. B., Bodede, S. O., Labulo, A. H., & Oseghale, C. O. (2016). Biosynthesis of silver nanoparticles using aqueous leaf extract of Thevetia peruviana Juss and its antimicrobial activities. *Applied Nanoscience, 6*(6), 903-912.

Paciorek-Sadowska, J., Borowicz, M., & Isbrandt, M. (2019). New poly (lactide-urethane-isocyanurate) foams based on bio-polylactide waste. *Polymers, 11*(3), 481.

Pai, F.-C., Chu, H.-H., & Lai, S.-M. (2020). Preparation and properties of thermally conductive PLA/PA 610 biomass composites. *Journal of Elastomers & Plastics, 52*(1), 53-69.

Pan, M., Hong, L., Xie, X., Liu, K., Yang, J., & Wang, S. (2021). Nanomaterials-Based Surface Protein Imprinted Polymers: Synthesis and Medical Applications. *Macromolecular chemistry and physics, 222*(1), 2000222.

Park, D. W., & Shim, S. E. (2010). A review on thermal conductivity of polymer composites using carbon-based fillers: carbon nanotubes and carbon fibers. *Carbon letters, 11*(4), 347-356.

Pérez-Fonseca, A., Robledo-Ortíz, J., González-Núñez, R., & Rodrigue, D. (2016). Effect of thermal annealing on the mechanical and thermal properties of polylactic acid–cellulosic fiber biocomposites. *Journal of Applied Polymer Science, 133*(31).

Pinto, V. C., Ramos, T., Alves, A., Xavier, J., Tavares, P., Moreira, P., & Guedes, R. M. (2017). Dispersion and failure analysis of PLA, PLA/GNP and PLA/CNT-COOH biodegradable nanocomposites by SEM and DIC inspection. *Engineering failure analysis, 71*, 63-71.

Qiao, J., & Qi, L. (2021). Recent progress in plant-gold nanoparticles fabrication methods and bio-applications. *Talanta, 223*, 121396.

Qiu, F., Liu, T.-s., Zhang, X., Chang, F., Shu, S.-l., Yang, H.-y., . . . Jiang, Q.-c. (2020). Application of nanoparticles in cast steel: An overview. *China Foundry, 17*(2), 111-126.

Qu, M., Nilsson, F., & Schubert, D. W. (2019). Novel definition of the synergistic effect between carbon nanotubes and carbon black for electrical conductivity. *Nanotechnology, 30*(24), 245703.

Rafique, M., Rafique, M. S., Kalsoom, U., Afzal, A., Butt, S. H., & Usman, A. (2019). Laser ablation synthesis of silver nanoparticles in water and dependence on laser nature. *Optical and Quantum Electronics, 51*(6), 1-11.

Rasal, R. M., Janorkar, A. V., & Hirt, D. E. (2010). Poly (lactic acid) modifications. *Progress in Polymer Science, 35*(3), 338-356.

Rashkov, I., Manolova, N., Li, S., Espartero, J., & Vert, M. (1996). Synthesis, characterization, and hydrolytic degradation of PLA/PEO/PLA triblock copolymers with short poly (l-lactic acid) chains. *Macromolecules, 29*(1), 50-56.

Rasmussen, S. C. (2018). Early history of conductive organic polymers *Conductive Polymers* (pp. 1-22): CRC Press.

Rebelo, R., Fernandes, M., & Fangueiro, R. (2017). Biopolymers in medical implants: a brief review. *Procedia engineering, 200*, 236-243.

Román-Ramírez, L. A., Mckeown, P., Jones, M. D., & Wood, J. (2018). Poly (lactic acid) degradation into methyl lactate catalyzed by a well-defined Zn (II) complex. *ACS Catalysis, 9*(1), 409-416.

Sadeghi, B., & Gholamhoseinpoor, F. (2015). A study on the stability and green synthesis of silver nanoparticles using Ziziphora tenuior (Zt) extract at room temperature. *Spectrochimica Acta Part A: Molecular and Biomolecular Spectroscopy, 134*, 310-315.

Saeidlou, S., Huneault, M. A., Li, H., & Park, C. B. (2012). Poly (lactic acid) crystallization. *Progress in Polymer Science, 37*(12), 1657-1677.

Salem, S. S., & Fouda, A. (2021). Green synthesis of metallic nanoparticles and their prospective biotechnological applications: an overview. *Biological Trace Element Research, 199*(1), 344-370.

Sheikh, K., & Shahrajabian, H. (2021). Experimental Study on Mechanical, Thermal and Antibacterial Properties of Hybrid Nanocomposites of PLA/CNF/Ag. *International Journal of Engineering, 34*(2), 500-507.

Shen, W., Wu, W., Liu, C., Wang, Y., & Zhang, X. (2020). Thermal conductivity enhancement of PLA/TPU/BN composites by controlling BN distribution and annealing treatment. *Plastics, Rubber and Composites, 49*(5), 204-213.

Shen, W., Wu, W., Liu, C., Wang, Z., & Huang, Z. (2020). Achieving a high thermal conductivity for segregated BN/PLA composites via hydrogen bonding regulation through cellulose network. *Polymers for advanced technologies, 31*(9), 1911-1920.

Simmons, H., Tiwary, P., Colwell, J. E., & Kontopoulou, M. (2019). Improvements in the crystallinity and mechanical properties of PLA by nucleation and annealing. *Polymer Degradation and Stability, 166*, 248-257.

Sin, L. T. (2012). *Polylactic acid: PLA biopolymer technology and applications*: William Andrew.

Singh, P., Ahn, S., Kang, J.-P., Veronika, S., Huo, Y., Singh, H., . . . Kim, Y. J. (2018). In vitro anti-inflammatory activity of spherical silver nanoparticles and monodisperse hexagonal gold nanoparticles by fruit extract of Prunus serrulata: a green synthetic approach. *Artificial cells, nanomedicine, and biotechnology, 46*(8), 2022-2032.

Speranza, G. (2021). Carbon nanomaterials: Synthesis, functionalization and sensing applications. *Nanomaterials, 11*(4), 967.

Spinelli, G., Lamberti, P., Tucci, V., Ivanova, R., Tabakova, S., Ivanov, E., . . . Silvestre, C. (2019). Rheological and electrical behaviour of nanocarbon/poly (lactic) acid for 3D printing applications. *Composites Part B: Engineering, 167*, 467-476.

Spinelli, G., Lamberti, P., Tucci, V., Kotsilkova, R., Ivanov, E., Menseidov, D., . . . Adami, R. (2019). Nanocarbon/poly (lactic) acid for 3d printing: Effect of fillers content on electromagnetic and thermal properties. *Materials, 12*(15), 2369.

Srithep, Y., Nealey, P., & Turng, L. S. (2013). Effects of annealing time and temperature on the crystallinity and heat resistance behavior of injection-molded poly (lactic acid). *Polymer Engineering & Science, 53*(3), 580-588.

Sun, J., Li, L., & Li, J. (2019). Effects of furan-phosphamide derivative on flame retardancy and crystallization behaviors of poly (lactic acid). *Chemical engineering journal, 369*, 150-160.

Sun, J., Yu, H., Zhuang, X., Chen, X., & Jing, X. (2011). Crystallization behavior of asymmetric PLLA/PDLA blends. *The Journal of Physical Chemistry B, 115*(12), 2864-2869.

Sury, S. V. J., Ulianas, A., & Aini, S. (2021). *Synthesis of Conducting Polyaniline with Photopolymerization Method and Characterization.* Paper presented at the Journal of Physics: Conference Series.

Taghizadeh, A., Taghizadeh, M., Jouyandeh, M., Yazdi, M. K., Zarrintaj, P., Saeb, M. R., . . . Gupta, V. K. (2020). Conductive polymers in water treatment: A review. *Journal of Molecular Liquids, 312*, 113447.

Takayama, T., Todo, M., & Tsuji, H. (2011). Effect of annealing on the mechanical properties of PLA/PCL and PLA/PCL/LTI polymer blends. *journal of the mechanical behavior of biomedical materials, 4*(3), 255-260.

Tarani, E., Papageorgiou, G. Z., Bikiaris, D. N., & Chrissafis, K. (2019). Kinetics of crystallization and thermal degradation of an isotactic polypropylene matrix reinforced with graphene/glass-fiber filler. *Molecules, 24*(10), 1984.

Tarani, E., Pušnik Črešnar, K., Zemljič, L. F., Chrissafis, K., Papageorgiou, G. Z., Lambropoulou, D., . . . Terzopoulou, Z. (2021). Cold Crystallization Kinetics and Thermal Degradation of PLA Composites with Metal Oxide Nanofillers. *Applied Sciences, 11*(7), 3004.

Terzopoulou, Z., Tarani, E., Kasmi, N., Papadopoulos, L., Chrissafis, K., Papageorgiou, D. G., . . . Bikiaris, D. N. (2019). Thermal decomposition kinetics and mechanism of in-situ prepared bio-based poly (propylene 2, 5-furan dicarboxylate)/graphene nanocomposites. *Molecules, 24*(9), 1717.

Tessema, A., Zhao, D., Moll, J., Xu, S., Yang, R., Li, C., . . . Kidane, A. (2017). Effect of filler loading, geometry, dispersion and temperature on thermal conductivity of polymer nanocomposites. *Polymer Testing, 57*, 101-106.

Trifol, J., van Drongelen, M., Clegg, F., Plackett, D., Szabo, P., & Daugaard, A. (2019). Impact of thermal processing or solvent casting upon crystallization of PLA nanocellulose and/or nanoclay composites. *Journal of Applied Polymer Science, 136*(20), 47486.

Urayama, H., Kanamori, T., Fukushima, K., & Kimura, Y. (2003). Controlled crystal nucleation in the melt-crystallization of poly (l-lactide) and poly (l-lactide)/poly (d-lactide) stereocomplex. *Polymer, 44*(19), 5635-5641.

Usunomena, U., & Ngozi, O. P. (2016). Phytochemical analysis and proximate composition of Vernonia amygdalina. *Int. J. Sci. World, 4*, 11-14.

Wang, N., Zhang, C., & Weng, Y. (2021). Enhancing gas barrier performance of polylactic acid/lignin composite films through cooperative effect of compatibilization and nucleation. *Journal of Applied Polymer Science, 138*(15), 50199.

Wang, X., Tang, Y., Zhu, X., Zhou, Y., & Hong, X. (2020). Preparation and characterization of polylactic acid/polyaniline/nanocrystalline cellulose nanocomposite films. *International journal of biological macromolecules, 146*, 1069-1075.

Wang, X., Zhang, X., Sun, L., Lee, D., Lee, S., Wang, M., . . . Palacios, T. (2018). High electrical conductivity and carrier mobility in oCVD PEDOT thin films by engineered crystallization and acid treatment. *Science advances, 4*(9), eaat5780.

Wang, Y., Ding, Y., Guo, X., & Yu, G. (2019). Conductive polymers for stretchable supercapacitors. *Nano Research*, 1-10.

Wang, Y., & Xia, Y. (2004). Bottom-up and top-down approaches to the synthesis of monodispersed spherical colloids of low melting-point metals. *Nano letters, 4*(10), 2047-2050.

Wei, Z., Shao, S., Sui, M., Song, P., He, M., Xu, Q., . . . Li, Y. (2019). Development of zinc salts of amino acids as a new class of biocompatible nucleating agents for poly (L-lactide). *European polymer journal, 118*, 337-346.

Wu, J., Zhu, L., Ning, T., & Lu, A. (2020). The effects of a complex nucleating agent with different ratios of MgF2/LiF on the crystallization and performance of lithium aluminum silicate glasses. *Journal of Non-Crystalline Solids, 540*, 120087.

Wu, W., Wu, C., Peng, H., Sun, Q., Zhou, L., Zhuang, J., . . . Li, R. K. (2017). Effect of nitrogen-doped graphene on morphology and properties of immiscible poly (butylene succinate)/polylactide blends. *Composites Part B: Engineering, 113*, 300-307.

Xiao, L., Wang, B., Yang, G., & Gauthier, M. (2012). Poly (lactic acid)-based biomaterials: synthesis, modification and applications. *Biomedical science, engineering and technology, 11*, 247-282.

Xu, L., Zhao, J., Qian, S., Zhu, X., & Takahashi, J. (2021). Green-plasticized poly (lactic acid)/nanofibrillated cellulose biocomposites with high strength, good toughness and excellent heat resistance. *Composites science and technology, 203*, 108613.

Xu, T., Wang, X., Zhang, X., & Bai, Z. (2022). Compact Ag nanoparticles anchored on the surface of glass fiber filter paper for SERS applications. *Applied Physics A, 128*(4), 1-8.

Yang, B., Wang, D., Chen, F., Su, L.-F., Miao, J.-B., Chen, P., . . . Liu, J.-W. (2019). Melting and crystallization behaviors of poly (lactic acid) modified with graphene acting as a nucleating agent. *Journal of Macromolecular Science, Part B, 58*(2), 290-304.

Yang, J., Hou, B., Wang, J., Tian, B., Bi, J., Wang, N., . . . Huang, X. (2019). Nanomaterials for the removal of heavy metals from wastewater. *Nanomaterials, 9*(3), 424.

Yang, L., & Zhen, W. (2019). Poly (lactic acid)/p-phenylenediamine functionalized graphene oxidized nanocomposites: Preparation, rheological behavior and biodegradability. *European polymer journal, 121*, 109341.

Yazdanshenas, M. E., & Shateri-Khalilabad, M. (2012). The effect of alkali pre-treatment on formation and adsorption of silver nanoparticles on cotton surface. *Fibers and Polymers, 13*(9), 1170-1178.

Ye, Y., Gong, L., Xiang, S., Zhang, Z., & Chen, B. (2020). Metal–organic frameworks as a versatile platform for proton conductors. *Advanced Materials, 32*(21), 1907090.

Yodahe, G. (2021). *Green Synthesis Of AgNPs Dispersed 3-Armed Gly Lac Macromolecule Matrix And Pla Film For Its Antimicrobial Activities.* ASTU.

Yu, W., Wang, X., Ferraris, E., & Zhang, J. (2019). Melt crystallization of PLA/Talc in fused filament fabrication. *Materials & Design, 182*, 108013.

Yuan, Y., Hu, Z., Fu, X., Jiang, L., Xiao, Y., Hu, K., . . . Lei, J. (2016). Poly (lactic acid) plasticized by biodegradable glyceryl lactate. *Journal of Applied Polymer Science, 133*(21).

Zhang, L., Deng, H., & Fu, Q. (2018). Recent progress on thermal conductive and electrical insulating polymer composites. *Composites Communications, 8*, 74-82.

Zhao, S., Liu, K., Zhou, S., Shi, Y., & Xin, Z. (2017). A novel self-dispersed β nucleating agent for isotactic polypropylene and its unique nucleation behavior and mechanism. *Polymer, 132*, 69-78.

APPENDIXES

Appendix -1: Particle size analyser (PSA), the particle size distribution of AgNPs

Size Distribution Report by Intensity
v2.2

Malvern

Sample Details

Sample Name: AgNPs
SOP Name: CNC.sop
General Notes:

File Name: Nano material.dts
Record Number: 273
Material RI: 1.59
Material Absorbtion: 0.010
Dispersant Name: Water
Dispersant RI: 1.330
Viscosity (cP): 0.8872
Measurement Date and Time: Tuesday, Dec 09, 2021...

System

Temperature (°C): 25.0
Count Rate (kcps): 22.0
Cell Description: Disposable sizing cuvette
Duration Used (s): 270
Measurement Position (mm): 0.85
Attenuator: 11

Results

		Size (d.nm):	% Intensity:	St Dev (d.n...
Z-Average (d.nm): 565	Peak 1:	56.45	66.5	5.353
PdI: 0.7	Peak 2:	3.05	33.5	0.1890
Intercept: 0.487	Peak 3:	0.000	0.0	0.000

Result quality : Refer to quality report

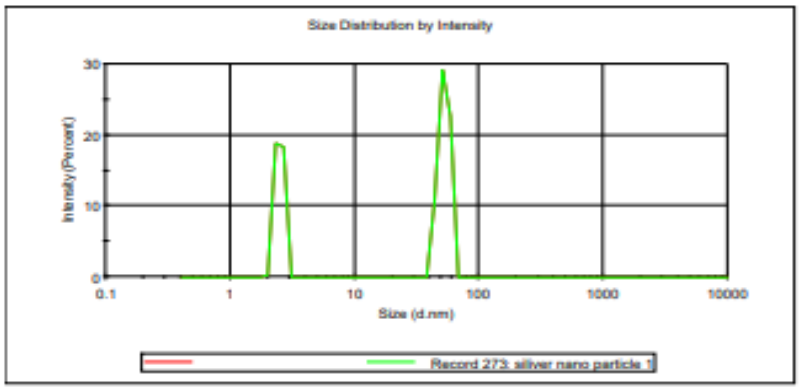

Appendix -2: ^{13}C-NMR Spectra for GLY-LAC 1:3 bio-conjugate

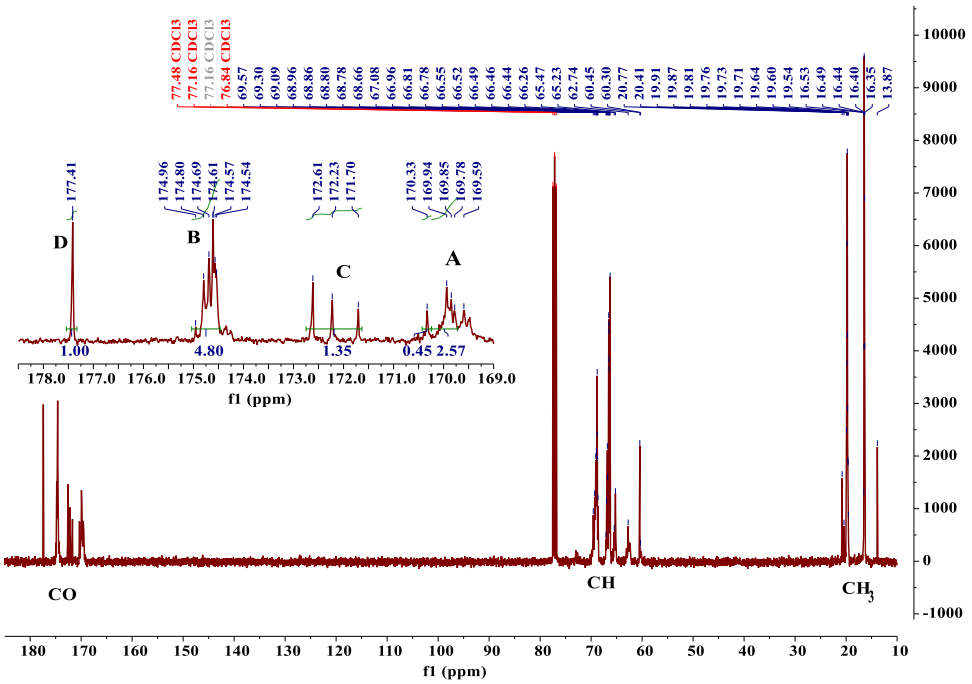

Appendix -3: ^{13}C-NMR Spectra for GLY-LAC 1:9 bio-conjugate

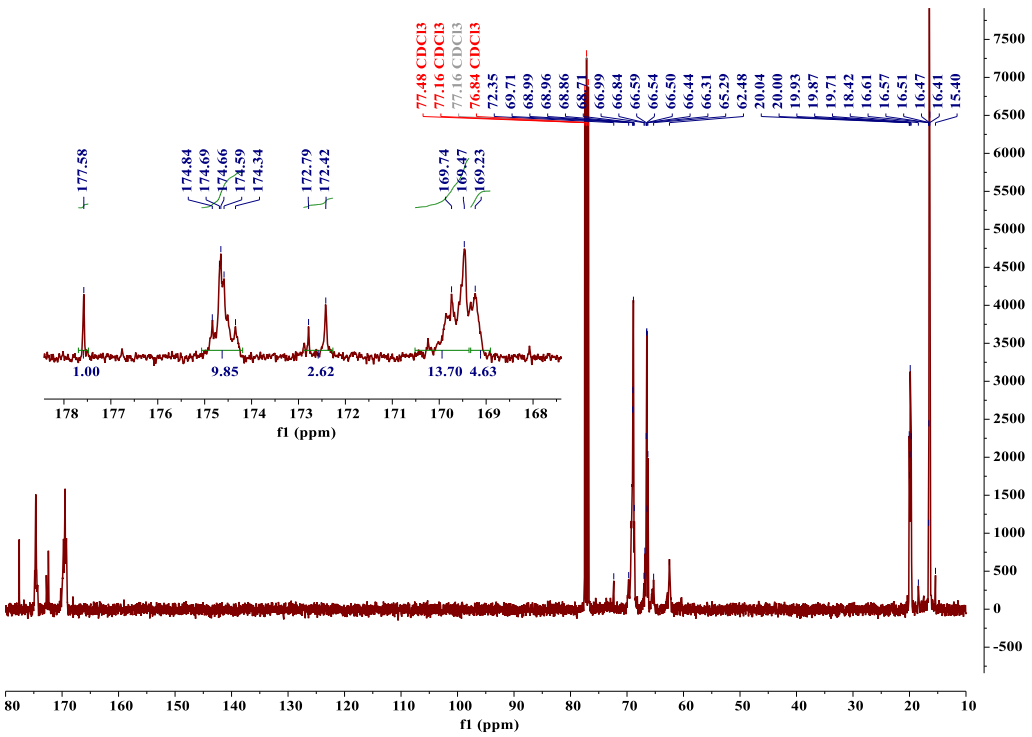

Appendix -4: ^{13}C-NMR Spectra for GLY-LAC 1:12 bio-conjugate

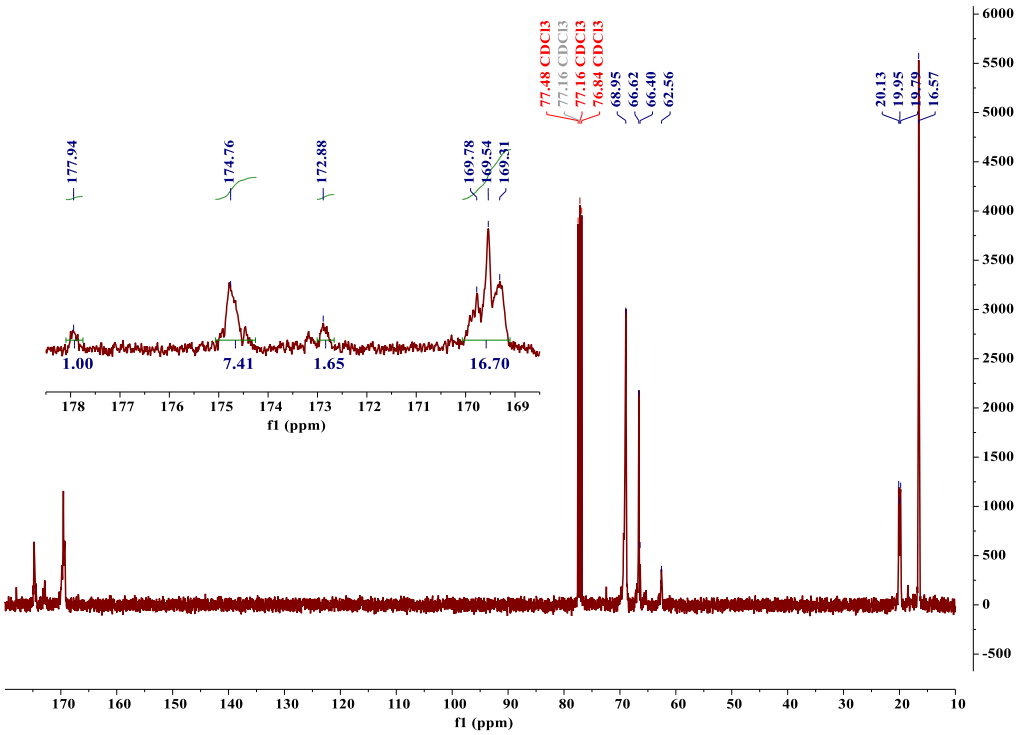

Appendix -5: ^{1}H-NMR Spectra for GLY-LAC 1:3 bio-conjugate

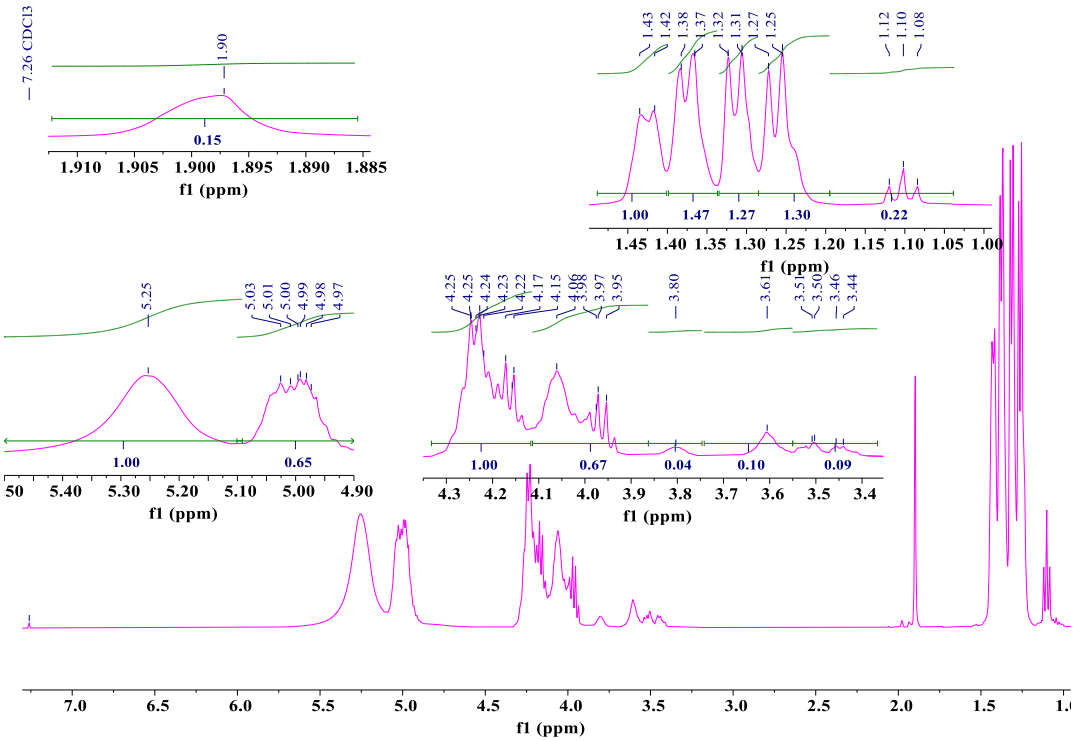

Appendix -6: DEPT 135-NMR Spectra for GLY-LAC 1:6 bio-conjugate

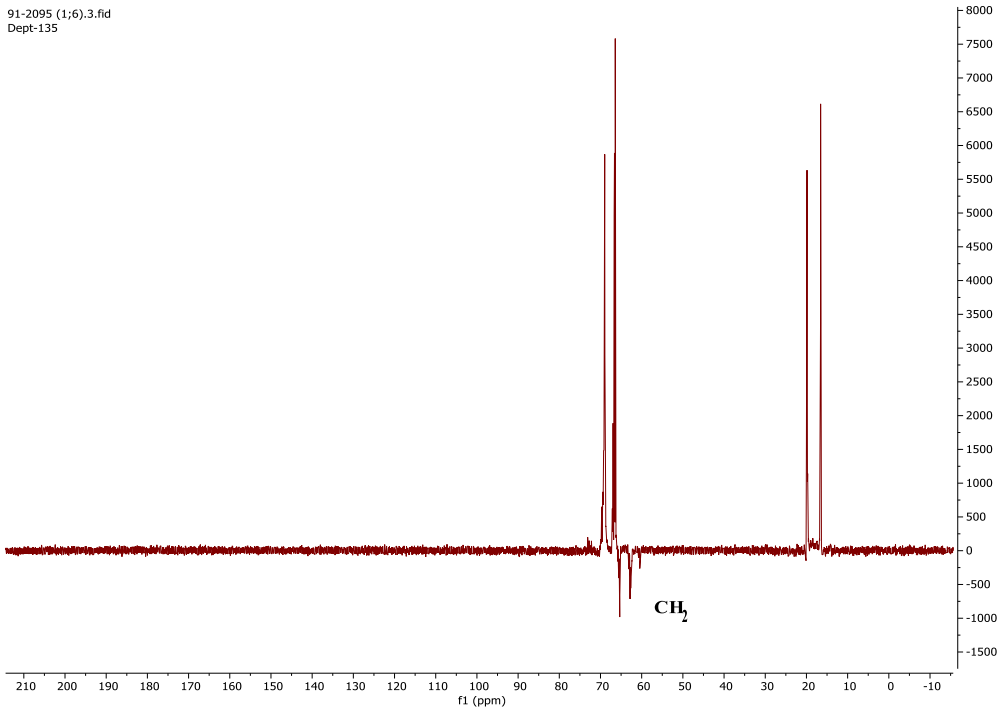

Appendix -7: ^{1}H-NMR Spectra for GLY-LAC 1:9 bio-conjugate

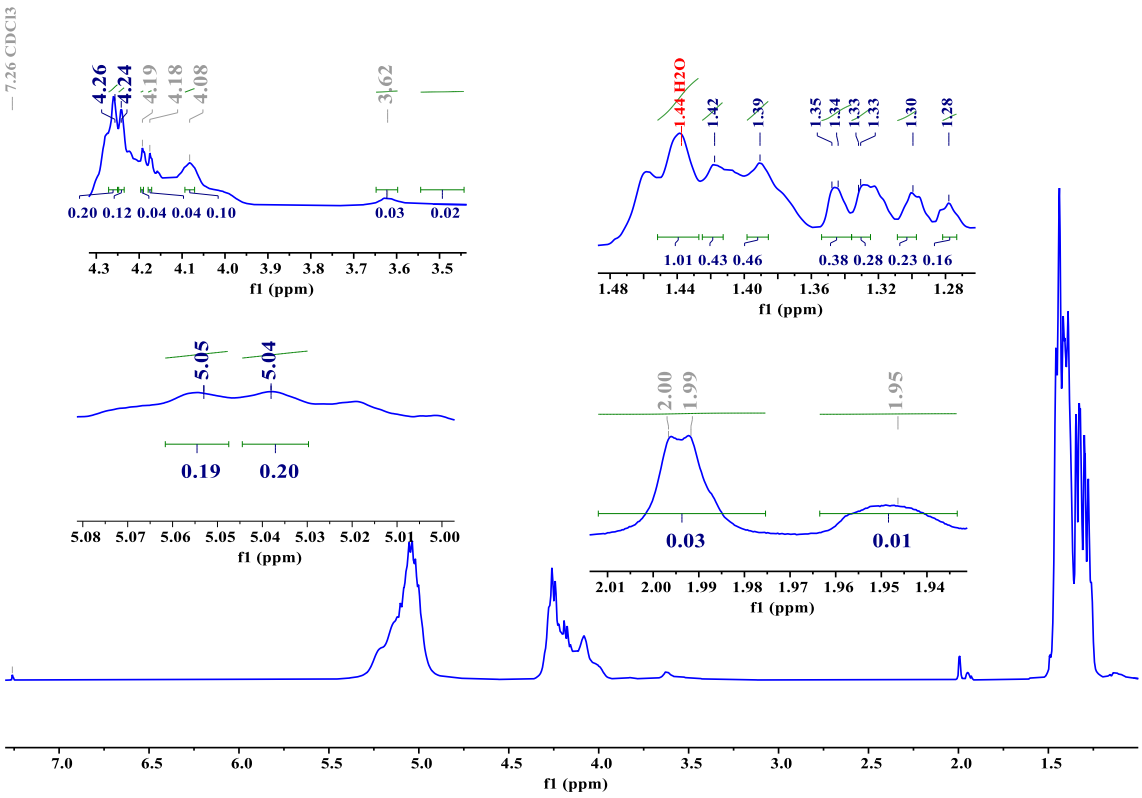

Appendix -8: ^{1}H-NMR Spectra for GLY-LAC 1:12 bio-conjugate

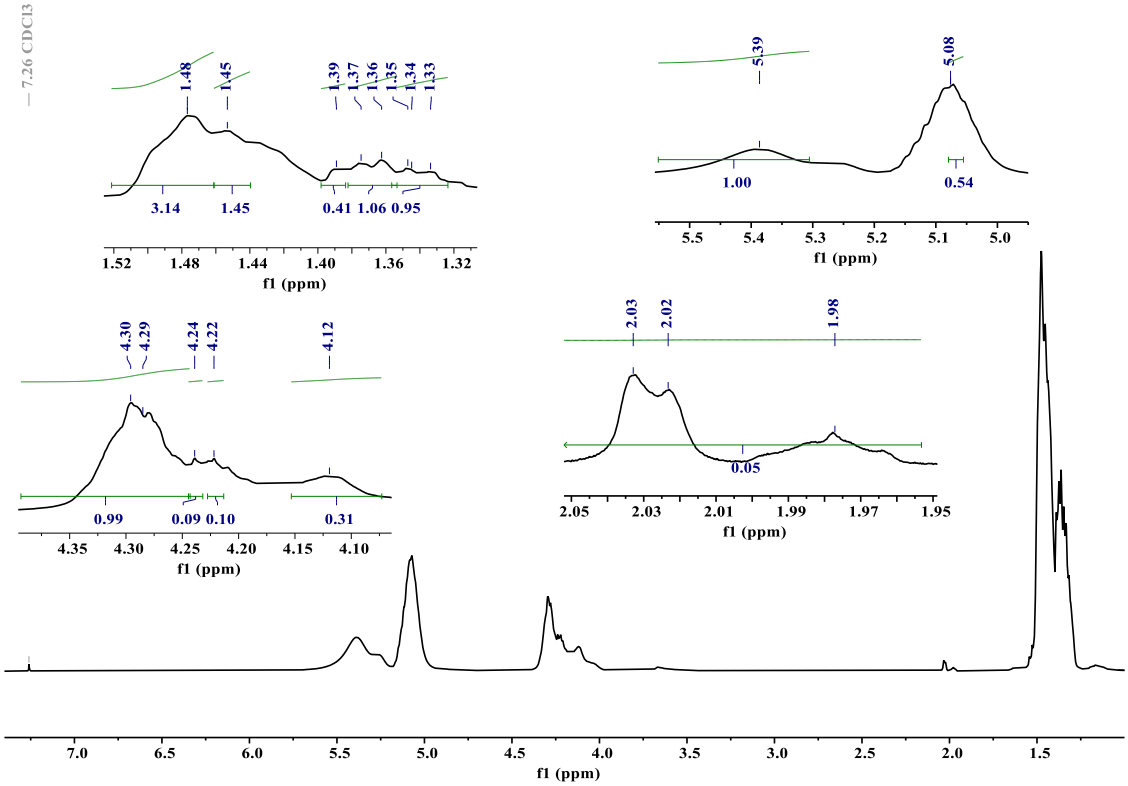

Appendix -9: Effects of AgNPs on the degree of crystallinity of PLA

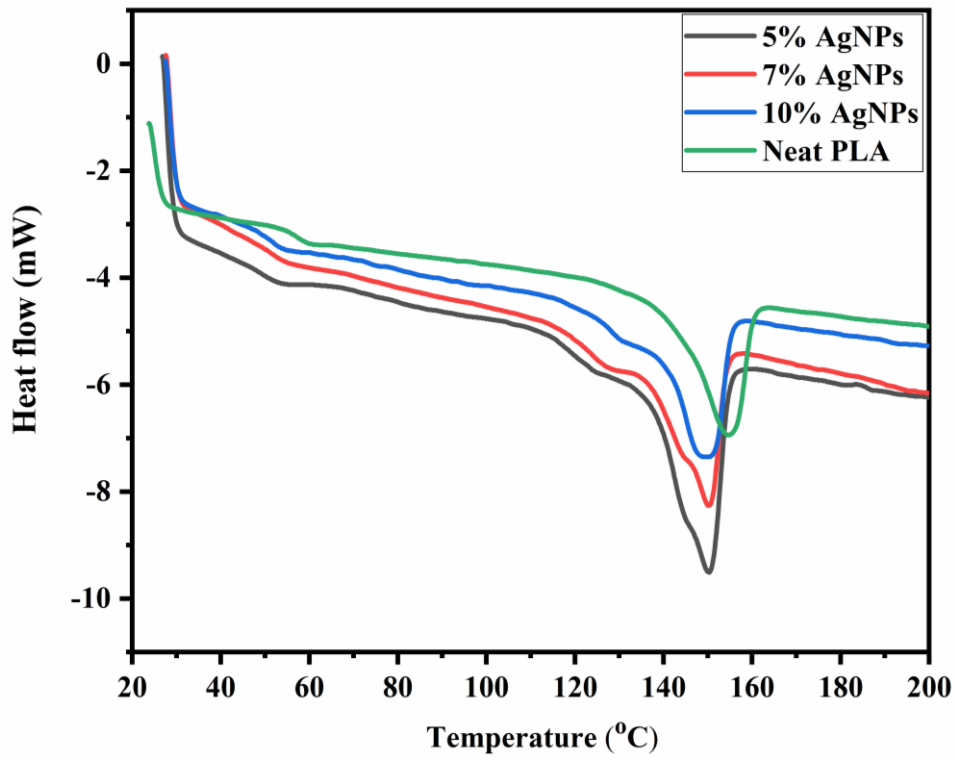

Appendix -10: Zeta potential

Zeta Potential Report

v2.3

Malvern

Sample Details

Sample Name: AgNPs without Cal.

SOP Name: Zeta potential test sample v2 DTS1070.sop

General Notes: This SOP is also suitable for most samples of conductivity less than 5 mS.

File Name:	Example Results.dts	**Dispersant Name:**	Water
Record Number:	264	**Dispersant RI:**	1.330
Date and Time:	Wednesday, December 1, 2021 3...	**Viscosity (cP):**	0.8872
		Dispersant Dielectric Constant:	78.5

System

Temperature (°C):	25.0	**Zeta Runs:**	12
Count Rate (kcps):	331.3	**Measurement Position (mm):**	2.00
Cell Description:	Clear disposable zeta cell	**Attenuator:**	6

Results

			Mean (mV)	Area (%)	St Dev (mV)
Zeta Potential (mV):	-27.2	**Peak 1:**	-27.2	100.0	4.52
Zeta Deviation (mV):	4.52	**Peak 2:**	0.00	0.0	0.00
Conductivity (mS/cm):	0.124	**Peak 3:**	0.00	0.0	0.00
Result quality :	Good				

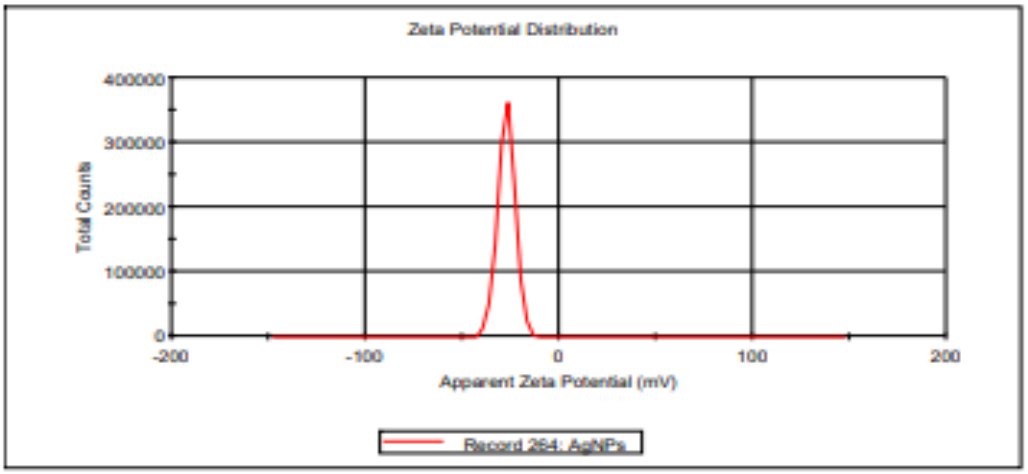

Appendix -11: Crystallite size of AgNPs without calcination

Peak position in (2θ)	Theta (θ)	FWHM	Crystalline size (nm)	D average (nm)
23.65496	11.82748	0.28794	28.18855036	
27.8273	13.91365	0.28814	28.40433972	
32.23213	16.116065	0.2882	28.69278162	
38.17864	19.08932	0.28778	29.21178353	
44.19857	22.09928	0.28778	29.79431345	
46.36427	23.182135	0.28789	30.01863759	30.48
54.92921	27.46461	0.28836	31.04928024	
57.55987	28.77994	0.28777	31.49704557	
64.58311	32.29155	0.28783	32.65030618	
77.33263	38.66631	0.28814	35.31123185	

Appendix -12: Crystallite size of Cal. AgNPs

Peak position in (2θ)	Theta (θ)	FWHM	Crystalline size (nm)	D average (nm)
27.85612	13.92807	0.25982	31.50233492	
32.2534	16.1267	0.27743	29.8082519	
38.23444	19.11722	0.26306	31.96223282	
44.42306	22.21153	0.34383	24.95724586	
46.22356	23.11178	0.31755	27.20053584	
54.79137	27.39568	0.34869	25.66113869	26.71
57.45679	28.728395	0.36237	25.00050237	
64.57817	32.289085	0.40863	22.99753227	
77.51906	38.78953	0.47875	21.28011421	

Appendix -13: d-Spacing values of AgNPs without calcination

Peak position in (2θ)	Theta (θ)	$d = \frac{n\lambda}{2sin\theta}$	Average d-Spacing (nm)
27.85612	13.92807	0.375819328	0.2204129
32.2534	16.1267	0.320345277	
38.23444	19.11722	0.277501553	
44.42306	22.21153	0.235535674	
46.22356	23.11178	0.204751195	
54.79137	27.39568	0.195678808	
57.45679	28.728395	0.16702061	
64.57817	32.289085	0.159996922	
77.51906	38.78953	0.144189438	

Appendix -14: d-Spacing values of AgNPs with calcination

Peak position in (2θ)	Theta (θ)	$d = \frac{n\lambda}{2sin\theta}$	Averaged-Spacing (nm)
27.85612	13.92807	0.320020391	0.2030518
32.2534	16.1267	0.277323403	
38.23444	19.11722	0.235204753	
44.42306	22.21153	0.203768461	
46.22356	23.11178	0.196241666	
54.79137	27.39568	0.167408148	
57.45679	28.728395	0.160259431	
64.57817	32.289085	0.144199274	